UNIVERSIDADE FEDERAL DE LAVRAS

ISABELA BRAGA BELCHIOR

AVALIAÇÃO DE QUEIMADAS POR SENSORIAMENTO REMOTO NO PARQUE NACIONAL DE ITATIAIA

LAVRAS – MG
2021

ISABELA BRAGA BELCHIOR

AVALIAÇÃO DE QUEIMADAS POR SENSORIAMENTO REMOTO NO PARQUE NACIONAL DE ITATIAIA

Tese apresentada à Universidade Federal de Lavras, como parte das exigências do Programa de Pós-Graduação em Engenharia Florestal, área de concentração em Ciências Florestais, para a obtenção do título de Doutora.

Prof. Dr. Luis Marcelo Tavares de Carvalho
Orientador

LAVRAS – MG

2021

ISABELA BRAGA BELCHIOR

AVALIAÇÃO DE QUEIMADAS POR SENSORIAMENTO REMOTO NO PARQUE NACIONAL DE ITATIAIA

REMOTE SENSING BURNS ASSESSMENT IN ITATIAIA NATIONAL PARK

Tese apresentada à Universidade Federal de Lavras, como parte das exigências do Programa de Pós-Graduação em Engenharia Florestal, área de concentração em Ciências Florestais, para a obtenção do título de Doutora.

APROVADA em 21 de dezembro de 2021

Dr. Luis Marcelo Tavares de Carvalho   UFLA

Dra. Thiza Falqueto Altoé   UFLA

Dr. Gabriel Araujo e Silva Ferraz   UFLA

Dr. Danton Diego Ferreira   UFLA

Dr. Allan Arantes Pereira   IFSULDEMINAS

Prof. Dr. Luis Marcelo Tavares de Carvalho
Orientador

LAVRAS – MG
2021

A minha amada mãe, Sueli Braga,

por ser minha maior incentivadora.

Dedico!

AGRADECIMENTOS

Primeiramente agradeço a Deus, por ter me sustentado e ter me dado forças para chegar até aqui. Pelo dom da vida e por abençoar sempre minha caminhada.

A Universidade Federal de Lavras (UFLA) e ao Programa de Pós-graduação em Engenharia Florestal. Agradeço ainda, os competentes docentes e funcionários desta instituição.

A Coordenação de Aperfeiçoamento de Pessoal de Nível Superior (CAPES) pela concessão de bolsa de estudo.

Ao meu orientador, Prof. Dr. Luis Marcelo, mais conhecido como passarinho, por todo conhecimento transmitido, pela confiança, apoio, incentivo e por demonstrar tanta empatia por seus orientados.

Aos gestores do Parque Nacional de Itatiaia, por apoiarem pesquisas multidisciplinares e por me acolherem para coletas de dados. Em especial agradeço ao Marcelo Motta por toda sua disponibilidade e auxílio.

Aos técnicos do LEMAF, em especial ao Thiago e Kalill pelo auxilio nas coletas de dados e troca de conhecimentos.

Ao professor Prof. Dr. Danton, por toda ajuda e pronto atendimento na elaboração dos algoritmos utilizados na tese.

As minhas companheiras de laboratório, Lizandra, Raphaela, Eveline e Samantha por toda ajuda com os processamentos de dados, conselhos, troca de vivências, momentos de descontração e pelo nossos papos no cantinho do café.

A minha mãe, Sueli Braga, que é minha grande inspiração e incentivadora, com certeza sem seu apoio não teria chegado até aqui. Você foi minha força motriz para finalização deste ciclo que sonhou comigo.

A minha família por todo o carinho e incentivo, especialmente meus avós Diva e Anizio, que com nossas conversas diárias sempre transmitiam palavras de conforto e estímulo, vocês foram essenciais nessa caminhada.

Ao meu namorado Douglas por sempre acreditar em mim, me colocando pra cima com suas palavras incentivadoras e amorosas, por toda sua paciência, por compreender o quão desafiadora é esta jornada e pelo presente maravilhoso, a Luna, que se tornou minha incansável e fiel companheira.

Aos meus amigos de Lavras, que se tornaram minha família mineira, e que levarei sempre comigo: Douglas, Bruna, Julio, Allison, Talles, Jaci, Gege e Rafa. E em especial agradeço a minha grande amiga Thayane (miglis) que sempre esteve ao meu lado desde o meu primeiro dia em solos lavrenses.

Aos escoteiros do Grupo Acauã que me acolheram com tanto afeto.

A todos que de alguma maneira contribuíram com esta conquista, agradeço!

"Não existe ensino que se compare ao exemplo."

(Robert Baden-Powell)

RESUMO GERAL

A ocorrência de incêndios florestais aumentou substancialmente nos últimos anos em todo mundo, sendo os padrões de atividade do fogo controlados pelo clima e impulsionados pelas mudanças climáticas. No Brasil o contexto não é diferente, apresentando aumento do número de incêndios e da extensão das áreas queimadas, influenciando negativamente na conservação dos biomas brasileiros, especialmente em áreas protegidas. Nesse sentido, esta tese foi conduzida no Parque Nacional de Itatiaia e pautada com a finalidade de analisar uma queima prescrita por meio de imagens RGB e multiespectral obtidas por VANT. De maneira geral, os resultados apontam que o método de classificação automática usando imagens RGB e multiespectral é preciso para discriminar a vegetação pré e pós queima (Artigo 1). Realizou-se também uma avaliação do uso de imagens de sensoriamento remoto de média resolução espacial para identificar áreas queimadas no interior e na área de amortecimento do parque e testada como uma alternativa para o refinamento dos dados de Registro de Ocorrência de Incêndios (ROIs), os resultados indicam que estas imagens (Landsat-8 e Sentinel-2) podem ser utilizadas para tornar a detecção de incêndios mais precisa em áreas protegidas (Artigo 2). Por fim, foi examinado a severidade do fogo e o tempo de permanência da mudança (cicatriz deixada pelo fogo na paisagem) em incêndios florestais e queimas prescritas e concluiu-se que queimas prescritas geram maior porcentagem de áreas com baixa e moderada severidade, já, incêndios florestais apresentam maiores áreas queimadas com moderada e alta severidade, além disso, essa análise permitiu inferir um tempo estimado para recuperação da vegetação queimada em cada área estudada (Artigo 3). Com isto, a obtenção e aprimoramento destes dados melhora o conhecimento sobre o papel ecológico do fogo e serve de subsídio aos gestores de unidades de conservação para um melhor planejamento de ações relacionadas ao manejo integrado do fogo.

Palavras-chave: VANT. GEOBIA. Incêndios Florestais. Severidade de queima. Unidade de Conservação.

GENERAL ABSTRACT

The occurrence of forest fires has substantially increased over the past few years across the world with patterns of fire activity being controlled by the climate and driven by climate changes. In Brazil, the context is no different with an increase in the number of fires as well as in the extension of burned areas, negatively influencing the conservation of the Brazilian biomes especially in protected areas. In this sense, the present thesis was developed at the Itatiaia National Park and it aimed at analyzing a prescribed fire using both RGB and multispectral imaging obtained by UAS. In general, results show that the automatic classification method using RGB and multispectral images is accurate in discriminating the vegetation both pre- and post-fire (Article 1). An evaluation of the use of medium-spatial-resolution satellite imagery was also carried out to identify burned areas in the interior and in the buffer zone of the park and tested as an alternative for the refinement of data from the Fire Occurrence Records (FORs). Results indicate that these images (Landsat-8 and Sentinel-2) may be used to make the detection of fires more accurate in protected areas (Article 2). Finally, the severity of the fire and how long the change remained (fire scars in the landscape) were examined in forest fires and prescribed fires and it was concluded that the last ones generate a higher percentage of areas with low to moderate severity whereas forest fires have larger areas burned with moderate to high severity; moreover, this analysis allowed us to infer an estimated time for the recovery of the burned vegetation in each area studied (Article 3). Thus, by obtaining and improving these data, it is possible to better understand the ecological role of the fire and it serves as a subsidy to managers of conservation units for a better planning of actions related to an integrated management of fire.

Keywords: UAV. GEOBIA. Wildfires. Fire severity. Protected areas.

SUMÁRIO

PRIMEIRA PARTE

1. INTRODUÇÃO

A ocorrência de incêndios aumentou substancialmente nos últimos anos em todo mundo (BARBERO et al., 2020; SUN et al., 2019). Um exemplo são os grandes incêndios florestais ocorridos recentemente, como os da Austrália em 2019-2020; no Brasil, especialmente na floresta amazônica em 2019 e 2020; no oeste dos Estados Unidos em 2018 e 2020; em British Columbia no Canadá, em 2017 e 2018 (XU et al., 2020).

Os frequentes incêndios vêm causando degradação da vegetação e estima-se que a perda florestal média induzida pelo fogo é cerca de 15% da perda florestal global, principalmente nas altas latitudes do norte (LIU; BALLANTYNE; COOPER, 2019). Além disso, os incêndios são responsáveis por queimar anualmente uma área do tamanho da União Europeia (GIGLIO et al., 2018).

Os padrões globais de atividade do fogo são controlados pelo clima, impulsionando a produtividade da vegetação e o acúmulo de combustível, bem como influencia na sua umidade por meio do aumento da demanda por evaporação e da diminuição da precipitação (BARBERO et al., 2020; BOWMAN et al., 2009). Assim, a medida que as mudanças climáticas pioram aumenta o risco de ocorrer incêndios florestais, pois a temporada de incêndios está começando cada vez mais cedo e terminando mais tarde (SUN et al., 2019; JOLLY et al., 2015). Projeções indicam que no final do século 21 a duração da temporada de incêndios e a frequência destes irão aumentar significativamente (SUN et al., 2019).

O Brasil segue esta tendência global, apresentando aumento do número de focos de incêndio e da extensão das áreas queimadas, com mais de 312.140 km^2 do país queimado em 2020 (INPE, 2020). A maior concentração de focos de calor ocorreu na Amazônia, Cerrado e no Pantanal, este último bioma apresentou 13% dos incêndios em nível nacional, um fato sem precedentes desde o início do registro de dados em 1998 (PIVELLO et al., 2021), chocando todo o país (MARENGO et al., 2021).

Além do clima mais seco e das mudanças no uso da terra por meio do desmatamento e fogo para limpeza de pasto que ampliam o risco de ocorrer incêndios florestais em todo país (PIVELLO et al., 2021), esta problemática é intensificada pela fraca governança florestal e resultado do governo atual (LIZUNDIA-LOIOLA; PETTINARI; CHUVIECO, 2020; ESCOBAR, 2019).

Neste contexto, a conservação dos biomas brasileiros principalmente em áreas protegidas está ameaçada, pois o atual governo é favorável à expansão das lavouras,

concomitantemente com a redução da política de conservação dos governos anteriores, diminuição dos investimentos na proteção de ecossistemas naturais, além de questionar os direitos de preservação de áreas indígenas (LIZUNDIA-LOIOLA; PETTINARI; CHUVIECO, 2020; SCHMIDT; ELOY, 2020).

A conduta do atual governo brasileiro resulta em um aumento dos incêndios em unidades de conservação federal, devido ao fogo usado para desflorestamento, gestão de pastagens e sistemas de corte e queima ultrapassar as fronteiras das propriedades privadas atingindo áreas protegidas.

Como é o caso Parque Nacional da Serra da Canastra que autoriza o uso do fogo por seus moradores desde 2002, porém a grande maioria utiliza o fogo indiscriminadamente (BERLINCK; LIMA, 2021). Outro exemplo é a vasta área queimada dentro de unidades de conservação na Amazônia, totalizando 20.960 km², tornando-a uma fonte de emissões de CO_2 (SILVA et al., 2021). De acordo com o MapBiomas (2021) no decorrer dos últimos 20 anos 18% da área queimada se localiza em áreas protegidas brasileiras.

O fogo é um dos principais fatores que afetam a degradação florestal, influencia na ciclagem de carbono, pode mudar a composição das espécies (GATTI et al., 2014; MEWS et al., 2013; LÍBANO; FELFILI, 2006) reduzir a circulação atmosférica de água e formação de nuvens por evapotranspiração (STAAL et al., 2020; MARENGO et al., 2018).

Quando os incêndios afetam áreas sensíveis ao fogo, onde as plantas não evoluíram sob a influencia do mesmo e não têm adaptações naturais há uma alta mortalidade causando efeitos ecológicos negativos (SCHMIDT et al., 2018; FRANCO et al., 2014).

Além disso, a tentativa de implementação de "fogo zero" no Brasil foi um grande impulsionador da ocorrência de grandes e mega incêndios (>50.000 ha) (FIDELIS et al., 2018; DURIGAN; RATTER, 2016), principalmente em ambientes propensos ao fogo, como o Cerrado e pastagens.

Devido à problemática e consequências do fogo em áreas protegidas, em 2010 foi desenvolvido o Manejo Integrado do Fogo (MIF), mudando o padrão de "fogo zero" para o fogo a favor da conservação da biodiversidade (BERLINCK; LIMA, 2021; SCHMIDT; ELOY, 2020). O MIF é uma estratégia que permite a integração das práticas culturais de manejo do fogo da população local (ELOY et al., 2019; FIDELIS et al., 2018) e tem por objetivo diminuir o risco de ocorrência de incêndios florestais, normalmente realizado por meio das queimas prescritas (PIVELLO et al., 2021).

As queimas prescritas visam à aplicação de fogo controlado no início na estação seca para manejo do material combustível em vegetação resistente ao fogo, resultando em mosaico

da vegetação para proteger as plantas sensíveis ao fogo, além disso, são sempre realizadas por especialistas do IBAMA e ICMBio (PIVELLO et al., 2021; SCHMIDT; ELOY, 2020).

Vários estudos indicam a efetividade dessas queimas controladas, como o de Durigan et al. (2020) que identificaram em Cerrado no sudeste do Brasil que estas queimas não afetaram a riqueza de vários vertebrados. Ainda no Cerrado, Berlinck e Lima (2021) obtiveram uma redução de 40% de incêndios em 2019 como resultado das ações do MIF. Em savana e manchas de pastagem estas queimas contribuem para proteger a floresta sensível ao fogo ao seu redor (BERLINCK; BATISTA, 2020).

Na Estação Ecológica Serra Geral do Tocantins, Parque Estadual do Jalapão e Parque Nacional da Chapada das Mesas um projeto piloto de MIF demonstrou de forma efetiva as várias técnicas para implementar a queima controlada em cada unidade de conservação, de maneira segura e eficiente (BEATTY, 2014). No Parque Nacional de Itatiaia desde 2017 foi implementado o MIF para gestão da paisagem, com a realização de queimas prescritas e aceiros negros com vistas a conservação de quatro alvos, sendo eles as formações florestais, a flora endêmica, o sapo-flamenguinho endêmico da Serra da Mantiqueira e os organossolos.

Apesar desses promissores resultados, o manejo da conservação usando as queimas prescritas ainda não é amplamente compreendido e aceito (OVERBECK; FERREIRA; PILLAR, 2016). Por este motivo, é importante a implementação de experimentos de avaliação e monitoramento para melhorar a compreensão entre o fogo, a vegetação e o homem, incluindo ecossistemas dependentes e sensíveis ao fogo e aperfeiçoar as estratégias do Manejo Integrado do Fogo (PIVELLO et al., 2021; BILBAO et al., 2019).

Assim, o monitoramento de incêndios e queimas prescritas no Brasil é realizado principalmente pelo Registro de Ocorrência de Incêndios (ROI) por meio de preenchimento de documento específico com as características do fogo (BONTEMPO et al., 2011). Além dessa estratégia, o fogo também é detectado/monitorado/avaliado por meio de sensoriamento remoto orbital. Como exemplo, o Instituto Brasileiro de Pesquisas Espaciais (INPE) fornece dados diários sobre focos ativos de calor por meio do processamento de dados de satélites.

Os dados de sensoriamento remoto orbital são uma valiosa ferramenta para avaliar a extensão e os impactos do fogo na vegetação, pois fornecem uma observação global e sistemática das condições do solo em diferentes resoluções espaciais, espectrais e temporais (LIZUNDIA-LOIOLA; PETTINARI; CHUVIECO, 2020). Nesse sentido, vários estudos científicos foram desenvolvidos usando satélites de resolução moderada, como produtos do *Moderate Resolution Imaging Spectroradiometer* (MODIS), para fornecer informações sobre o fogo em contexto global, como o de Humber et al. (2019); Andela et al. (2019); Earl;

Simmonds (2018); Laurent et al. (2018); Giglio et al. (2018); Nogueira et al. (2016); Hantson; Pueyo; Chuvievo (2015); Giglio et al. (2009); e na perspectiva regional (SANTANA et al., 2020; ROSSI; SANTOS, 2020; FUSCO et al., 2019; PANISSET et al., 2017; SÁ et al., 2017; VERAVERBEKE et al., 2014; MAEDA et al., 2011; FREEBORN; WOOSTER; ROBERTS, 2011).

Além disso, sensores com pixels de melhor resolução espacial, como a série Landsat (30 m) vêm sendo usados para determinar a extensão da área queimada, severidade do fogo e monitorar os efeitos pós-fogo (KONKATHI; SHETTY, 2021; CARDIL et al, 2019; SANTOS et al., 2018; QUINTANO; FERNÁNDEZ-MANSO; FERNÁNDEZ-MANSO, 2018; DALDEGAN et al., 2014; BASTARRIKA; CHUVIECO; MARTÍN, 2011; ESCUIN; NAVARRO; FERNÁNDEZ, 2008). E mais recentemente dados de Sentinel-2 (10m) estão sendo utilizados para a mesma finalidade (KONKATHI; SHETTY, 2021; BROVKINA et al., 2020; ROTETA et al., 2019; NEDKOV, 2018; QUINTANO; FERNÁNDEZ-MANSO; FERNÁNDEZ-MANSO, 2018; NAVARRO et al., 2017; MARTINIS et al., 2017; VERHEGGHEN et al., 2016).

Apesar da ampla utilização do sensoriamento orbital para análise de incêndios florestais algumas limitações podem ser detectadas, como o clima, principalmente a grande presença de nuvens nas imagens, que afeta negativamente a disponibilidade de dados (JANG et al., 2019; ALLISON et al., 2016). Além disso, como o tempo de revisita é alto, a exemplo dos satélites Landsat (16 dias) e Sentinel-2 (5 dias) inviabiliza a detecção em tempo real de incêndios (BARMPOUTIS et al., 2020; ALLISON et al., 2016) e a baixa resolução espacial de alguns satélites não possibilita a detecção de pequenos incêndios (ALLISON et al., 2016).

Nesse contexto, recentemente as aeronaves pilotadas remotamente surgiram como inovação ao sensoriamento remoto orbital apresentando um crescente interesse científico (LALIBERTE; RANGO, 2011) principalmente devido à vantagem de serem operadas a partir de locais remotos para obter informações de áreas de difícil acesso (HUNG; XU; SUKKARIEH, 2014), além da flexibilidade na programação dos voos e possibilidade de voo em baixas altitudes, permitindo a obtenção de imagens de altíssimas resoluções temporais e espaciais (por exemplo, pixels de alguns centímetros) (VON BUEREN et al., 2015; HUNG; XU; SUKKARIEH, 2014; TURNER; LUCIEER; WATSON, 2012; XIANG; TIAN, 2011).

Apesar dessas vantagens, pesquisas relacionadas a incêndios florestais ainda são baseadas normalmente em maneiras mais convencionais, particularmente por esses sistemas não permitem missões de detecção ou mapeamento de longo alcance e duração (ALLISON et al., 2016). Poucos estudos foram realizados nesta temática, uma busca feita na plataforma

Web of Science usando as palavras-chave: *uav and wildfire* (em inglês para maior abrangência) foi possível identificar 104 artigos, trocando a palavra *uav* para *uas* um total de 36 resultados foram encontrados e mudando de *uas* para *drone* 63 pesquisas foram documentadas. Realizando a busca na mesma sequência, porém trocando o termo *wildfire* por *forest fire*, encontramos um total de 247, 43 e 104 artigos, respectivamente.

Pode-se observar que ainda existe uma lacuna de conhecimento sobre o uso de VANTs na detecção, mapeamento e monitoramento pós-incêndios, sobretudo em áreas protegidas no Brasil, especialmente em campos de altitude, uma formação dominada por gramíneas restrita aos picos do sudeste do Brasil, de alta biodiversidade e presença de espécies endêmicas (SAFFORD, 1999) onde até o presente momento não foram encontrados resultados publicados na literatura.

Nesse contexto, esta tese foi pautada com a finalidade de obter mais informações sobre o uso de imagens RGB e multiespectrais coletadas com VANTs e imagens orbitais para a avaliação de incêndios florestais e queimas controladas em unidades de conservação e seus efeitos de curto prazo sobre a vegetação; comparar a severidade da queima e a permanência da mudança em incêndios florestais e queimas prescritas; além de testar o uso de sensoriamento remoto como ferramenta aplicável para tornar os dados de registro de ocorrência de incêndios (ROIs) mais robustos. A obtenção e aprimoramento destes dados servirão de subsidio aos gestores de unidades de conservação para um melhor planejamento de ações relacionadas ao manejo integrado do fogo.

A presente tese foi estruturada em duas partes, a primeira composta pela introdução geral e um breve referencial teórico e a segunda pelos artigos científicos oriundos das análises realizadas. Estes capítulos individuais fornecem uma extensa revisão de literatura sobre os assuntos abordados.

O primeiro artigo intitulado por Imagens RGB e multiespectral derivadas de veículos aéreos não tripulados para o mapeamento de campos de altitude e queima prescrita tem como objetivo analisar uma queima prescrita realizada na parte alta do Parque Nacional de Itatiaia com intuito de fragmentação da vegetação e também nesta mesma área realizar uma classificação supervisionada orientada a objeto de vegetação de campos de altitude obtida por meio de imagens RGB e multiespectrais coletadas com veículos aéreos não tripulados (VANTs), sendo eles o Phantom 4 Pro e Matrice 100.

O segundo capítulo cujo título é Efetividade do uso de dados de sensoriamento remoto para identificação de incêndios florestais em unidades de conservação brasileiras foi conduzido com o propósito de avaliar o uso de imagens de sensoriamento remoto de média

resolução espacial (Landsat-8 e Sentinel-2) para a identificação de áreas queimadas no Parque Nacional de Itatiaia e ser uma alternativa para o refinamento dos dados de Registro de Ocorrência de Incêndios (ROIs) que são coletados *in situ*. Além disso, foram gerados mapas de recorrência de incêndios entre 2013 e 2018 que é uma importante ferramenta para os gestores melhorarem as estratégias do MIF pela identificação de áreas mais vulneráveis ao fogo.

O terceiro capítulo intitulado Avaliação de curto prazo da recuperação da vegetação após incêndios florestais e queimadas prescritas em unidade de conservação na Mata Atlântica foi proposto com o intuito de analisar a severidade do fogo e o tempo de permanência da mudança (cicatriz deixada pelo fogo na paisagem) em incêndios florestais e queimas prescritas no Parque Nacional de Itatiaia usando imagens de sensoriamento remoto orbital de média resolução espacial, Sentinel-2 (10m) e computação na nuvem da plataforma do *Google Earth Engine* (GEE).

2. REFERENCIAL TEÓRICO

2.1. Unidades de Conservação no Brasil (UCs)

O Brasil abriga cerca de 10% de todas as espécies vegetais no mundo, caracterizando-o assim como região peculiar e diversificada fisionomicamente, resultando em uma elevada diversidade nos vários biomas presentes no país (MYERS et al., 2000).

O Cerrado ocupa cerca de 20% de toda a área do Brasil, sendo caracterizado por um mosaico de formações vegetais distribuídas heterogeneamente (pastagem, savana e floresta) (RIBEIRO; WALTER, 2008). Apresenta alta biodiversidade tropical (BONANOMI et al., 2019) e é considerado um *hotspots* da biodiversidade mundial (CEPF, 2016). Entretanto, nos últimos 55 anos perdeu mais da metade da sua área original (LAPOLA et al., 2014).

A Amazônia é outro bioma que também abriga importantes centros de diversidade biológica e cultural que devem ser protegidos (FINER et al., 2015). A Amazônia Legal Brasileira é uma região de 521.742.300 hectares sendo que aproximadamente 30% da mesma estão sob alguma forma de proteção, dentro de uma das 532 áreas protegidas (PFAFF et al., 2015).

Já, a Mata Atlântica é uma das maiores florestas tropicais das Américas, cobrindo originalmente cerca de 150 milhões de hectares. Embora já tenha perdido em torno 88% de sua extensão original de 1.350.000 km² (LOPES et al., 2018), ela ainda mantém 8.000 espécies endêmicas de plantas vasculares, anfíbios, répteis, aves e mamíferos, sendo que as plantas endêmicas e vertebrados perfazem pelo menos 2% do total de espécies a nível mundial. Em decorrência destas características, ela é classificada como um dos 36 centros mundiais de diversidade (CEPF, 2016).

Essa vasta biodiversidade brasileira vem sendo protegida legalmente por meio das unidades de conservação (UCs). Um terço da extensão do Brasil é ocupado por áreas protegidas, que são manejadas e regulamentadas pelo governo federal, estadual e municipal, formando 3 categorias de proteção, sendo elas: proteção integral, que permitem apenas o uso indireto de recursos naturais; de uso sustentável, que visam conciliar conservação com o manejo dos recursos e áreas indígenas (OLIVEIRA et al., 2017).

Estas áreas protegidas constituem uma estratégia essencial para a conservação da biodiversidade, reduzindo as taxas de perdas de habitat e mantendo sua integridade (D'AMICO et al., 2020; GRAY et al., 2016; BUTCHART et al., 2012; MARGULES; PRESSEY; WILLIAMS, 2002). Além disso, são importantes, pois foram delineadas com o intuito de proteger porções significativas de diferentes tipos de vegetação natural e auxiliar na

manutenção da vida na Terra enquanto geram vários benefícios a humanidade (FIGUEROA; SÁNCHEZ-CORDERO, 2008).

Apesar da grande essencialidade destas áreas apenas uma pequena proporção do território nacional é ocupada por elas. Além disso, muitas vêm sofrendo com os incêndios florestais frequentes, devido a mudanças nos regimes de fogo causados por atividades humanas, aumento da temperatura e mudança nos padrões de precipitação (HALOFSKY; PETERSON; HARVEY, 2020; BOWMAN et al., 2020).

Ainda que o Código Florestal Brasileiro (Lei 12.651/2012) inicialmente proíba o uso do fogo, este admite exceções, como o Art. 38, que permite o emprego da queima controlada em Unidades de Conservação, em conformidade com o respectivo plano de manejo e mediante prévia aprovação do órgão gestor da UC, visando ao manejo conservacionista da vegetação nativa, cujas características ecológicas estejam associadas evolutivamente à ocorrência do fogo.

Sendo este um grande avanço desde políticas de exclusão do fogo, ou de "fogo zero" que predominaram no Brasil no século XX (SAMPAIO et al., 2016). Pois, como foi verificado, o resultado global desta exclusão do fogo, são as incidências de incêndios cada vez mais danosos à vegetação, ao solo e às bacias hidrográficas, que geram um custo econômico cada vez maior com o combate a esses incêndios (MYERS, 2006).

Devido à problemática do fogo em áreas protegidas, em 2010 foi desenvolvido o Manejo Integrado do Fogo (MIF), mudando o padrão de "fogo zero" para o fogo a favor da conservação da biodiversidade (BERLINCK; LIMA, 2021; SCHMIDT; ELOY, 2020). O MIF é uma estratégia que permite a integração das práticas culturais de manejo do fogo da população local (ELOY et al., 2019; FIDELIS et al., 2018) e tem por objetivo diminuir o risco de ocorrência de incêndios florestais, normalmente realizado por meio das queimas prescritas (PIVELLO et al., 2021).

As queimas prescritas visam à aplicação de fogo controlado no início na estação seca para manejo do material combustível em vegetação resistente ao fogo, resultando em mosaico da vegetação para proteger as plantas sensíveis ao fogo, além disso, são sempre realizadas por especialistas do IBAMA e ICMBio (PIVELLO et al., 2021; SCHMIDT; ELOY, 2020).

Alguns programas de queimas prescritas vêm sendo implementados no Brasil, como o programa para realizar acordos comunitários e emitir autorizações para queimada controlada nas comunidades rurais do entorno do Mosaico de Carajás, iniciado pelo Instituto Brasileiro do Meio Ambiente e dos Recursos Naturais Renováveis (Ibama), com a finalidade de

diminuição do risco de incêndios florestais e a proteção da biodiversidade. Neste programa foi obtido sucesso na prevenção de incêndios florestais (MARTINS et al., 2016).

O Projeto de Cooperação Brasil-Alemanha "Prevenção, Controle e Monitoramento de Incêndios Florestais no Cerrado" vem sendo realizado com o intuito de reduzir os gases de efeito estufa e proteger a biodiversidade de três Unidades de Conservação: Estação Ecológica Serra Geral do Tocantins, Parque Estadual do Jalapão e Parque Nacional da Chapada das Mesas. Este projeto piloto de Manejo Integrado do Fogo demonstrou de forma efetiva as várias técnicas para implementar a queima controlada em cada UC, de maneira segura e eficiente (BEATTY, 2014).

Outras pesquisas indicam a efetividade dessas queimas controladas, como o de Durigan et al. (2020) que identificaram em Cerrado no sudeste do Brasil que estas queimas não afetaram a riqueza de vários vertebrados. Ainda no Cerrado, Berlinck e Lima (2021) obtiveram uma redução de 40% de incêndios em 2019 como resultado das ações do MIF. Em savana e manchas de pastagem estas queimas contribuem para proteger a floresta sensível ao fogo ao seu redor (BERLINCK; BATISTA, 2020).

No Parque Nacional de Itatiaia desde 2017 foi implementado o MIF para gestão da paisagem, com a realização de queimas prescritas e aceiros negros com vistas a conservação de quatro alvos, sendo eles as formações florestais, a flora endêmica, o sapo-flamenguinho endêmico da Serra da Mantiqueira e os organossolos.

2.2. Incêndios Florestais

Os incêndios florestais são amplamente reconhecidos como um dos distúrbios ambientais mais críticos que afetam a degradação florestal, influenciam na ciclagem de carbono, podem mudar a composição das espécies (GATTI et al., 2014; MEWS et al., 2013; LÍBANO; FELFILI, 2006), afetam a química atmosférica, com emissão de aerossóis e gases de efeito estufa (KNORR; JIANG; ARNETH, 2016); reduzem a circulação atmosférica de água e formação de nuvens por evapotranspiração (STAAL et al., 2020; MARENGO et al., 2018); diminuem a biodiversidade e a retenção de água, causam degradação e erosão do solo por meio de uma série de modificações em sua natureza física, química e biológica (SANSEVERO et al., 2017; REDIN et al., 2011; CHUVIECO et al., 2010).

Por outro lado, o fogo é uma parte natural de muitos ecossistemas, ajudando a promover a diversidade, manter a integridade, composição de espécies e contribuir para a regeneração natural (KELLY; BROTONS, 2017; ODION et al., 2014) e sua supressão pode

causar um redução na quantidade de espécies vegetais (BOND; KEELEY, 2005) e aumento de grandes incêndios devido ao acumulo de biomassa.

A ocorrência de incêndios aumentou substancialmente nos últimos anos em todo mundo (BARBERO et al., 2020; SUN et al., 2019). Um exemplo são os grandes incêndios florestais ocorridos recentemente, como os da Austrália em 2019-2020; no Brasil, especialmente na floresta amazônica em 2019 e 2020; no oeste dos Estados Unidos em 2018 e 2020; em British Columbia no Canadá, em 2017 e 2018 (XU et al., 2020).

O Brasil segue esta tendência global, apresentando aumento do número de focos de incêndio e da extensão das áreas queimadas, com mais de 312.140 km^2 do país queimado em 2020 (INPE, 2020). A maior concentração de focos de calor ocorreu na Amazônia, Cerrado e no Pantanal, este último bioma apresentou 13% dos incêndios em nível nacional, um fato sem precedentes desde o início do registro de dados em 1998 (PIVELLO et al., 2021), chocando todo o país (MARENGO et al., 2021):

Os padrões globais de atividade do fogo são controlados pelo clima, impulsionando a produtividade da vegetação e o acúmulo de combustível, bem como influencia na sua umidade por meio do aumento da demanda por evaporação e da diminuição da precipitação (BARBERO et al., 2020; BOWMAN et al., 2009). Assim, à medida que as mudanças climáticas pioram aumenta o risco de ocorrer incêndios florestais, pois a temporada de incêndios está começando cada vez mais cedo e terminando mais tarde (SUN et al., 2019; JOLLY et al., 2015). Projeções indicam que no final do século 21 a duração da temporada de incêndios e a frequência destes irão aumentar significativamente (SUN et al., 2019).

Além do clima mais seco e das mudanças no uso da terra por meio do desmatamento e fogo para limpeza de pasto que ampliam o risco de ocorrer incêndios florestais em todo país (PIVELLO et al., 2021), esta problemática é intensificada pela fraca governança florestal e resultado das políticas do presidente Jair Bolsonaro (LIZUNDIA-LOIOLA; PETTINARI; CHUVIECO, 2020; ESCOBAR, 2019).

Em geral, quando ocorre um evento de incêndio a maioria dos ecossistemas são modificados, com queima de parte ou total da vegetação, resultando em perturbação da atividade biológica, gerando custos ambientais, econômicos e sociais (VIANA-SOTO; AGUADO; MARTÍNEZ, 2017; BASTOS et al ., 2011). Assim, esse evento depende de uma variedade de fatores biológicos e ambientais e da interação entre eles, como intensidade, duração, extensão e período do ano em que ocorrem os incêndios (SHIMABUKURO et al., 2020; BASTOS et al., 2011). Devido a isso, é complexo mapear e modelar padrões pós-incêndio porque esses fatores afetam a resiliência da vegetação. No entanto, constituem uma

questão fundamental na ecologia florestal espacial que está relacionada ao fogo (TEODORO; AMARAL, 2019).

2.3. Parque Nacional de Itatiaia

O Parque Nacional de Itatiaia (PNI) foi o primeiro parque criado no Brasil, por meio do Decreto n. 1.713, de 14 de junho de 1937, assinado pelo presidente Getúlio Vargas. Seu nome é originário da língua Puri que significa "pedra cheia de picos" (ICMBIO, 2014b). Está localizado a sudoeste do Estado do Rio de Janeiro, abrangendo os municípios de Resende e Itatiaia e ao sul de Minas Gerais nos municípios de Bocaina de Minas e Itamonte, região do Maciço do Itatiaia, na Serra da Mantiqueira (ICMBIO, 2014b).

A área original do parque era de 11.943 hectares, porém, em 20 de setembro de 1982 pelo Decreto no 87.586, teve sua área ampliada para aproximadamente 30.000 ha (ICMBIO, 2014a). Sua área de atuação administrativa estende–se por uma faixa de 3 km de largura dos seus limites, de forma a abranger as principais áreas de mata contígua e atuar sobre aqueles impactos ambientais que mais diretamente influenciam a unidade (ICMBIO, 2014c).

Apresenta relevo montanhoso com afloramentos rochosos e variação de altitude de cerca de 540 m no extremo sul do PNI a 2.791,55 m em seu ponto culminante, o Pico das Agulhas Negras. Há quatro tipos de classe de solos no interior do Parque com abundância de solos rasos e jovens, sendo: Cambissolos, a classe predominante, ocorrendo nas encostas das Montanhas; áreas de maiores altitudes e/ou com maiores declividades ocorrem os Neossolos Litólicos, entre afloramentos rochosos; o Argissolo vermelho-amarelo distrófico em pequena fração, na parte sul e o Latossolo encontrado próximo à comunidade Vargem Grande (ICMBIO, 2014b).

O clima segundo a classificação de Koppen é o mesotérmico com verão brando sem estação seca (Cpb) ocorrendo nas partes baixas das encostas e o mesotérmico, para as áreas acima de 1600 m de altitude, com verão brando que constitui a estação chuvosa (Cwb), no qual a precipitação média anual varia de 1250 mm a 2500 mm. Segundo o Plano de manejo a temperatura média para o Planalto varia de 8,4 ℃ no inverno a 13,6 ℃ nos meses mais quentes, sendo comum a ocorrência de temperaturas negativas no inverno e, a umidade relativa do ar de aproximadamente 83% em dezembro e 62% em junho (ICMBIO, 2014b).

O parque encontra-se inserido na Mata Atlântica, possuindo diversas fitofisionomias, como Floresta Ombrófila Densa Montana, Floresta Ombrófila Densa Altomontana, Floresta Estacional Semidecidual Montana, Floresta Ombrófila Mista Altomontana e Campos de altitude (VELOSO; RANGEL FILHO; LIMA, 1991; ICMBIO, 2014b), sendo que este último

é encontrado em altitudes acima 2300 m, onde predomina matriz campestre graminóide, conhecida como páramo brasileiro (SAFFORD, 2001).

As ocorrências de incêndios florestais no PNI são catalogadas por meio do Registro de Ocorrência de Incêndios (ROIs) que é o conjunto de dados oficial de incêndios ocorridos em áreas protegidas no Brasil, disponível no Centro Nacional de Prevenção e Combate a Incêndios Florestais (PREVFOGO), associado ao Instituto Brasileiro do Meio Ambiente e dos Recursos Naturais Renováveis (IBAMA), foi criado na década de 1990 objetivando sistematizar as ocorrências e reunir informações para o desenvolvimento de estratégias de prevenção e minimização da ocorrência de incêndios florestais em áreas protegidas (BONTEMPO et al., 2011). Em 2007 foi criado o Instituto Chico Mendes (ICMBio), que passou a ser responsável pela formação de um banco de dados do Sistema Nacional de Informações sobre Incêndios (SISFOGO) e, desde então, apenas algumas unidades de conservação continuam utilizando os ROIs, como é o caso do PNI.

No Parque Nacional de Itatiaia os dados de ROIs são coletados no local da ocorrência pelos brigadistas desde 2008 utilizando o *Global Navigation Satellite System* (GNSS) e digitalizados em polígonos (referente à queima) em ambiente de SIG. Estes dados são constituídos de *shapefiles* anuais contendo informações sobre incêndios florestais, como a geolocalização da ocorrência e a quantificação da área queimada.

A presença do fogo no Parque Nacional de Itatiaia vem sendo documentada a um bom tempo (BRADE, 1956; RIBEIRO; MEDINA, 2002; AXIMOFF; RODRIGUES, 2011) e suas ocorrências estão relacionadas principalmente por ação antrópica. Pesquisas de Aximoff; Rodrigues (2011) e Tomzhinski; Ribeiro; Fernandes (2012) reuniram informações de registros de incêndios desde 1937, sendo que a partir 2008 se iniciou o mapeamento das áreas atingidas por meio de GPS.

Por meio destas análises, obtiveram que a área queimada de 2001 a 2008 dentro e no entorno do Parque foi de 5.724 ha (FIGURA 1), e que maioria dos incêndios ocorreu em área de pastagens (49%), contudo a maior extensão atingida foi nos campos de altitude (49,6%), atingindo uma área de 2.937,3 ha (AXIMOFF; RODRIGUES, 2011).

Figura 1 - Áreas atingidas por incêndios no período de 2001 a 2008 no interior do PNI (barras pretas) e em seu entorno (barras brancas).
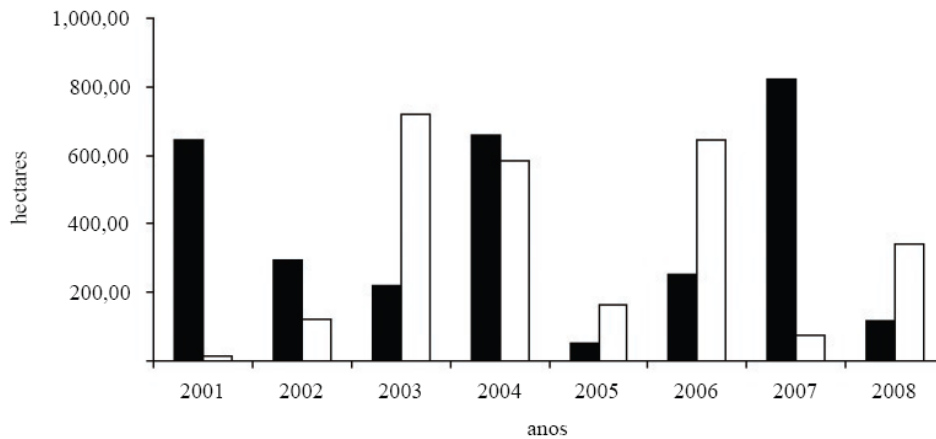
Fonte: adaptado de Aximoff; Rodrigues (2011).

Tomzhinski; Ribeiro; Fernandes (2012) analisaram 332 registros de incêndios florestais, entretanto nem todos os registros incluíam informações sobre a área atingida, além disso, nos anos anteriores a 2008 essa medida era visualmente estimada. Assim, na Figura 2 estão apresentadas as áreas afetadas pelos incêndios de 1937 a 2011 obtidas por Tomzhinski; Ribeiro; Fernandes (2012). Estes autores encontraram que o mês com maior número de ocorrências foi agosto (35%) e maior área queimada em setembro (57%). Além disso, 78% incêndios foram localizados acima de 2.000 m de altitude.

Figura 2 - Distribuição anual das áreas queimadas por meio de registros de incêndios de 1937 a 2011, no PNI e entorno de 3km.
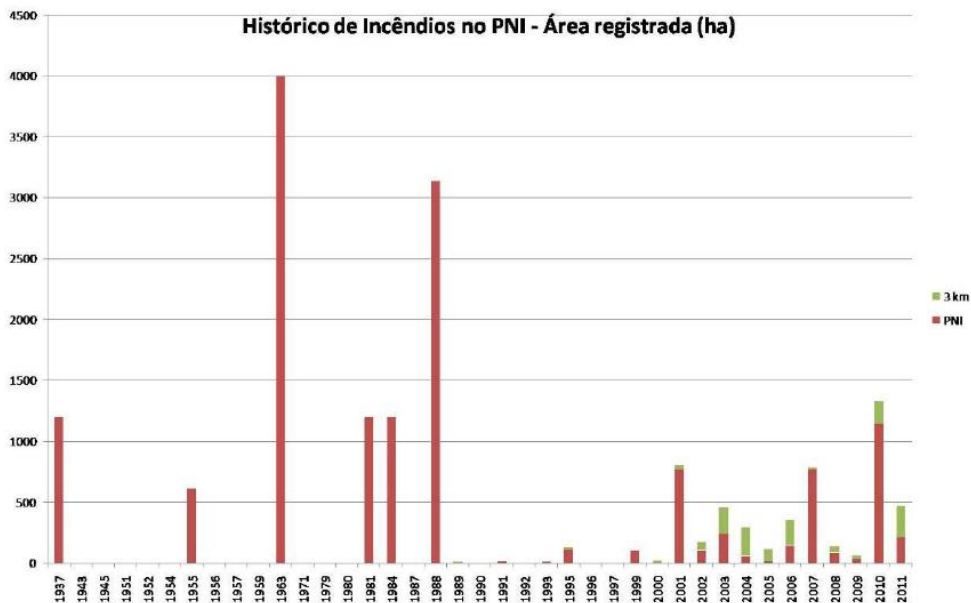
Fonte: adaptado de Tomzhinski; Ribeiro; Fernandes (2012).

Além desses estudos, mais recentemente Belchior et al. (2020) constataram que entre 2008 e 2016 um total de 3.435,64 hectares foram queimados no PNI, com maior recorrência de fogo em campos antrópicos e pastagens relacionadas ao uso de gado.

Alguns estudos sobre os efeitos do fogo na vegetação de campos de altitude do PNI foram realizados, como o de biogeografia das ilhas de vegetação sobre rocha do Planalto, no qual foi encontrado que ocorrência de incêndios está associada com o desaparecimento de determinadas espécies da flora, como a *Doryopteris feei* (endêmicas do Planalto), além da substituição da flora por algumas gramíneas e/ou espécies mais resistentes ao fogo (RIBEIRO; MEDINA, 2002).

Aximoff (2011) avaliou a presença do fogo nos campos de altitude do Parque Nacional de Itatiaia e as espécies ameaçadas de extinção presentes neste ecossistema, e encontrou que mais de 70% dos incêndios atingiram essa formação vegetacional e que o impacto causado pelo fogo está reduzindo as populações de algumas espécies ameaçadas e não tolerantes a ele.

Pesquisa sobre regeneração natural pós-fogo nos campos de altitude aponta que regeneração da vegetação ocorreu relativamente rápido, sendo que sítios entre quatro e sete anos apresentaram estrutura, composição e riqueza similares ao sítio com 25 anos de regeneração. Entretanto, não foram registradas algumas das espécies endêmicas e ameaçadas de extinção pós-fogo (AXIMOFF; NUNES-FREITAS; BRAGA, 2016).

Nesse contexto, as queimas prescritas são uma alternativa para a minimização dos incêndios florestais de grandes proporções que vem acarretando perda da biodiversidade dos campos de altitude. Estas queimas de baixa intensidade envolvem a aplicação deliberada de fogo aos combustíveis florestais sob condições específicas, a fim de atingir metas de manejo bem definidas (FERNANDES; BOTELHO, 2003). Essas metas incluem reduzir a carga de combustível superficial em áreas sujeitas a longos períodos de estiagem (FERNÁNDEZ; VEJA; FONTURBEL, 2013) e, consequentemente redução do risco de incêndios florestais e proteção da biodiversidade (LEIGH; NOBLE, 1981).

2.4. Sensoriamento Remoto no Mapeamento e Monitoramento da Vegetação

O sensoriamento remoto é uma ferramenta que utiliza dados de vários tipos de sensores para medir a quantidade de energia eletromagnética refletida e emitida por objetos ou área geográfica à distância (JENSEN, 2015; SCHOWENGERDT, 2006).

Uma das principais aplicações de dados de sensoriamento remoto é no mapeamento e monitoramento, visando compreender a dinâmica da superfície da Terra (RODRIGUEZ-

GALIANO et al., 2012) além de monitorar as mudanças em seu uso e cobertura (PANDE-CHHETRI et al., 2017).

O mapeamento por meio do sensoriamento remoto apresenta vantagens em relação às técnicas de mapeamento baseadas exclusivamente em pesquisas de campo, como a cobertura de grandes áreas geográficas, aquisição periódica de dados e possibilidade de registro de informações espectrais em diferentes regiões do espectro eletromagnético (LUMBIERRES et al., 2017). O sensoriamento remoto pode complementar as técnicas de estudo de campo a partir da coleta de informações em diversas escalas temporais, espectrais e espaciais, tornando o monitoramento da paisagem mais eficiente (GÓMEZ et al., 2012).

Nesse contexto, muitos estudos foram desenvolvidos utilizando satélites de resolução moderada, devido à vantagem de imagearem largas áreas com alto período de revisita. Por exemplo, o espectrorradiômetro de imagem de resolução moderada (MODIS) que fornece observações globais diárias em resolução espacial de 250m a 1km. Embora as imagens de sensores de resolução grosseira, como o MODIS, sejam normalmente superiores aos dados de resolução mais fina em termos de sua frequência de revisita, eles carecem de detalhes espaciais para capturar características de superfície para muitas aplicações, como para detectar e estimar pequenas mudanças na vegetação, tornando necessária a utilização de resoluções espaciais e temporais mais altas.

Este fato se tornou possível a partir da disponibilidade gratuita de dados dos satélites Landsat e Sentinel, iniciando uma nova era para o monitoramento dos recursos terrestres (ROY et al., 2014; DRUSCH et al., 2012).

A série de satélites Landsat é uma das de maior sucesso da história fornecendo dados por mais de 40 anos. Os sensores a bordo das primeiras missões Landsat foram *Multispectral Scanner* (MSS), e posteriormente atualizados para *Thematic Mapper* (TM) no Landsat-4 (lançado em 1982), Landsat-5 (lançado em 1984) e *Enhanced Thematic Mapper Plus* (ETM +) no Landsat -7 (lançado em 1999) e o mais recente, Landsat-8 (CHEN et al., 2019). Suas imagens tem resolução espacial de 30 m a 60 m com uma missão de revisita de 16 dias (WULDER et al., 2019), essa frequência temporal é considerada baixa, comparada com imagens de resolução mais grosseira, que são quase diárias.

Esta questão pode ser contornada com aprimoramento da resolução espacial e temporal do satélite Sentinel-2 (AMOS; PETROPOULOS; FERENTINOS, 2019). O Sentinel-2 faz parte da missão de observação da Terra do Programa Copernicus (DRUSCH et al., 2012). Possui bandas do visível e do infravermelho próximo (NIR) com resolução espacial

de 10 m, as bandas do infravermelho têm resolução espacial de 20 m e as demais bandas têm 60 m (RAIYANI et al., 2021).

Quando comparado a outros satélites de média resolução espacial, como o Landsat, oferece dados aprimorados, especialmente na resolução temporal e espacial (NOVELLI et al., 2016). Suas características valiosas são: a alta resolução temporal de cinco dias, imagens multiespectrais e dados de acesso livre (AMOS; PETROPOULOS; FERENTINOS, 2019).

Como resultado, a utilização destes satélites possibilita que as informações sejam obtidas rapidamente e em grandes escalas espaciais, proporcionando aquisições mais frequentes e possibilitando o monitoramento detalhado necessário, como exemplo, para revelar a severidade e a dinâmica pós-incêndio de curto prazo em ecossistemas que se recuperam rapidamente, como savanas tropicais e pastagens (PÉREZ-CABELLO; MONTORIO; ALVES, 2021).

Contudo, as tecnologias convencionais do sensoriamento remoto, como os satélites, apresentam desvantagens, como o acesso restrito, elevado custo de obtenção de imagens, operação e limitações de seus produtos, baixa resolução temporal, contaminação das imagens por nuvens (PANEQUE-GÁLVEZ et al., 2014; WHITEHEAD; HUGENHOLTZ, 2014).

Nesse sentido, uma tecnologia que vem ganhando destaque são os Veículos aéreos não tripulados (VANTs). Sendo que o monitoramento com a utilização de imagens obtidas por esses veículos, combinam as vantagens do tradicional mapeamento de sensoriamento remoto e o nível de detalhamento alcançado pelo trabalho de campo, preenchendo a lacuna de escala entre as observações baseadas em campo e observações aéreas ou por satélite em larga escala (LUCIEER et al., 2014).

2.4.1. Veículos aéreos não tripulados (VANTs)

O desenvolvimento e a disseminação de tecnologias militares trouxeram inovações para o sensoriamento remoto. Uma dessas tecnologias são os Veículos Aéreos Não Tripulados (VANTs), também denominados de Aeronave Pilotada Remotamente (APR), Sistema de Aeronave Não Tripulado (SANT) ou Drones (WATTS; AMBROSIA; HINKLEY, 2012). Os VANTs são aeronaves que não possuem piloto a bordo, podendo ser pilotadas remotamente ou autônomas (ICAO, 2011).

Os VANTs consistem em componentes da aeronave, sensor e uma estação de controle no solo, esta última operada por uma ou mais pessoas. Sendo estes, classificados em asa fixa ou rotativa. As rotativas são mais autônomas, possuem decolagem e pouso vertical, geralmente são menores e de menor peso em relação às asas fixas (SANTOS et al., 2019). Por

outro lado, as asas fixas são utilizadas em coletas em grandes distâncias, atingem maiores velocidades que as rotativas, embora sejam mais pesadas, maiores e com custos mais elevados (ROMEO et al., 2015).

Há um crescente interesse em usar dados de VANT em aplicações no sensoriamento remoto de recursos naturais (LALIBERTE; RANGO, 2011). Esse interesse surge devido a uma série de vantagens que os VANTs possuem sobre outras plataformas de sensoriamento remoto. Em primeiro lugar, eles requerem uma infraestrutura mínima e podem, assim, ser operados a partir de locais remotos para obter informações de locais de difícil acesso (HUNG; XU; SUKKARIEH, 2014).

Outras vantagens são relacionadas a menores custos de aquisição de imagem (RANGO et al., 2006; TORRES-SÁNCHEZ et al., 2014; GAO et al., 2018), flexibilidade da programação dos voos e possibilidade de voo em baixas altitudes, permitindo a obtenção de imagens de altas resoluções temporais e espaciais (por exemplo, pixels de alguns centímetros) (XIANG; TIAN, 2011; TURNER; LUCIEER; WATSON, 2012; HUNG; XU; SUKKARIEH, 2014; VON BUEREN et al., 2015).

Devido isso, os VANTs contribuem para o mapeamento e monitoramento de ecossistemas naturais, zonas agrícolas entre outros ambientes em um nível de detalhes dificilmente obtidos em outros métodos (GETZIN et al., 2011).

Ao passo que essa tecnologia de obtenção de dados fornece benefícios, novos obstáculos são encontrados, como a dificuldade de imageamento de grandes áreas, pois as baterias possuem uma duração limitada, resultando em baixa autonomia de voo (ROMEO et al., 2015). Demanda um vasto tempo no processamento das imagens para obtenção dos produtos e muitas vezes possui uma baixa resolução espectral (SANTOS et al., 2019).

Algumas câmeras usadas nos VANTs contêm apenas três bandas visíveis (RGB) gerando uma resolução espectral limitada. Assim, pela falta de bandas de infravermelho, geralmente as bandas do visível não são suficientes para identificar e classificar a vegetação (LIU, 2018). No entanto, estudos encontraram soluções para classificação de vegetação com apenas as bandas RGB (TORRES-SÁNCHEZ; LÓPEZ-GRANADOS; PEÑA, 2015; LALIBERTE; RANGO, 2009; LALIBERTE et al., 2010).

2.5. Análise de imagem baseada em objetos geográficos

A partir dos anos 2000 tem-se usado com maior frequência a Análise de Imagem Baseada em Objetos Geográficos (*Geographic Object-based Image Analysis*-GEOBIA) para extrair e analisar objetos geográficos a partir de imagens de alta resolução espacial

(BLASCHKE et al., 2014). Em contraste com os métodos por pixel, a GEOBIA utiliza objetos de imagem gerados por segmentação para reproduzir a percepção humana dos objetos reais no solo (HAY; CASTILLA, 2008).

Na classificação de imagens podem ser empregados dois diferentes métodos: pixel a pixel e por objetos. Ambos os métodos funcionam na classificação de unidades para classes através de múltiplos algoritmos (DURO; FRANKLIN; DUBÉ, 2012). Na classificação pixel a pixel, há o emprego da informação espectral de cada pixel sem considerar outros atributos (YAN et al., 2006). Já, a classificação por regiões ou objetos avalia os segmentos, ou seja, pixels agrupados em compartimentos homogêneos da cena. O segmento pode ser entendido como uma região discreta em uma imagem que é internamente coerente e diferente do seu entorno (CASTILLA; HAY, 2008), sendo que para esta segmentação pode ser usado uma gama de informações adicionais, como atributos espaciais, espectrais e de textura (BLASCHKE, 2010; CÁNOVAS-GARCÍA; ALONSO-SARRÍA, 2015).

Apesar do uso mais recentemente de GEOBIA, a classificação de imagens por este método vem apresentando boa precisão em muitos estudos (LALIBERTE; RANGO, 2009; KIM et al., 2011; PANDE-CHHETRI et al., 2017 LIU; ABD-ELRAHMAN, 2018). Dean e Smith (2003) comparando classificação orientada a objeto com baseada em pixel para diferentes satélites e sensores, concluíram que a baseada em objeto foi superior quando é aumentada a resolução espacial da imagem. Já, Blaschke (2009) obteve que a utilização de análise orientada a objeto na classificação de imagens apresenta avanços tanto na classificação de fisionomias de vegetação quanto na extração de informações quantitativas sobre a vegetação.

Essa melhor precisão é obtida pela extração de várias características do objeto, como textura, forma, relações topológicas, relação hierárquica entre os níveis de segmentação, aproximando-se assim dos processos cognitivos humanos (CAMARGO et al., 2009; TARABALKA; BENEDIKTSSON; CHANUSSOT, 2009; MYINT et al., 2011; CHEN et al., 2011).

Na classificação de imagens orientada a objetos há duas etapas principais, a primeira é a segmentação da imagem, que visa dividir uma imagem em regiões espacialmente contínuas e homogêneas (PEKKARINEN, 2002; DESCLÉE et al., 2006) e a segunda etapa está relacionada com classificação dessas regiões.

A segmentação é um ponto chave da GEOBIA relacionada à qualidade da classificação final (BAATZ; HOFFMANN; WILLHAUC, 2008). Esta etapa pode ser explicada como: supondo que R represente toda a região espacial ocupada por uma imagem,

então a segmentação particiona R em n sub-regiões (R1, R2...Rn), assim, cada pixel se enquadra dentro de uma região, conforme sua similaridade com o pixel vizinho (GONZALES; WOODS, 2010).

Entre os métodos de segmentação, para as análises baseadas em objetos, o mais utilizado é o algoritmo de segmentação multiresolução (*Multiresolution Segmentation*), baseado no crescimento das regiões (BAATZ; SCHAPE, 2000). O primeiro passo na aplicação deste algoritmo é considerar cada pixel na imagem como um objeto, e iterativamente, pares de objetos são unidos em objetos maiores (BLASCHKE, 2010), com intuito de minimizar a heterogeneidade interna de cada objeto.

Em cada iteração, os objetos são mesclados se o objeto recém-gerado não exceder um limite de heterogeneidade definido pelas seguintes configurações de algoritmo: escala, forma e compacidade (TORRES-SÁNCHEZ; LÓPEZ-GRANADOS; PEÑA, 2015). Sendo um verdadeiro desafio definir parâmetros de segmentação apropriados para cada particularidade (HAY et al., 2005).

O parâmetro da forma considera a junção de dois parâmetros, compacidade e suavidade. Compacidade é definida como a razão da área da região com o raio da circunferência circunscrita. A suavidade refere-se aos limites existentes entre as regiões, sendo que, quanto mais limites existentes, maior é o índice da forma (BLASCHKE, 2010). Assim, um alto valor de compacidade produz segmentos menores e mais compactos, por outro lado, um alto valor de suavidade gera segmentos com bordas suaves, características de alvos naturais (BAATZ; SHAPE, 2000; KRESSLER; STEINNOCHER, 2006).

O parâmetro de escala influencia o número máximo de pixels heterogêneos presentes em um objeto, limitando a amplitude de variação no tamanho e no número dos objetos gerados (COUTO JUNIOR, 2011) assim, o valor de escala controla o tamanho final dos segmentos, quanto maior o valor para esse parâmetro, mais liberdade é dada ao crescimento da região (LALIBERTE; RANGO, 2009).

Em alguns casos, os objetos resultantes da segmentação multiresolução não correspondem a elementos na paisagem e são chamados de objetos primitivos (BENZ et al., 2004). Assim, em alguns casos, há a necessidade de utilizar outros algoritmos de fusão para mesclarem esses objetos em um conjunto de objetos maiores, que estão mais relacionados a elementos da paisagem (BENZ et al., 2004; YAN et al., 2006).

Nesse sentido, a segmentação pelo algoritmo de diferenças espectrais (*Spectral Difference*) pode ser utilizada para reduzir o número de objetos e assim melhorar a correspondência espacial entre objetos primitivos e elementos da paisagem. Este algoritmo

mescla dois objetos se a diferença entre o valor médio de suas características for menor que um limite chamado de diferença espectral máxima (CÁNOVAS-GARCÍA; ALONSO-SARRÍA, 2015).

Em estudos de Esch et al. (2008) e Zabala; Cea; Pons (2012), os melhores resultados de segmentação foram obtidos aplicando uma combinação de segmentação pelos algoritmos multiresolução e diferença espectral.

Depois de realizada a segmentação, procede-se a segunda etapa da GEOBIA, a classificação dessas regiões criadas. Devido ao volume de dados gerados na análise de imagem baseada em objetos, algoritmos de mineração de dados são utilizados com intuito de diminuir a dimensionalidade do conjunto de dados (LALIBERTE; FREDRICKSON; RANGO, 2007). Estes métodos são considerados não paramétricos, pois eles não necessitam que os dados sigam alguma distribuição em particular (RUIZ, 2015). Entre os métodos mais utilizados de mineração de dados está o *Random Forest* (RF) (BREIMAN, 2001).

A mineração dos dados por meio do por meio do RF ocorre realizando avaliações da importância da variável dos recursos prontos para uso, essa medida é um indicativo da importância de cada variável utilizada no classificador. Este algoritmo tenta identificar os recursos mais explicativos no espaço de recursos que são essenciais para melhorar o desempenho da classificação (WANG et al., 2013).

Portanto, a última etapa da GEOBIA é a classificação dos objetos nas suas devidas classes correspondentes a qual é realizada utilizando algoritmos de aprendizado de máquina, que têm sido cada vez mais usados para classificar grandes quantidades de dados complexos (GAŠPAROVIĆ et al., 2020), como os obtidos por SR. Entre esses algoritmos grande destaque na literatura é encontrado pelo *Random Forest* e Redes Neurais Artificiais.

RF é um algoritmo bastante utilizado em sensoriamento remoto, vários estudos demonstram bons resultados de classificação de imagem (GAŠPAROVIĆ et al., 2020; GAO et al., 2018; DE CASTRO et al., 2018; RODRIGUEZ-GALIANO; CHICA-RIVAS 2012; RODRIGUEZ-GALIANO et al., 2012; ZHANG; XIE 2013). Este fato pode estar associado a ele possuir adequada capacidade de lidar com conjuntos de dados de alta dimensão, mesmo com um pequeno número de amostras de treinamento, tornando-o adequado para processamento de dados de alta resolução espacial (STEFANSKI; MACK; WASKE, 2013; GONÇALVES et al., 2016).

RF, introduzido incialmente por Breiman (2001) é uma poderosa técnica de aprendizado de máquina para classificação, regressão e outras tarefas. Este algoritmo gera várias árvores de decisão baseado em amostras aleatórias dos dados de treinamento, assim

cada árvore de decisão é cultivada usando um subconjunto de dados que contém cerca de dois terços das instâncias e os nós são divididos usando as melhores variáveis de divisão entre os selecionados aleatoriamente do subconjunto de variáveis. Os dados restantes podem ser usados para obter uma classificação teste, bem como determinar a importância de características (BREIMAN, 2001; GAO et al., 2018).

O classificador de RF requer dois parâmetros para construir o modelo: o número de árvores de decisão e o número de variáveis usadas em cada divisão para fazer a árvore crescer (LEI MA et al., 2017). Valores padrão ou recomendados podem ser utilizados. As configurações padrão para o número de árvores são 500, entretanto, esse parâmetro pode ser facilmente adaptado durante o treinamento do classificador (STEFANSKI; MACK; WASKE, 2013). Este classificador requer muito menos parâmetros de classificação do que técnicas semelhantes de aprendizado de máquina (DE CASTRO et al., 2018).

Outro algoritmo bastante utilizado em SR são as Redes Neurais Artificiais (*Artificial Neural Network* -ANN). Elas são estruturas de mapeamento não linear baseadas na função do cérebro humano. Possuem várias classes como: rede *convolutional neural* networks (CNN), *deep neural network* (DNN) *Single-layer perceptron* (SLP) *Multilayer Perceptron* (MLP) (ABIODUN et al., 2019).

Redes neurais multicamadas (MLP) são uma classe de redes neurais *feedforward* (ABIODUN et al., 2019) aprendem rapidamente com alta generalização e têm uma poderosa capacidade de autoaprendizagem (LIAN et al., 2015). Eles são compostos de camadas de entrada, ocultas e de saída, o número de entradas e saídas é determinado com base nos objetivos da pesquisa. A entrada recebe o sinal, uma saída toma uma decisão ou predição sobre a entrada e, no meio, tem um número arbitrário de camadas ocultas que são o verdadeiro motor computacional do MLP (ABIODUN et al., 2019).

Vários estudos mostraram a eficácia do algoritmo de aprendizado de máquina de Redes Neurais Artificiais (RNA), especialmente MLP, quando aplicado na classificação de sensoriamento remoto (CARVAJAL-RAMÍREZ et al. 2019; IIZUKA et al., 2018; DUARTE-CARVAJALINO et al., 2018; BARRERO; PERDOMO, 2018; NEVALAINEN et al., 2017).

2.6. Avaliação de Similaridade
2.6.1. *Shape, Theme, Edge, Position* (STEP)

Shape, Theme, Edge, Position é um método proposto por Lizarazo (2014), que utiliza as características temáticas e geométricas dos objetos, como forma, borda, posição para gerar uma matriz de similaridade. Ele usa amostras de objetos de referência e de objetos

classificados para gerar as métricas de similaridade. Primeiro, é necessário um conjunto de verdades de campo (objetos de referência), e em seguida, esses dados são sobrepostos às amostras de objetos classificados. Portanto, todos os objetos classificados que se cruzam com a referência são selecionados para a análise.

A qualidade temática foi determinada pela similaridade do tema (T) que se refere a uma cobertura do solo e quantifica a porcentagem de objetos classificados que correspondem aos objetos de referência (LIZARAZO, 2014).

$$T = A_{int}/A_{ref} \tag{1}$$

Sendo: A_{int} a área de interseção entre o objeto classificado e o objeto de referência e A_{ref} a área do objeto de referência.

Enquanto a precisão geométrica foi avaliada pelos índices de borda (E), forma (S) e posição (P). A similaridade de borda analisa os limites dos objetos (internos e externos), calculando as porcentagens dos limites do objeto de referência que coincidem com os limites do objeto classificado (LIZARAZO, 2014).

A equação considera porcentagem das linhas de borda dos objetos classificados que coincidem com a borda do objeto de referência e então é dividido pelo perímetro do limite do objeto de referência (Equação 2).

$$E = \left(l_{int}/p_{ref}\right)^{k} \tag{2}$$

Sendo: l_{int} comprimento de borda do objeto classificado e p_{ref} o perímetro do objeto de referência. O valor k é definido como +1 caso l_{int} for menor ou igual p_{ref}, enquanto k é igual a -1 quando l_{int} for maior que p_{ref}.

Além disso, a similaridade de borda considera a banda *épsilon*, considerada uma largura de incerteza relacionada ao objeto de referência, ou seja, é uma margem relacionada à probabilidade de encontrar a linha (borda) verdadeira (LIZARAZO, 2014).

A similaridade de formas compara a geometria de objetos de referência e classificados considerando um índice de compactação. Para isso é utilizado o índice de perímetro normalizado (NPI) (Equação 3) (LIZARAZO, 2014).

$$NPI = P_{eac}/P_{obj} \tag{3}$$

Sendo: P_{eac} o perímetro do círculo e P_{obj} o perímetro do objeto.

Este índice se baseia na razão do perímetro de um círculo de área igual do objeto comparado e o perímetro verdadeiro do objeto. Assim por meio do NPI é realizada uma comparação entre o objeto classificado e o objeto de referência (Equação 4).

$$S = r_{npi^k} \tag{4}$$

Sendo: r_{npi} a razão entre os NPIs dos objetos classificados e de referência e k +1 quando o resultado de r_{npi} é menor ou igual a 1, e -1 quando o resultado é maior que 1.

A similaridade de posição avalia a posição do centroide de objetos classificados e de referência. Este índice é calculado utilizando a distancia euclidiana entre os centroides dos objetos, sendo dividida pelo diâmetro de área circular combinada (circulo que possui área igual à soma das áreas dos objetos de referência e classificado) (Equação 5).

$$P = 1 - d_{cent}/d_{cac} \tag{5}$$

Sendo: d_{cent} a distância euclidiana entre o centroide do objeto de referência classificado correspondente e d_{cac} o diâmetro da área circular combinada.

Os valores dos índices de similaridade STEP variam de 0 a 1, em que 0 se refere a objetos sem similaridade e 1 indica que existe uma concordância completa (LIZARAZO, 2014).

Os índices de similaridade são gerados para os objetos individuais, em que os objetos são avaliados separadamente e apresentados em uma matriz em que as colunas indicam os objetos classificados e as linhas equivalem aos objetos de referência. Esta matriz individual pode ser agregada por classe temática e a nova matriz expressa a matriz de similaridade STEP integrada, em que o número resultante de linhas e colunas corresponde ao número de classes temáticas (LIZARAZO, 2014).

REFERÊNCIAS

ABIODUN. O. I. et al. Comprehensive Review of Artificial Neural Network Applications to Pattern Recognition. **IEEE Access**, v. 7, p. 158820-158846, 2019.

ALLISON, R. S. et al. Airborne Optical and Thermal Remote Sensing for Wildfire Detection and Monitoring. **Sensors**, v. 16, n. 8, p. 1-29, 2016.

AMOS, C.; PETROPOULOS, G. P.; FERENTINOS, K. P. Determining the use of Sentinel-2A MSI for wildfire burning & severity detection. **International Journal of Remote Sensing**, v. 40, n. 3, p. 905-930, 2019.

ANDELA, N. et al. The Global Fire Atlas of individual fire size, duration, speed and direction. **Earth System Science Data**, v. 11, p. 529–552, 2019.

AXIMOFF, I. O que Perdemos com a Passagem do Fogo pelos Campos de altitude do Estado do Rio de Janeiro? **Biodiversidade Brasileira**, n. 2, p. 180-200, 2011.

AXIMOFF, I.; ALEVES, R.G.; RODRIGUES, R.C. Campos de altitude do Itatiaia: aspectos ambientais, biológicos e ecológicos. **Boletim do Parque Nacional do Itatiaia**, Rio de Janeiro, n. 18, 74p., 2014.

AXIMOFF, I.; NUNES-FREITAS, A.F.; BRAGA, J.M.A. Regeneração natural pós-fogo nos campos de altitude no Parque Nacional do Itatiaia, Sudeste do Brasil. **Oecologia Australis**, v. 20, n. 2, p. 62-80, 2016.

AXIMOFF, I.; RODRIGUES, R.C. Histórico dos incêndios florestais no Parque Nacional do Itatiaia. **Ciência Florestal**, Santa Maria, v. 21, n. 1, p. 83-92, 2011.

BAATZ, M.; SCHAPE, A. Multiresolution segmentation: an optimization approach for high quality multi-scale image segmentation. **Journal of Photogrammetry and Remote Sensing**, v. 58, p. 12-23, 2000.

BAATZ, M.; HOFFMANN, C.; WILLHAUCK, G. Progressing from object-based to object-oriented image analysis. In: BLASCHKE, T.; LANG, S.; HAY, G.J. **Object based image analysis**. Springer, New York, p. 29-42. 2008.

BARBERO, R. et al. Attributing Increases in Fire Weather to Anthropogenic Climate Change Over France. **Frontiers in Earth Science**, v. 8, p. 1-11, 2020.

BARMPOUTIS, P. et al. A Review on Early Forest Fire Detection Systems Using Optical Remote Sensing. **Sensors**, v. 20, n. 22, p. 1-26, 2020.

BARRERO, O.; PERDOMO, S. A. RGB and multispectral UAV image fusion for Gramineae weed detection in rice fields. **Precision Agriculture**, v. 19, p. 809-822, 2018.

BASTARRIKA, A.; CHUVIECO, E.; MARTÍN, M.P. Mapping burned areas from Landsat TM/ETM+ data with a two-phase algorithm: balancing omission and commission erros. **Remote Sensing of Environment**, v. 115, n. 4, p. 1003-1012, 2011.

BASTOS, A. et al. Modelling post-fire vegetation recovery in Portugal. **Biogeosciences**, v.8, p. 3593–3607, 2011.

BEATTY, R. **Projeto de cooperação Brasil-Alemanha "Prevenção, controle e monitoramento de incêndios florestais no Cerrado".** Programas piloto de manejo integrado do fogo - Relatório de Planejamento e Implementação. 15p. 2014.

BELCHIOR, I. B. et al. Occurrence and recurrence of forest fires in Itatiaia National Park between 2008 and 2016. **Biodiversidade Brasileira**, v. 10, n. 1, p. 72, 2020.

BENZ, U. et al. Multi-resolution, object oriented fuzzy analysis of remote sensing data for GIS-ready information. **ISPRS Journal of Photogrammetry and Remote Sensing,** v.58, p. 239–258, 2004.

BERLINCK, C. N.; LIMA, L. H. A. Implementation of Integrated Fire Management in Brazilian Federal Protected Areas: Results and Perspectives. **Biodiversidade Brasileira**, v. 11, n. 2, p. 128-138, 2021.

BERLINCK, C. N.; BATISTA, E. K. L. Good fire, bad fire: it depends on who burns. **Flora**, v. 268, p. 1-4, 2020.

BILBAO, B. et al. Sharing multiple perspectives on burning: towards a participatory and intercultural fire management policy in Venezuela, Brazil, and Guyana. **Fire**, v. 2, n. 3, p. 1-33, 2019.

BLASCHKE, T. Object based image analysis for remote sensing. **ISPRS Journal of Photogrammetry and Remote Sensing,** v. 65, n. 1, p. 2-16, 2010.

BLASCHKE, T. et al. Geographic object-based image analysis – towards a new paradigm. **ISPRS Journal of Photogrammetry and Remote Sensing,** v. 87, p. 180–191, 2014.

BONANOMI, J. et al. Protecting forests at the expense of native grasslands: Land-use policy encourages open-habitat loss in the Brazilian *cerrado* biome. **Perspectives in Ecology and Conservation**, v. 17, n. 1, p. 26-31, 2019.

BOND, W. J.; KEELEY, J. E. Fire as a global "herbivore": The ecology and evolution of flammable ecosystems. **Trends in Ecology & Evolution**, v. 20, n. 7, p. 387–394, 2005.

BONTEMPO, G. C. et al. Registro de Ocorrência de Incêndio (ROI): evolução, desafios e recomendações. **Biodiversidade Brasileira**, n. 2, p. 247-263, 2011.

BOWMAN, D. M. J. S. et al. Fire in the Earth system. **Science**, v. 324, p. 481-484, 2009.

BOWMAN, D. M. J. S. et al. Vegetation fires in the anthropocene. **Nature Reviews Earth & Environment**, v. 1, p. 500–515, 2020.

BRADE, A.C. A flora do Parque Nacional do Itatiaia. **Boletim do Parque Nacional do Itatiaia**, n. 5, p. 1-114, 1956.

BREIMAN, L. Random forests. **Machine Learning**, v. 45, n. 1, p. 5–32, 2001.

BROVKINA, O. et al. Monitoring of post-fire forest scars in Serbia based on satellite Sentinel-2 data. **Geomatics, Natural Hazards and Risk**, v. 11, n. 1, p. 2315-2339, 2020.

BUTCHART, S. H. M. et al. Protecting Important Sites for Biodiversity Contributes to Meeting Global Conservation Targets. **PLOS ONE**, v. 7, n. 3, 2012.

CAMARGO, F.F. et al. Geomorphological Mapping Using Object-Based Analysis and ASTER DEM in the Paraíba do Sul Valley, Brazil. **International Journal of Remote Sensing**, v. 30, n. 24, p. 6613-6620, 2009.

CÁNOVAS-GARCÍA, F.; ALONSO-SARRÍA, F. A local approach to optimize the scale parameter in multiresolution segmentation for multispectral imagery. **Geocarto International,** v. 30, n. 8, p. 937–961, 2015.

CARDIL, A. et al. Fire and burn severity assessment: Calibration of Relative Differenced Normalized Burn Ratio (RdNBR) with field data. **Journal of Environmental Management**, v. 235, p. 342–349, 2019.

CARVAJAL-RAMÍREZ, F. et al. Evaluation of Fire Severity Indices Based on Pre- and Post-Fire Multispectral Imagery Sensed from UAV. **Remote Sensing**, v. 11, n. 9, p. 1-19, 2019.

CEPF - Critical Ecosystem Partnership Fund. **Announcing the World's 36th Biodiversity Hotspot: The North American Coastal Plain (2016, November)**. Available: http://www.cepf.net/news/top_stories/Pages/Announcing-the-Worlds-36th- Biodiversity-Hotspot.aspx.

CHEN, G. et al. A multiscale geographic object based image analysis to estimate lidar-measured forest canopy height using Quickbird imagery. **International Journal of Geographical Information Science**, v. 25, p. 37–41, 2011.

CHEN, Y. et al. Remote sensing for vegetation monitoring in carbon capture storage regions: A review. **Applied Energy**, v. 240, n. p. 312-326, 2019.

CHUVIECO E. et al. Development of a frame work for fire risk assessment using remote sensing and geographic information system technologies. **Ecological Modelling**, v. 221, n. 1, p. 46–58, 2010.

COUTO JUNIOR, A.C.S. **Monitoramento do cerrado em Minas Gerais usando análises estatísticas baseadas em objetos:** uma abordagem em diferentes escalas. 2011. 78p. Dissertação (Mestrado em Engenharia Florestal) – Universidade Federal de Lavras, Lavras, 2011.

DALDEGAN, G. A. et al. Spatial patterns of fire recurrence using remote sensing and GIS in the Brazilian savanna: Serra do Tombador Nature Reserve, Brazil. **Remote Sensing**, v. 6, p. 9873-9894, 2014.

D'AMICO, A. R. et al. Environmental diagnoses and effective planning of Protected Areas in Brazil: Is there any connection? **PLoS ONE**, v. 15, n. 12, p. 1-13, 2020.

DEAN, A.M.; SMITH, G.M. An evaluation of per-parcel land cover mapping using maximum likelihood class probabilities**. International Journal of Remote Sensing**, v. 24, p. 2905–2920, 2003.

DE CASTRO, A. I. et al. An automatic random forest-obia algorithm for early weed mapping between and within crop rows using UAV imagery. **Remote Sensing**, v. 10, n. 2, p. 1-21, 2018.

DESCLÉE, B.; BOGAERT, P.; DEFOURNY, P. Forest change detection by statistical object-based method. **Remote Sensing of Environment,** v. 102, p. 1–11, 2006.

DRUSCH, M. et al. Sentinel-2: ESA's optical high-resolution mission for GMES operational services. **Remote Sensing of Environment**, v. 120, n.15, p.25-36, 2012.

DUARTE-CARVAJALINO, J. M. et al. Evaluating Late Blight Severity in Potato Crops Using Unmanned Aerial Vehicles and Machine Learning Algorithms. **Remote Sensing**, v. 10, n. 10, p. 1-17, 2018.

DURIGAN, G. et al. No net loss of species diversity after prescribed fires in the Brazilian savanna. **Frontiers in Forest and Global Change**, v. 3, n. 13, p. 1-15, 2020.

DURIGAN, G.; RATTER, J. A. The need for a consistent fire policy for Cerrado conservation. **Journal of Applied Ecology**, v. 53, p.11-15, 2016.

DURO, D.C.; FRANKLIN, S.E.; DUBÉ, M.G. A comparison of pixel-based and object-based image analysis with selected machine learning algorithms for the classification of agricultural landscapes using SPOT-5 HRG imagery. **Remote Sensing of Environment**, v. 118, p. 259-272, 2012.

EARL, N. SIMMONDS, I. Spatial and Temporal Variability and Trends in 2001–2016 Global Fire Activity. **Journal of Geophysical Research: Atmospheres**, v. 123, n. 5, p. 2524–2536, 2018.

ELOY, L. et al. From fire suppression to fire management: advances and resistances to changes in fire policy in the savannas of Brazil and Venezuela. **Geographical Journal**, v. 185, p. 10-22, 2019.

ESCH, T. et al. Improvement of image segmentation accuracy based on multiscale optimization procedure. IEEE Geoscience and Remote Sensing Letters, v. 5, p. 463–467, 2008.

ESCOBAR, H. Amazon fires clearly linked to deforestation, scientists say. **Science,** v. 365, n. 6456, p. 853, 2019.

ESCUIN, S.; NAVARRO, R.; FERNÁNDEZ, P. Fire severity assessment by using NBR (Normalized Burn Ratio) and NDVI (Normalized Difference Vegetation Index) derived from LANDSAT TM/ETM images. **International Journal of Remote Sensing**, v. 29, n. 4, p. 1053-1073, 2008.

FERNANDES, P.M.; BOTELHO, H.S. A review of prescribed burning effectiveness in fire hazard reduction. **International Journal of Wildland Fire**, v. 12, p. 117–128, 2003.

FERNÁNDEZ, C.; VEGA, J. A.; FONTURBEL, T. Shrub resprouting response after fuel reduction treatments: comparison of prescribed burning, clearing and mastication. **Journal of Environmental Management**, v.117, p.235- 241, 2013.

FIDELIS, A. et al. The year 2017: megafires and management in the Cerrado. **Fire**, v. 1, n. 3, p. 1-11, 2018.

FIGUEROA, F., SÁNCHEZ-CORDERO, V. Effectiveness of natural protected areas to prevent land use and land cover change in Mexico. **Biodiversity and Conservation**, v. 17, p. 3223–3240, 2008.

FINER, M. et al. Future of oil and gas development in the western Amazon. **Environmental Research Letters**, v. 10, n. 2, p. 1-6, 2015.

FRANCO, A. C. et al. Cerrado vegetation and global change: the role of functional types, resource availability and disturbance in regulating plant community responses to rising CO_2 levels and climate warming. **Theoretical and Experimental Plant Physiology**, v. 26, p. 9–38, 2014.

FRANÇA, H.; RAMOS NETO, M. B.; SETZER, A. **O Fogo no Parque Nacional das Emas**. Ministério do Meio Ambiente – MMA. Brasília, 140p. 2007.

FREEBORN, P. H.; WOOSTER, M. J.; ROBERTS, G. Addressing the spatiotemporal sampling design of MODIS to provide estimates of the fire radiative energy emitted from Africa. **Remote Sensing of Environment**, v. 115, n. 2, p. 475–489, 2011.

FUSCO, E. J. et al. Detection rates and biases of fire observations from MODIS and agency reports in the conterminous United States. **Remote Sensing of Environment**, v. 220, p. 30–40, 2019.

GAŠPAROVIĆ, M. et al. An automatic method for weed mapping in oat fields based on UAV imagery. **Computers and Electronics in Agriculture**, v. 173, p. 1-12, 2020.

GATTI, L. V. et al. Drought sensitivity of Amazonian carbon balance revealed by atmospheric measurements. **Nature**, v. 506, p. 76–80, 2014.

GAO, J. et al. Fusion of pixel and object-based features for weed mapping using unmanned aerial vehicle imagery. **International Journal of Applied Earth Observation and Geoinformation**, v. 67, p. 43–53, 2018.

GETZIN, S. et al. Size dominance regulates tree spacing more than competition within height classes in tropical Cameroon. **Journal of Tropical Ecology**, v. 27, n. 01, p. 93-102, 2011.

GIGLIO, L. et al. The collection 6 MODIS burned area mapping algorithm and product. **Remote Sensing of Environment**, v. 217, p. 72-85, 2018.

GIGLIO, L. et al. An active-fire based burned area mapping algorithm for the MODIS sensor. **Remote Sensing of Environment**, v. 113, n. 2, p. 408–420, 2009

GRAY, C. L. et al. Local biodiversity is higher inside than outside terrestrial protected areas worldwide. **Nature Communications**, v. 7, p. 1-7, 2016.

GÓMEZ, C. et al. Modeling forest structural parameters in the mediterranean pines of central Spain using QuickBird-2 imagery and classification and regression tree analysis (CART). **Remote Sensing**, v. 4, n. 1, p. 135–159, 2012.

GONÇALVES, J. et al. Evaluating an unmanned aerial vehicle-based approach for assessing habitat extent and condition in fine-scale early successional mountain mosaics. **Applied Vegetation Science**, v. 19, p. 132–146, 2016.

GONZALEZ, R. C.; WOODS, R. E. **Processamento digital de imagens**. 3. ed. São Paulo: Pearson, 2010. 624 p.

HALOFSKY, J. E.; PETERSON, D. L.; HARVEY, B. J. Changing wildfire, changing forests: the effects of climate change on fire regimes and vegetation in the Pacific Northwest, USA. **Fire Ecology**, v. 16, n. 4, p. 1-26, 2020.

HANTSON, S.; PUEYO, S.; CHUVIECO, E. Global fire size distribution is driven by human impact and climate. **Global Ecology and Biogeography**, v. 24, n. 1, p. 77–86, 2015.

HAY, G.J. et al. An automated object-based approach for the multiscale image segmentation of forest scenes. **International Journal of Applied Earth Observation and Geoinformation**. V. 7, p. 339–359, 2005.

HAY, G.J., CASTILLA, G. Geographic Object-Based Image Analysis (GEOBIA). In: Blaschke, T., Lang, S., Hay, G.J. (Eds.), Object-Based Image Analysis – Spatial Concepts for Knowledge-Driven **Remote Sensing Applications**, p. 77–92, 2008.

HUNG, C.; XU, Z.; SUKKARIEH, S. Feature Learning Based Approach for Weed Classification Using High Resolution Aerial Images from a Digital Camera Mounted on a UAV. **Remote Sensing**, v. 6, p. 12037-12054, 2014.

ICAO- International Civil Aviation Organization. Circular 328: **Unmanned Aircraft Systems (UAS)**. 2011. ISBN 978-92-9231-751-5.

ICMBio – Instituto Chico Mendes de Biodiversidade. **Plano de Manejo Parque Nacional do Itatiaia Revisão – Encarte 1**. Brasília, 47p., 2014a. Disponível em: <http://www.icmbio.gov.br/portal/component/content/article?id=2181:parna-do-itatiaia>.

ICMBio – Instituto Chico Mendes de Biodiversidade. **Plano de Manejo Parque Nacional do Itatiaia Revisão – Encarte 3**. Brasília, 215p., 2014b. Disponível em: <http://www.icmbio.gov.br/portal/component/content/article?id=2181:parna-do-itatiaia>.

ICMBio – Instituto Chico Mendes de Biodiversidade. **Plano de Manejo Parque Nacional do Itatiaia Revisão – Encarte 4**. Brasília, 77p., 2014c. Disponível em: <http://www.icmbio.gov.br/portal/component/content/article?id=2181:parna-do-itatiaia>.

IIZUKA, K. et al. Advantages of unmanned aerial vehicle (UAV) photogrammetry for landscape analysis compared with satellite data: A case study of postmining sites in Indonesia. **Cogent Geoscience**, v. 4, n. 1, p. 1-15, 2018.

INPE – **INSTITUTO NACIONAL DE PESQUISAS ESPACIAIS**. Available: https://queimadas.dgi.inpe.br/queimadas/portal. 2020.

JANG, E. et al. Detection and Monitoring of Forest Fires Using Himawari-8 Geostationary Satellite Data in South Korea. **Remote Sensing**, v. 11, n. 3, p. 1-25, 2019.

JENSEN, J.R. **Introductory Digital Image Processing**: A Remote Sensing Perspective, 4 ed., Prentice-Hall, Inc., Upper Saddle River, New Jersey, 544 p. 2015.

JOLLY, W. M. Climate-induced variations in global wildfire danger from 1979 to 2013. **Nature Communication**, v. 6, n. 7537, p. 1-11, 2015.

KELLY, L. T.; BROTONS, L. Using fire to promote biodiversity. **Science**, v. 355, n. 6331, p.1264-1265, 2017.

KIM, M. et al. Multi-scale GEOBIA with very high spatial resolution digital aerial imagery: scale, texture and image objects. **International Journal of Remote Sensing**, v. 32, n. 10, 2825–2850, 2011.

KNORR, W.; JIANG, L.; ARNETH, A. Climate, CO_2 and human population impacts on global wildfire emissions. **Biogeosciences**, v. 13, p. 267–282, 2016.

KONKATHI, P.; SHETTY, A. Inter comparison of post-fire burn severity indices of Landsat-8 and Sentinel-2 imagery using Google Earth Engine. **Earth Science Informatics**, v. 14, p. 645–653, 2021.

KRESSLER, F.P.; STEINNOCHER, K. Image data and LIDAR – an ideal combination matched by object oriented analysis. In: Geographic Object-Based Image Analysis, 1, 2006. Salzburg University, Austria. **Proceedings…** Salzburg: Salzburg University 2006.

LALIBERTE A.S.; FREDRICKSON, E.L.; RANGO, A. Combining Decision Trees with Hierarchical Object-oriented Image Analysis for Mapping Arid Rangelands. **Photogrammetric Engineering & Remote Sensing**, v. 73, n. 2, p. 197–207, 2007.

LALIBERTE, A.S. et al. Acquisition, orthorectification, and object-based classification of unmanned aerial vehicle (UAV) imagery for rangeland monitoring. **Photogrammetric Engineering & Remote Sensing**, v. 76, n. 6, p. 661-672, 2010.

LALIBERTE, A.S.; RANGO, A. Texture and scale in object-based analysis of sub-decimeter resolution unmanned aerial vehicle (UAV) imagery. **IEEE Transactions on Geoscience and Remote Sensing**, v. 47, n. 3, p. 761–770, 2009.

LALIBERTE, A.S.; RANGO, A. Image Processing and Classification Procedures for Analysis of Subdecimeter Imagery Acquired with an Unmanned Aircraft over Arid Rangelands. **GIScience & Remote Sensing**, v. 48, n. 1, p. 4–23, 2011.

LAPOLA, D. M. et al. Pervasive transition of the Brazilian land-use system. **Nature Climate Change**, v 4, n. 1,p. 27–35, 2014.

LAURENT, P et al. FRY, a global database of fire patch functional traits derived from space-borne burned area products. **Scientific Data**, v. 5, p. 1-12, 2018.

LEIGH, J.H.; NOBLE, J.C. The role of fire in the management of rangelands in Australia. In Fire and the Australian Biota; Grove, R.H., Noble, I.R., Eds.; **Australian Academy of Science**, p. 471–495, 1981.

LEI MA. et al. Evaluation of Feature Selection Methods for Object-Based Land Cover Mapping of Unmanned Aerial Vehicle Imagery Using Random Forest and Support Vector Machine Classifiers. **International Journal of Geo-Information**, v. 6, n. 2, p. 1-21, 2017.

LIAN, C. et al. Multiple neural networks switched prediction for landslide displacement. **Engineering Geology**, v. 186, p. 91–99, 2015.

LIBANO, A. M.; FELFILI, J. M. Mudanças temporais na composição florística e na diversidade de um cerrado sensu stricto do Brasil Central em um período de 18 anos (1985-2003). **Acta Botanica Brasilica**, v. 20, p. 927-936, 2006.

LIU, J. **Combined method for vegetation classification based on visible bands from UAV images: a case study for invasive wild parsnip plants**. 2018. 93p. Dissertação (Mestrado em Environmental Studies) - Queen's University, Canadá, 2018.

LIU, J.; ABD-ELRAHMAN, A. An Object-Based Image Analysis Method for Enhancing Classification of Land Covers Using Fully Convolutional Networks and Multi-View Images of Small Unmanned Aerial System. **Remote Sensing**, v. 10, p. 1-24, 2018.

LIU, Z.; BALLANTYNE, A. P.; COOPER, L. A. Biophysical feedback of global forest fires on surface temperature. **Nature Communications**, v.10, p. 1-9, 2019.

LIZARAZO, I. Accuracy Assessment of Object-Based Image Classification: Another STEP. **International Journal of Remote Sensing**, v. 35, n. 16, p. 6135–6156, 2014.

LIZUNDIA-LOIOLA, J.; PETTINARI, M. C.; CHUVIECO, E. Temporal Anomalies in Burned Area Trends: Satellite Estimations of the Amazonian 2019 Fire Crisis. **Remote Sensing**, v. 12, n. 151, p. 1-8, 2020.

LOPES, E. R. N. et al. Losses on the Atlantic Mata vegetation induced by land use changes. **Cerne**, v. 24, n. 2, p. 121-232, 2018.

LUCIEER, A. et al. Using an Unmanned Aerial Vehicle (UAV) to capture micro-topography of Antarctic moss beds. **International Journal of Applied Earth Observation and Geoinformation**, v. 27, Part A, p. 53–62, 2014.

LUMBIERRES, M. et al. Modeling Biomass Production in Seasonal Wetlands Using MODIS NDVI Land Surface Phenology. **Remote Sensing**, v. 9, n. 4, p. 1-18, 2017.

MAEDA, E. E. et al. Fire risk assessment in the Brazilian Amazon using MODIS imagery and change vector analysis. **Applied Geography**, v. 31, n. 1, p. 76-84, 2011.

MapBiomas **- Projeto de Mapeamento Anual do Uso e Cobertura da Terra no Brasil**. 2021. Disponível em: https://mapbiomas.org/noticias?cama_set_language=pt-BR.

MARENGO, J. A. et al. Extreme drought in the Brazilian Pantanal in 2019-2020: characterization, causes and impacts. **Frontiers Water**, v. 3, p. 1-20, 2021.

MARENGO, J. A. et al. Changes in climate and land use over the Amazon region: current and future variability and trends. **Frontiers in Earth Science**, v. 6, p. 1-21, 2018.

MARGULES, C. R.; PRESSEY, R. L.; WILLIAMS, P. H. Representing biodiversity: Data and procedures for identifying priority areas for conservation. **Journal of Biosciences**, v. 27, p.309-326, 2002.

MARTINS, F.M. et al. Grupos de Queimada Controlada para Prevenção de Incêndios Florestais no Mosaico de Carajás. **Biodiversidade Brasileira**, v. 6, n. 2, p. 121-134, 2016.

MARTINIS, S. et al. Mapping burn scars, fire severity and soil erosion susceptibility in Southern France using multisensoral satellite data. In **Proceedings...** IEEE International Geoscience and Remote Sensing Symposium (IGARSS), Fort Worth, TX, USA, 2017, p. 1099–1102.

MEWS, H. A. et al. Influência de agrupamentos de bambu na dinâmica pós-fogo da vegetação lenhosa de um cerrado típico, Mato Grosso, Brasil. **Rodriguésia**, v. 64, p. 211-221, 2013.

MIRANDA, H.S., NETE, W.N., NEVES, B.M.C. **Caracterização das queimadas de Cerrado.** In: MIRANDA, H.S., Efeitos Do Regime Do Fogo Sobre a Estrutura de Comunidades de Cerrado: Resultados do Projeto Fogo. IBAMA/MMA, Brasília, 144p, 2010.

MYINT, S. W. et al. Per-pixel vs. object-based classification of urban land cover extraction using high spatial resolution imagery. **Remote Sensing of Environment,** v. 115, n. 5, p. 1145-1161, 2011.

MYERS, N. et al. Biodiversity hotspots for conservation priorities. **Nature**, n. 403, p. 853-845, 2000.

MYERS, R.L. **Convivendo com o fogo – Manutenção dos ecossistemas & subsistência com o Manejo Integrado do Fogo**. The Nature Conservancy**,** 36p. 2006.

NAVARRO, G. et al. Evaluation of forest fire on Madeira Island using Sentinel-2A MSI imagery. **International Journal of Applied Earth Observation and Geoinformation,** v. 58, p. 97–106, 2017.

NEDKOV, R. Quantitative assessment of forest degradation after fire using ortogonalized satellite images from SENTINEL-2. **Comptes Rendus de l'Academie Bulgare des Sciences**, v. 71, n. 1, p. 83–86, 2018.

NEVALAINEN, O. et al. Individual Tree Detection and Classification with UAV-Based Photogrammetric Point Clouds and Hyperspectral Imaging. **Remote Sensing**, v. 9, n. 3, p. 1-34, 2017.

NOGUEIRA, J. M. P. et al. Can we go beyond burned area in the assessment of global remote sensing products with fire patch metrics? **Remote Sensing**, v. 9, n. 7,p. 1-18, 2016.

NOVELLI, A. Performance evaluation of object based greenhouse detection from Sentinel-2 MSI and Landsat 8 OLI data: A case study from Almería (Spain). **International Journal of Applied Earth Observation and Geoinformation**, v. 52, p. 403–411, 2016.

ODION, D. C. et al. Examining historical and current mixed-severity fire regimes in ponderosa pine and mixed-conifer forests of western North America. **PLoS ONE**, v. 9, n. 2, p. 1-14, 2014.

OVERBECK, G. E., FERREIRA, P. M. A., PILLAR, V. D. Conservation of mosaics calls fora perspective that considers all types of mosaic-patches. Reply to Luza et al. **Natureza & Conservação**, v. 14, n. 2, p. 152–154, 2016.

PANDE-CHHETRI, R. et al. Object-based classification of wetland vegetation using very high-resolution unmanned air system imagery. **European Journal of Remote Sensing**, v. 50, n. 1, p. 564–576, 2017.

PANEQUE-GÁLVEZ, J. et al. Small Drones for Community-Based Forest Monitoring: An Assessment of Their Feasibility and Potential in Tropical Areas. **Forests,** v. 5, n. 6, p. 1481-1507, 2014.

PANISSET, J. et al. Assigning dates and identifying areas affected by fires in Portugal based on MODIS data. **Anais da Academia Brasileira de Ciências**, v. 89, n. 3, p. 1487-1501, 2017.

PEKKARINEN, A. Image segment – based spectral features in the estimation of timber volume. **Remote Sensing of Environments**, v. 82, p. 349 – 359, 2002.

PÉREZ-CABELLO, F.; MONTORIO, R.; ALVES, D. B. Remote sensing techniques to assess post-fire vegetation recovery. **Current Opinion in Environmental Science & Health**, v. 21, p.1-9, 2021.

PFAFF, A. et al. Protected Areas' Impacts on Brazilian Amazon Deforestation: Examining Conservation – Development Interactions to Inform Planning. **PLOS ONE**, v. 10, n. 7, p. 1-17, 2015.

PIVELLO, V. R. et al. Understanding Brazil's catastrophic fires: Causes, consequences and policy needed to prevent future tragedies. **Perspectives in Ecology and Conservation**, v. 19, p. 233–255, 2021

QUINTANO, C.; FERNÁNDEZ-MANSO, A.; FERNÁNDEZ-MANSO, O. Combination of Landsat and Sentinel-2 MSI data for initial assessing of burn severity**. International Journal of Applied Earth Observation and Geoinformation**, v. 64, p. 221– 225, 2018.

RADOUX, J.; BOGAERT, P. Good Practices for Object-Based Accuracy Assessment. **Remote Sensing**, v. 9, n. 7, p. 1-23, 2017.

RAIYANI, K. et al. Sentinel-2 Image Scene Classification: A Comparison between Sen2Cor and a Machine Learning Approach**. Remote Sensing**, v. 13, p. 1-22, 2021.

RANGO, A. et al. Using Unmanned Aerial Vehicles for Rangelands: Current Applications and Future Potentials. **Environmental Practice**, v. 8, n. 3, p. 159–168, 2006.

REDIN, M. et al. Impactos da queima sobre atributos químicos, físicos e biológicos do solo. **Ciência Florestal**, v. 21, n. 2, p. 381-392, 2011.

RIBEIRO, K. T.; MEDINA, B. M. O. Estrutura, Dinâmica e Biogeografia das Ilhas de Vegetação Sobre Rocha do Planalto do Itatiaia. **Boletim do Parque Nacional do Itatiaia**, Rio de Janeiro, n. 10, 84p., 2002.

RIBEIRO, J. F.; WALTER, B. M. As principais fitofisionomias do bioma cerrado. In: Cerrado: Ecologia e Flora, eds S. M. Sano, S. P. Almeida, and J. F. Ribeiro (Planaltina: Embrapa Cerrados), p. 151–199, 2008.

RODRIGUEZ-GALIANO, V.F.; CHICA-RIVAS, M. Evaluation of different machine learning methods for land cover mapping of a Mediterranean area using multi-seasonal Landsat images and Digital Terrain Models. **International Journal of Digital Earth**, v. 7, p. 492–509, 2012.

RODRIGUEZ-GALIANO, V.F.; GHIMIRE, B.; ROGAN, J.; CHICA-OLMO, M.; RIGOL-SANCHEZ, J. P. An assessment of the effectiveness of a random forest classifier for land-cover classification. **ISPRS Journal of Photogrammetry and Remote Sensing**, v. 67, p. 93-104, 2012.

ROMERO, V. R. et al. Perspectivas de la tecnología VANT en el cultivo de palma de aceite: monitorización del cultivo mediante imágenes aéreas de alta resolución. **Revista Palmas**, v. 36, n. 3, p. 25-41, 2015.

ROSSI, F. S.; SANTOS, G. A. A. Fire dynamics in Mato Grosso State, Brazil: the relative roles of gross primary productivity. **Big Earth Data**, v. 4, n. 1, p. 23-44, 2020.

ROTETA, E. et al. Development of a Sentinel-2 burned area algorithm: Generation of a small fire database for sub-Saharan Africa. **Remote Sensing of Environment**, v. 222, p. 1–17, 2019.

ROY, D.P. Landsat-8: science and product vision for terrestrial global change research. **Remote Sensing of Environment**, v. 145, n. 5, p. 154–172, 2014.

RUIZ, L.F.C. **Uma abordagem de classificação da cobertura da terra em imagens obtidas por veículo aéreo não tripulado**. 2015. Dissertação (Mestrado em Sensoriamento Remoto) - Universidade Federal do Rio Grande do Sul, Porto Alegre. 104p. 2015.

SÁ, A. C. L. et al. Evaluating fire growth simulations using satellite active fire data. **Remote Sensing of Environment**, v. 190, p. 302–317, 2017.

SAFFORD, H. D. Brazilian páramos I. An introduction to the physical environment and vegetation of the *campos de altitude*. **Journal of Biogeography**, v. 26, p. 693-712, 1999.

SAMPAIO, A.B. et al. Editorial - Manejo do Fogo em Áreas Protegidas. **Biodiversidade Brasileira**, v. 6, n. 2, p 1-3, 2016.

SANTANA, N. C. et al. Comparison of Post-fire Patterns in Brazilian Savanna and Tropical Forest from Remote Sensing Time Series. **ISPRS International Journal of Geo-Information**, v. 9, n. 11, p. 1-19, 2020.

SANTOS, J. F. C. et al. Potentials and limitations of remote fire monitoring in protected areas. **Science of The Total Environment**, v. 616-617, p. 1347-1355, 2018.

SANTOS, L. M. Use of remotely piloted aircraft in precision agriculture: A review. **Dyna**, v. 86, n. 10, p. 284-291, 2019.

SANSEVERO, J. B. B. et al. Past land-use and ecological resilience in a lowland Brazilian Atlantic Forest: implications for passive restoration. **New Forest**, v. 48, p. 573–586, 2017.

SCHMIDT, I. B. et al. Fire management in the Brazilian Savanna: first steps and the way forward. **Journal of Applied Ecology**, v. 55, p.2094-2101, 2018.

SCHMIDT, I. B.; ELOY, L. Fire regime in the Brazilian Savanna: Recent changes, policy and management. **Flora**, v. 268, p. 1-5, 2020.

SCHOWENGERDT, R.A. **Remote sensing**: Models and methods for image processing. 3 ed. New Delhi: Elsevier. 515 p. 2006.

SHIMABUKURO, Y. E. et al. Mapping Burned Areas of Mato Grosso State Brazilian Amazon Using Multisensor Datasets. **Remote Sensing**, v. 12, n. 22, p. 1-23, 2020.

SILVA, C. et al. **The hidden emissions: how Amazon wildfires can boost Brazil's CO_2 emissions**. Policy Brief. Instituto de Pesquisa Ambiental da Amazônia, Brasília, DF. p. 1-6, 2021.

SOARES, R. V.; BATISTA, A. C. **Incêndios florestais**: controle, efeitos e uso do fogo. Curitiba, 2007. 264 p.

STAAL, A. et al. Feedback between drought and deforestation in the Amazon. **Environmental Research Letters**, v. 15, p. 1-9, 2020.

STEFANSKI, J.; MACK, B.; WASKE, B. Optimization of Object-Based Image Analysis With Random Forests for Land Cover Mapping. **IEEE Journal of Selected Topics in Applied Earth Observations and Remote Sensing**, v. 6, n. 6, p. 1-13, 2013.

SUN, Q. et al. Global heat stress on health, wildfires, and agricultural crops under different levels of climate warming. **Environment International**, v. 128, p. 125-136, 2019.

TARABALKA, Y.; BENEDIKTSSON, J. A.; CHANUSSOT, J. Spectral–spatial classification of hyperspectral imagery based on partitional clustering techniques. **IEEE Transactions on Geoscience and Remote Sensing**, v. 47, n. 8, p. 2973-2987, 2009.

TEODORO, A.; AMARAL, A. A Statistical and Spatial Analysis of Portuguese Forest Fires in Summer 2016 Considering Landsat 8 and Sentinel 2A Data. **Environments**, v. 6, n. 3, p. 1-17, 2019.

TOMZHINSKI, G.W.; RIBEIRO, K.T.; FERNANDES, M.C. Análise Geoecológica dos Incêndios Florestais do Parque Nacional do Itatiaia. **Boletim do Parque Nacional do Itatiaia**, Rio de Janeiro, n. 15, 164 p., 2012.

TORRES-SÁNCHEZ, J.; LÓPEZ-GRANADOS, F.; PEÑA, J.M. An automatic object-based method for optimal thresholding in UAV images: Application for vegetation detection in herbaceous crops. **Computers and Electronics in Agriculture**, v. 114, p. 43–52, 2015.

TORRES-SÁNCHEZ. J. et al. Multi-temporal mapping of the vegetation fraction in early-season wheat fields using images from UAV. **Computers and Electronics in Agriculture**, v. 103, p. 104- 113, 2014.

TURNER, D.; LUCIEER, A. WATSON, C. An automated technique for generating georectified mosaics from ultra-high resolution unmanned aerial vehicle (UAV) imagery, based on structure from motion (SFM) point clouds. **Remote Sensing**, v. 4, n. 5, p. 1392-1410, 2012.

VELOSO, H.P.; RANGEL FILHO, A.L.R.; LIMA, J.C.A. **Classificação da vegetação brasileira, adaptada a um sistema universal**. Rio de Janeiro: IBGE, Departamento de Recursos Naturais e Estudos Ambientais, 124p., 1991.

VERAVERBEKE, S. et al. Mapping the daily progression of large wildland fires using MODIS active fire data. **International Journal of Wildland Fire**, v. 23, p. 655–667, 2014.

VERHEGGHEN, A. et al. The potential of Sentinel satellites for burnt area mapping and monitoring in the Congo Basin forests. **Remote Sensing**, v. 8, n. 12, p. 1-22, 2016.

VIANA-SOTO, A.; AGUADO, I.; MARTÍNEZ, S. Assessment of postfire vegetation recovery using fire severity and geographical data in the mediterranean region (Spain). **Environments**, v. 4, n. 4, p. 1-17, 2017.

VON BUEREN, S.K. et al. Deploying four optical UAV-based sensors over grassland: challenges and limitations. **Biogeosciences**, n. 12, p. 163–175, 2015.

WANG, J. et al. Maximum weight and minimum redundancy: a novel framework for feature subset selection. **Pattern Recognition,** v. 46, n. 6, p. 1616–1627, 2013.

WATTS, A.C.; AMBROSIA, V.G.; HINKLEY, E.A. Unmanned Aircraft Systems in Remote Sensing and Scientific Research: Classification and Considerations of Use. **Remote Sensing**, v. 4, p. 1671-1692, 2012.

WHITEHEAD, K.; HUGENHOLTZ, C.H. Remote sensing of the environment with small unmanned aircraft systems (UASs), part 1: A review of progress and challenges. **Journal of Unmanned Vehicle Systems,** v. 2, p. 69–85, 2014.

WULDER, M. A. et al. Current status of Landsat program, science, and applications. **Remote Sensing of Environment**, v. 225, p. 127-147, 2019.

XIANG, H., TIAN, L. Development of a low-cost agricultural remote sensing system based on an autonomous unmanned aerial vehicle (UAV). **Biosystems Engineering**, v. 108, n. 2, p. 174–190, 2011.

XU, R. et al. Wildfires, Global Climate Change, and Human Health. **The New England Journal of Medicine**, v. 383, n. 22, p. 2173-2181, 2020.

YAN G. et al. Comparison of pixel-based and object-oriented image classification approaches-a case study in a coal fire area, Wuda, Inner Mongolia, China. **International Journal of Remote Sensing,** v. 27, p. 4039–4055, 2006.

YE, S.; PONTIUS, R. G.; RAKSHIT, R. A review of accuracy assessment for object-based image analysis: From per-pixel to per-polygon approaches. **ISPRS Journal of Photogrammetry and Remote Sensing**, v. 141, p. 137-147, 2018.

ZABALA, A.; CEA, C.; PONS, X. Segmentation and thematic classification of color orthophotos over non-compressed and JPEG 2000 compressed images. **International Journal of Applied Earth Observation and Geoinformation**, v. 15, p. 92-104, 2012.

ZHANG, C.; XIE, Z. Object-based vegetation mapping in the Kissimmee River watershed using HyMap data and machine learning techniques. **Wetlands**, v. 33, p. 233– 244, 2013.

SEGUNDA PARTE – ARTIGOS

ARTICLE 1 - RGB and multispectral imagery derived from unmanned aerial vehicle for mapping of *campos de altitude* and prescribed fire

Abstract

Unmanned aerial vehicle (UAV) technology has rapidly improved in recent years and provided the ability to acquire high spatial and temporal resolution data, resulting in better environmental monitoring. In this paper, geographic object-based image analysis (GEOBIA) and machine learning techniques were applied to classify *campos de altitude* vegetation using RGB (Red, Green, Blue, bands) and multispectral images before and after a prescribed fire. Image classification was used to generate three vegetation classes that were assessed by RGB and multispectral sensors pre- (shrubs, grass, and non-vegetated) and post- (burned, not burned, and non-vegetated) prescribed fire. From a fuel perspective, the area analysed by RGB and multispectral images determined that 14.8% and 27.3% of vegetation did not burn, respectively. This incomplete removal of fuel is a trait of prescribed fire, causing vegetation spatial discontinuity through specific fire conditions. Our findings showed that the automatic classification method using RGB and multispectral images is accurate for discriminating pre- and postfire vegetation. Therefore, RGB images overcome the limitations of poor spectral resolution and are suitable for distinguishing vegetation

Keywords: UAV. Image classification. GEOBIA. Controlled burning.

1. INTRODUCTION

Unmanned aerial vehicle technology has been developed in recent years, and its improvement has been observed. This technology makes it possible to fly at lower heights than satellites and to obtain decimetre spatial resolution, fly designated routes according to demands (VENTURI et al., 2016; YANG et al., 2017), and have low cost, easy operation (LALIBERT; RANGO, 2009; COLOMINA et al., 2014; MATESE et al., 2015; MANFREDA et al., 2018, GAO et al., 2018), and great flexibility (LARRINAGA; BROTONS, 2019), while maintaining a high level of accuracy (MAMAGHANI; SALVAGGIO, 2019).

This technology is being increasingly applied to several monitoring tasks using various types of sensors (FREEMAN; FREELAND, 2015). The most common and affordable sensors employed in UAV surveys are off-the-shelf digital cameras with red, green and blue (RGB) bands (ZHANG et al., 2016; ZHENG et al., 2018). Low-cost RGB cameras have been successfully used in mapping vegetation in different environments (AYHAN; KWAN, 2020; ASHAPURE et al., 2019; DÍAZ-VARELA et al., 2018; PALACE et al., 2018; AHMED et al., 2017; FENG; LIU; GONG, 2015; TORRES-SÁNCHEZ; LÓPEZ-GRANADOS; PEÑA, 2015; LALIBERTE et al., 2010; LALIBERTE; RANGO, 2009).

Multispectral cameras permit us to obtain spectral information in the RGB, red edge, and NIR bands for vegetation applications (YAO; QIN; CHEN, 2019). Several surveys have used these multispectral cameras (XU et al., 2020; ASHAPURE et al., 2019; KWAK; NO-WOOK, 2019; FRANKLIN; AHMED, 2018; BARRERO; PERDOMO, 2018; AHMED et al., 2017; TORRES-SÁNCHEZ et al., 2013). Nevertheless, it is important to note that this type of camera is significantly more expensive than conventional RGB (GAŠPAROVIĆ et al., 2020).

Additionally, RGB and multispectral sensors have been applied to monitor fire events, allowing flights to be carried out in the immediate postfire situation given the provided control of the revisit time (MCKENNA et al., 2017). Burned areas can be estimated by analysing the electromagnetic spectrum to detect changes in the spectral characteristics of land cover before and after the occurrence of fires (CHUVIECO et al., 2019; SAMIAPPAN et al., 2019).

In Brazil, fire activity is influenced mainly by land-use change and is a management practice used to create and maintain cattle pasture and to expand the agricultural frontier (PIVELLO et al., 2021). However, when realized without proper knowledge, this practice might result in uncontrolled forest fires.

In this context, prescribed fire is often used by land managers as an effective tool for reducing uncontrolled fire hazards. Therefore, fire is introduced under specific environmental conditions with an established duration and rate of spread (FERNANDEZ-CARRILLO; MCCAW; TANASE, 2019). Prescribed fire not only reduces the biomass available to burn in a subsequent uncontrolled wildfire (VAILLANT; FITES-KAUFMAN; STEPHENS, 2009) but can also be beneficial for vegetation, as in Brazilian savanna (*Cerrado*) and paramos (*campos de altitude*), because fire with low-to-moderate intensity can accelerate the availability of nutrients and organic matter (MAGALLANES et al., 2020).

In order to analyse high-resolution UAV imagery, machine learning algorithms have been increasingly used to classify large amounts of complex data (GAŠPAROVIĆ et al., 2020). Several studies have shown the effectiveness of artificial neural network (ANN) machine learning algorithms, especially multilayer perceptrons (MLPs), when applied in remote sensing classification (CARVAJAL-RAMÍREZ et al. 2019; IIZUKA et al., 2018; DUARTE-CARVAJALINO et al., 2018; BARRERO; PERDOMO, 2018; NEVALAINEN et al., 2017). These studies have indicated that the advantage of this method is the ability to derive patterns and trends from large data, which could be difficult to extract using other techniques and to relate them to specific desirable characteristics (ALVES et al., 2017; IIZUKA et al., 2017).

On the other hand, random forest (RF) has been used for the same purpose for higher accuracy (GAŠPAROVIĆ et al., 2020; GAO et al., 2018; DE CASTRO et al., 2018; DUARTE-CARVAJALINO et al., 2018; MICHEZ et al., 2016; PÉREZ-ORTIZ et al., 2016) since it requires fewer classification parameters than similar machine learning techniques (DE CASTRO et al., 2018).

Despite the increased UAV-derived products in the published literature evaluating land cover and burned vegetation, the practices of drone-based multispectral and RGB for mapping Brazilian paramos have yet to be developed by the research community. Furthermore, the performance of different sensors onboard UAVs for the same purpose has rarely been compared.

Thus, our objective was (i) to compare RGB and multispectral centimetric-scale orthomosaics to classify a complex mosaic of shrubs within a grass matrix interspersed with rock outcrops, (ii) to assess a prescribed fire impact on land cover, and (iii) to develop a low-cost methodological approach to analyse vegetation for supporting protected areas fire management.

1.1. MATERIALS AND METHODS

1.2. Study area

The area of study is the Itatiaia National Park (INP), located in southern Rio de Janeiro and north-eastern Minas Gerais states (22°15' and 22°30'S, 44°30' and 44°45'W), in the highest part of the Mantiqueira mountain range. It covers an area of approximately 30,000 hectares and has a 3 km buffer zone starting from the park's perimeter (FIGURE 1.1), which protects its surroundings, reducing possible negative impacts on the conservation unit. This area has mountainous relief with rocky outcrops and altitudes varying from approximately from 540 meters up to 2,791 meters at its highest point, Agulhas Negras Peak (ICMBio, 2014).

The park is located in the Atlantic Forest Biome and presents several phytophysiognomies, such as dense ombrophilous forest, high-montane dense ombrophilous forest, semideciduos forest, montane mixed ombrophilous forest, and *campos de altitude* (high grassland) (VELOSO; RANGEL FILHO; LIMA, 1991; ICMBio, 2014). The last is the focus of this study (FIGURE 1.2) and is also known as Brazilian paramos, due to their similarities to the high regions of the Andes and the mountains of Central America (SAFFORD, 1999).

Figure 1.1 - The geopolitical boundary and landscape of study site during the prescribed fire, in Itatiaia National Park, Brazil.
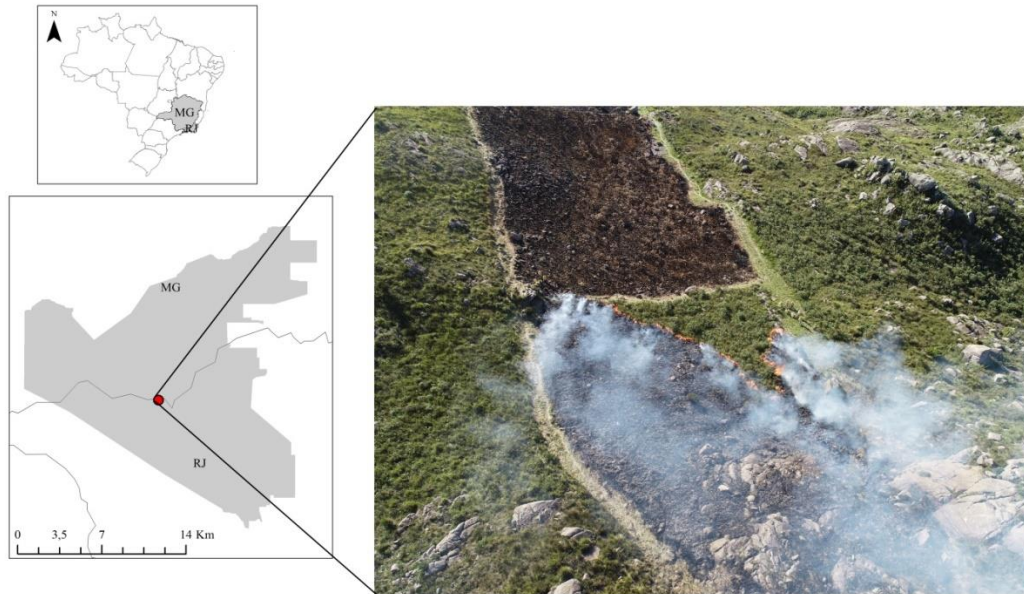
Source: from the author (2021).

Campos de altitude are grass-dominated formations restricted to the highest summits of the south-eastern Brazilian highlands composed of igneous or metamorphic rocks in the Mantiqueira and Mar Mountains (SAFFORD, 1999). As the altitude increases, tree and shrub individuals decrease, giving way to the fields at an average altitude of 2300 m. In this phytophysiognomy, approximately 415 plant species have already been recorded, including herbs, shrubs, lianas, and trees, with the grass family (*Poaceae*) having the largest number of species (AXIMOFF; ALVES; RODRIGUES, 2014).

Figure 1.2 - *Campos de altitude* vegetation in Itatiaia Natonal Park.

Source: from the author (2021).

The general methodological flowchart is illustrated in Figure 1.3 and includes several steps, such as image acquisition through UAV, preprocessing, image segmentation, feature extraction, classification, and classification accuracy assessment.

Figure 1.3. Flowchart of the applied methodology.
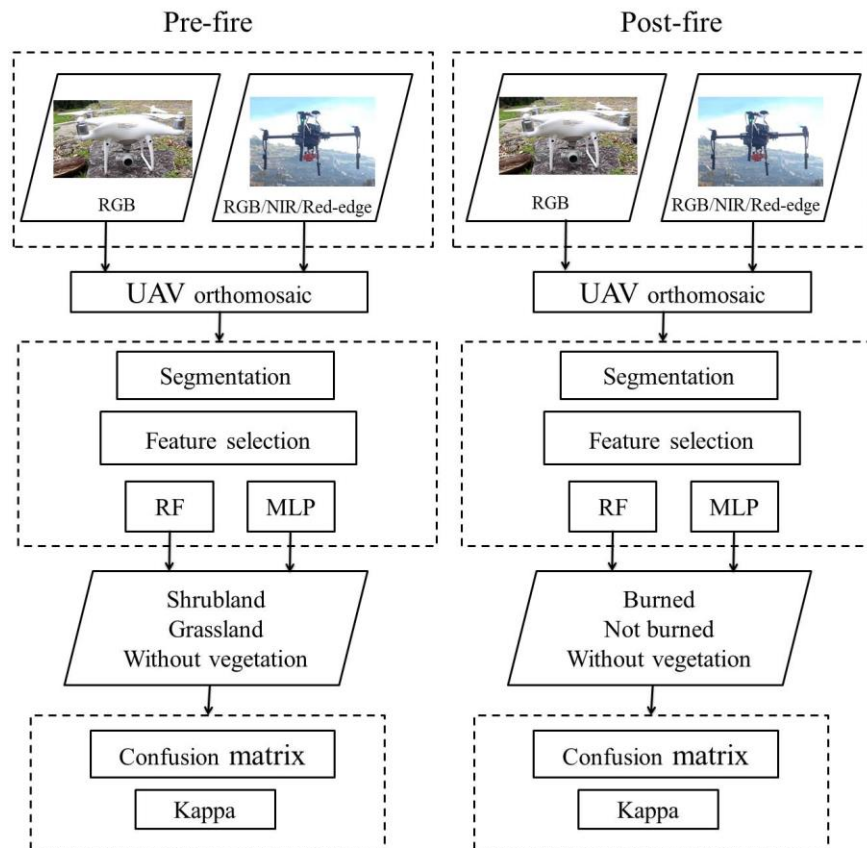
Source: from the author (2021).

1.3. Data collection and processing

The airborne campaigns were conducted using DJI UAVs: Phantom 4 Pro and Matrice 100, on May 22, 2019, in pre- and post-prescribed fire events. However, preflight site visits were performed to identify obstacles and brief information about topographic constraints that may affect flight planning.

The Phantom 4 Pro is an aircraft formed by titanium and magnesium alloys, providing resistance and lightness to the equipment; it weighs 1388 g, including batteries and propellers. The UAV has a flight autonomy of almost 30 minutes and is equipped with a sensor that has a 20 megapixel resolution, with a maximum shutter speed of 1/2000 s, which eliminates possible distortions in the images of moving scenes. The camera can record blue, green, and red (RGB) bands.

Matrice 100 is a completely customizable and programmable aircraft with a carbon fibre structure that provides lightness and resistance in addition to reducing vibrations, expansion bays that allow adding components to the equipment and a compartment for the installation of the additional battery, giving higher-flight autonomy, achieving 40 minutes. MicaSense's RedEdge-M camera was attached to this aircraft, which has five sensors able to collect data in blue, green, red, near infrared (NIR), and red-edge bands. This camera was chosen because it is currently one of the best performing UAV multispectral cameras (TADDIA et al., 2020).

This camera has a global positioning system (GPS), with a reflectance panel composed of material with an almost Lambertian behaviour in which the calibration in the laboratory provided spectral characteristics, and a downwelling light sensor (DLS), which measures the environmental light during the flight for all bands and records this information, which was used in this study to correct the illumination changes during flights. In addition, the RedEdge-M camera is also interfaced with a standard onboard GNSS that provides georeferencing information, and the coordinates are stored within the Exif metadata of every single shot.

In our research, the flight plan was defined in the DroneDeploy app for the collection made with the Phantom 4 Pro with a flight altitude of 240 m for prefire and 120 m for postfire. A Pix4DCapture app was used with Matrice 100, with a flight altitude of 90 m pre- and postfire and with 80% front and side overlap for all flights. Additionally, the images of the known reflectance panel were always acquired holding the multispectral camera directly above the panel at no more than 1 m distance just before and just after each flight.

The imagery were processed using reconstruction techniques, SfM (structure from motion), and multispectral, radiometric corrections were performed based on DLS data and images of a known reflectance panel. The advantage of using the DLS and known reflectance panel is that precise and trustworthy reflectance values could be computed and issues due to changes in the irradiance may be corrected by DLS measurements (TADDIA et al., 2020).

Reflectance is not directly measured by sensors; rather, they measure at-sensor radiance, the radiant flux received by the sensor. At-sensor radiance measurements are stored as arbitrary digital numbers (DNs) (ASSMANN et al., 2019). In this study, for RGB images, the classification was solely based on the DN, and conversion from DN values to reflectance was not performed due to not having known reflectance data for the Phantom camera and the complexity of determining the spectral sensitivity for each channel of the sensor. Since the conversion of the DN values into reflectance was not conducted, the results of the digital

orthophoto are qualitative (CANDIAGO et al., 2015), and these results cannot be directly compared with images from other dates.

The processed images generated georeferenced orthomosaics, with a spatial resolution of 7.2 cm/pixel for the RGB prefire and 4.3 cm/pixel for postfire. The multispectral pre- and postfire data show 6.1 and 6.2 cm/pixel, respectively. Afterwards, the orthomosaics were resampled using the pixel aggregate method for 7.2 cm/pixel to be compatible with the analysis.

1.4. Reference data set

Field trips were carried out in Itatiaia National Park to make visual recognition and to obtain *in situ* ground referencing of vegetation cover to assist with the development of digital vegetation maps. During these trips, georeferenced data from the vegetation classes were collected, aided by GPS. Additionally, visual inspection of vegetation classes was realized to collect and compose the reference dataset.

1.5. Geographic Object-Based Image Analysis (GEOBIA)

From the images collected with the UAV, geographic object-based image analysis was performed to identify 3 classes of vegetation in prefire analyses: grasslands (dominant undergrowth with a predominance of grasses), shrubland (a predominance of *Baccharis uncinella*, *Machaerina ensifolia*, and *Cortaderia modesta*) and non-vegetated areas (rocky outcrops and bare ground). Three classes were used postfire: burned, unburned vegetation, and non-vegetated.

1.5.1. Segmentation

Image segmentation was performed using an algorithm based on the region growth technique, known as multiresolution segmentation (MRSA) (BAATZ; SCHAPE, 2000; BENZ et al., 2004).

The segmentation parameter values were adjusted using a trial and error procedure based on a visual assessment (ZHANG; FRITTS; GOLDMAN, 2008). Visual interpretation is generally the most significant way to parameterize segmentations in natural environments (RÄSÄNEN et al., 2013). The visible bands (RGB) in the case of the image obtained by the Phantom and the visible, infrared, and red-edge bands of RedEgde's sensor were equally balanced in the segmentation parameter.

The thresholds used for these parameters were determined empirically based on the expertise of the image interpreter. For the pre- and postfire multispectral orthomosaics, the parameters of scale, shape, and compactness were set to 2, 0.6, and 0.9, respectively.

For the RGB pre- and postfire orthomosaics, the parameters were set: 15 for the scale, 0.4 for the shape, and 0.8 for the compactness. After establishing an initial segmentation level, a second segmentation was performed to join some objects belonging to the same class. For this, the spectral difference segmentation algorithm was used, which unites neighbouring objects that do not exceed the maximum spectral difference (a user-defined limit) (ESCH et al., 2008; ZYLSHAL et al., 2016). Thus, the objects generated in the multiresolution segmentation were merged to produce the final objects, and the parameter was 5.

1.5.2. Feature computation and selection

Metrics were extracted from the objects to be used as inputs for classifier algorithms. These inputs are shown in Table 1.1 and include spectral, textural, and shape features.

RGB orthomosaic feature selection used the spectral, textural, and shape characteristics of the red, green, and blue bands; band ratio; vegetation indices as excess green (ExG); red–green ratio (RGRI); normalized red–green difference (NGRDI); and visible-band difference vegetation (VDVI). The same features were used for the multispectral orthomosaic adding the red-edge and NIR bands, and the indices were normalized difference red-edge (NDRE) normalized difference vegetation index (NDVI) and chlorophyll index (CI).

Five texture metrics were derived from the grey level co-occurrence matrix (GLCM), based on Haralick; Shanmugam; Dinstein (1973): entropy, standard deviation, correlation, mean, and contrast. These derivatives are computed through symmetric matrices for neighbouring pixels at 0°, 45°, 90°, or 135°, and in this study, the approach used was in "all the directions".

Tabe 1.1 - Classification input features.

Type of metrics	Inputs	Description
Spectral	Average brightness values for the red, green and blue (RGB), red-edge, NIR bands; Standard deviation; Overall brightness; Maximum difference; Band ratio: Blue/(Red+Blue+Green)	Basic statistics of pixel values of objects in R, G, B, Red-edge, NIR bands

	Red/(Red+Blue+Green) Green/(Red+Blue+Green)	
Vegetation Indexes	ExG = 2*G – R - B RGRI = R/G VDVI= (2*G – R – B)/(2*G + R + B) NGRDI = (G – R)/(G + R) NDVI = (NIR – Red) / (NIR + Red); NDRE = (NIR- Red-edge)/(NIR+ Red-edge); CI = (NIR/ Red-edge) - 1	The vegetation index combine different spectral bands of objects ExG (WOEBBECKE et al., 1995) RGRI (VERRELST et al., 2008) VDVI (WANG et al., 2015) NDVI (ROUSE et al., 1974) NGRDI (TUCKER, 1979) NDRE (BARNES et al., 2000) CI (GITELSON et al., 2005)
Texture	Entropy; Standard deviation; Homogeneity; Dissimilarity; Mean; Contrast	Texture features calculated by GLCM algorithm (HARALICK; SHANMUGAM; DINSTEIN, 1973)
Shape	Area; Border length; Border index; Shape index; Thickness; Asymmetry; Compactness; Length; Length/Thickness; Length/Width	Shape features refer to object geometry information, which is calculated from the pixels that form it.

Source: from the author (2021).

As a large number of features were extracted from the objects, 31 and 35 to RGB and multispectral data, respectively, metric selection was performed using random forest (BREIMAN, 2001) and analysed by conducting evaluations of the variable importance of the ready-to-use features. This measure is an indication of the importance of each variable used in the classifier. Of all samples, 70% were used for training, and the remaining 30% were used in the validation. This algorithm attempts to identify the most explanatory resources in the resource space that are essential to improve classification performance (WANG et al., 2013).

1.5.3. Supervised classification

Data were divided into three classification schemes. The first is composed of a multispectral image and an RGB image of the same area and the same pre-fire date. The second scheme has pre- and post-fire RGB images of the same area. And the last scheme is composed of a clipping of the multispectral image of the first scheme (pre-fire) and a multispectral image of the corresponding area in the post-fire.

In this study, the training and validation datasets were randomly sampled, and 70/30 of the samples were used for training and validation purposes.

The RF machine learning method was chosen due to its ability to handle high-dimensional remote sensing datasets (LAWRENCE; WOOD; SHELEY, 2006; STUMPF; KERLE, 2011), making it interesting for high-resolution spatial data processing (GONÇALVES et al., 2016). Additionally, it has been widely used in remote sensing classification research due to its good performance (STUMPF; KERLE, 2011; STEFANSKI; MACK; WASKE, 2013; MICHEZ et al., 2016; KULKARNI; LOWE, 2017).

The RF is an ensemble classifier that produces multiple decision trees (BELGIU; DRĂGUŢ, 2016) and requires a few parameters to build the model, including the number of trees and the number of randomly selected predictor variables (RODRIGUEZ-GALIANO et al., 2012; LEI MA et al., 2017). Thus, random forest offers less complex and high-performance computations (REZAEIAN; AMIRFATTAHI; SADRI, 2014). In this study, we used a random forest classifier consisting of 100 decision trees.

The forward structure of the ANN used in this study was the multilayer perceptron (MLP) with a hyperbolic tangent function trained by the backpropagation method designed to map a set of input vectors to a set of output vectors (HU et al., 2019). Artificial neural networks are nonlinear mapping structures based on the function of the human brain.

MLPs learn quickly with high generalization and have a powerful self-learning capacity (LIAN et al., 2015). They are composed of input, hidden, and output layers, and the number of inputs and outputs is determined based on research objectives. In this case, the number of neurons in the input layer was defined according to the number of attributes to be used per sample, and in the output layer, it was equal to the number of vegetation classes being discriminated against, in this study composed by 3 classes. The input receives the signal, an output makes a decision or prediction about the input, and in between they have an arbitrary number of hidden layers that are the true computational engine of the MLP; in this study, the number of hidden layers that were used was 30.

1.5.4. Accuracy assessment

Accuracy assessment calculates the percentage of the classified map that approximates the field reality. In this study, a validation dataset was created that did not overlap with the dataset used as input in classification algorithms. Visual field inspection concomitant with the flight survey allowed identification and refinement of classes. Due to the high spatial

resolution of imagery, visual inspection is very reliable for assessing accuracy (LECHNER et al., 2012).

For all classifications, a confusion matrix was created to assess the accuracy metrics that provided information regarding overall, user and producer accuracies (CONGALTON; GREEN, 2019) and the Kappa index (COHEN, 1960). A Kappa value of 1 indicates total agreement, while 0 represents no agreement (GONÇALVES et al., 2016).

2. RESULTS

2.1. Variable importance (VI)

The most important variables in each imagery classification were examined by the RF algorithm. In summary, the features that have values higher than 0.5 and higher values of GLCM texture, which were used later in classification, are shown in Tables 1.2 and 1.3.

The average of the "out-of-bag" importance value resources of the 31 preditors to RGB orthomosaics pre- and postfire was approximately 0.30 and 0.26, respectively. The highest values for RGB prefire were found for the spectral attributes (TABLE 1.2), while the lowest importance value was found for shape features with values less than 0.28.

Table 1.2 - Values of VI for RGB pre and post-fire evaluated by Random Forest.

	Importance values		
	> 0.5	**> 0.7**	**Texture GLCM**
RGB pre-fire 1 scheme	Blue Brightness Green Maximum difference MeanRGB NGRDI RGRI Red VDVI	Blue Maximum difference MeanGreen Red VDVI	Stde Homogeneity
RGB pre-fire 2 scheme	Blue Brightness Maximum difference Mean green Green Red VDVI	Blue Maximum difference	Entropy Homogeneity
RGB post-fire	Blue Brightness ExG Green Mean green/blue	Blue	Mean Dissimilarity

VDVI	

Regarding the 35 predictors of multispectral orthomosaics, the mean importance values prefire and postfire were 0.31 and 0.30, respectively. The lowest importance value for both analyses was found for shape features, which may indicate that these characteristics are not efficient in classifying the vegetation complex mosaic (Campos de altitude). For multispectral data pre- and postfire, the spectral features provide the highest values of "out-of-bag" importance (TABLE 1.3).

Table 1.3 - Values of VI for Multispectral pre and post-fire evaluated by Random Forest.

|	**Features values**		
	> 0.5	**> 0.7**	**Texture GLCM**
Multispectral pre-fire	CI ExG Maximum difference Mean green and red-edge bands NDRE NDVI NGRDI RGRI VDVI	ExG Maximum difference NDVI	Stde Dissimilarity
Multispectral post-fire	Brightness Maximum difference Mean blue, red, and red-edge bands NDVI	Maximum difference Mean green NDVI	Stde Contrast

2.2. Classification

The RGB and multispectral orthomosaics are shown in Figures 1.4, 1.5, and 1.6. In both prefire orthomosaics (1 scheme), the contrast between shrubland and grassland vegetation was not very clear, especially using RGB data.

Figure 1.4 – Images used in first classification scheme a) Multispectral pre-fire and b) RGB pre-fire, in true-color composite (Red, Green, Blue).
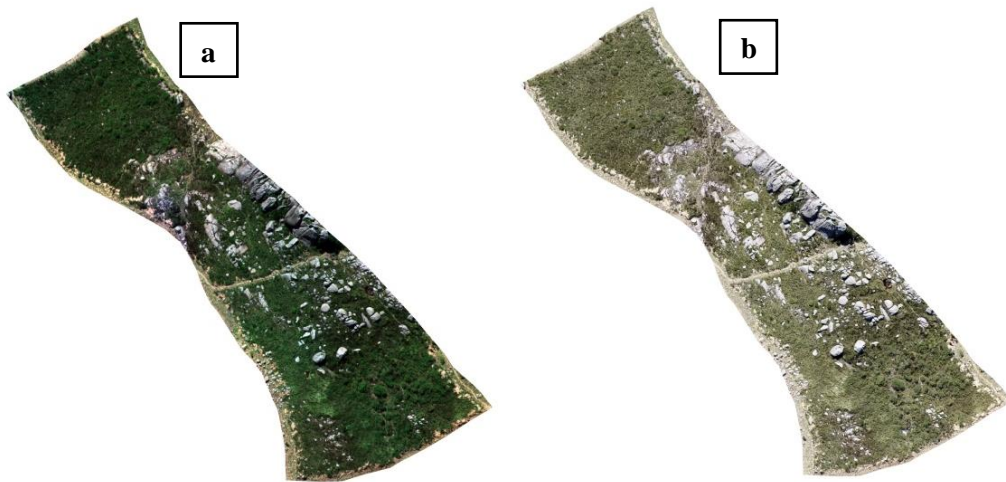
Source: from the author (2021).

Figure 1.5 - Images used in second classification scheme a) RGB pre-fire and b) RGB post-fire, in true-color composite (Red, Green, Blue).
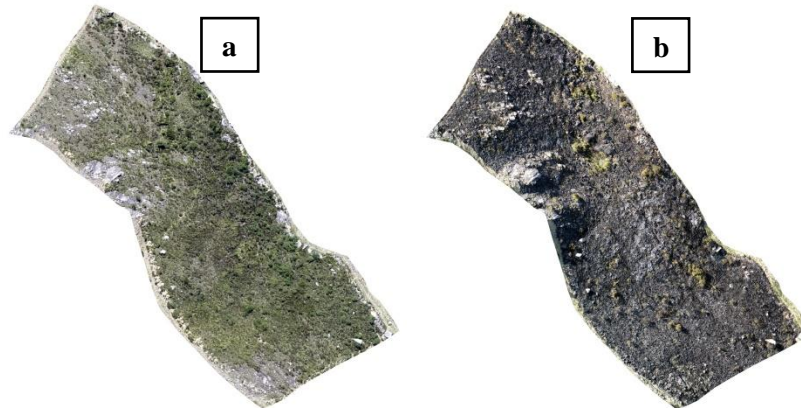
Source: from the author (2021).

Figure 1.6 - Images used in third classification scheme a) Multispectral pre-fire and b) Multispectral post-fire, in false-color composite (NIR, Red, Green).
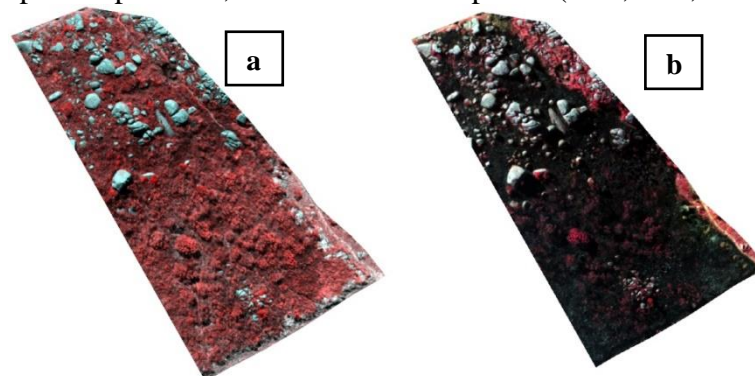
Source: from the author (2021).

GEOBIA was employed to produce maps in all classification schemes. Although spectral metrics were the most important feature selected by RF to RGB and multispectral

pre- and postfire data, we used the two best texture metrics to add spectral to evaluate whether they improved the classifications.

Our results confirm, in the first classification scheme, the combination of texture metrics, GLCM homogeneity, and standard deviation using the random forest algorithm for mapping vegetation cover in *campos de altitude* increases the quality of the final classification map for RGB data, as the authors expected. The accuracy was almost 0.34% higher than using only spectral attributes (TABLE 1.4), which resulted in the classification map illustrated in Figure 1.7.

Table 1.4 - Accuracy metrics for first classification scheme.

Classifier	Feature combination	RGB Pre-fire		Multispectral Pre-fire	
		Overall accuracy (%)	Kappa	Overall accuracy (%)	Kappa
MLP	> 0.5	96.67	0.95	97.83	0.97
	> 0.7	94.67	0.92	97.33	0.96
	> 0.7 + texture	95.00	0.93	96.83	0.95
RF	> 0.5	97.00	0.96	97.50	0.96
	> 0.7	96.67	0.94	96.50	0.95
	> 0.7 + texture	97.33	0.96	96.67	0.95

Source: from the author (2021).

In the multispectral case, the use of texture metrics added to the spectral for the MLP and RF algorithms did not produce the best accuracy results, but the values were near the maximum obtained with spectral features, which was 97.83% (TABLE 1.4), obtained with MLP, and Figure 1.7 shows the classification map produced.

Figure 1.7 - Classification maps for first scheme generated by a) MLP using > 0.5 feature combination and b) RF using > 0.7 + texture feature combination.
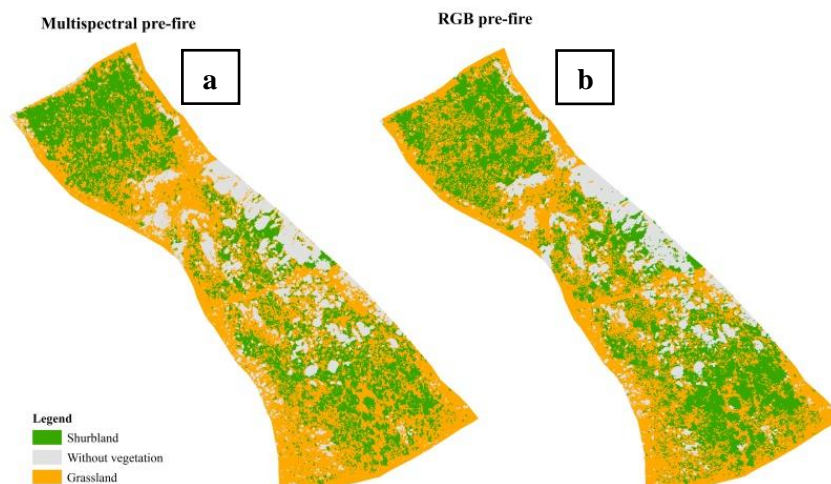
We assessed the accuracy of the classification algorithm by comparing the validation dataset selected randomly to the land cover generated by the algorithm and created a confusion matrix. Therefore, the MLP algorithm trained with spectral features obtained 97.83% overall classification accuracy using the multispectral sensor data in the first classification scheme. Some confusion between shrub and grassland cover occurred, but the assertiveness of these classes was almost the same, 97% and 96.5%, respectively. For non-vegetated areas, the classification presented 100% user accuracy (TABLE 1.5).

Table 1.5 – Confusion matrix for MLP using > 0.5 feature combination in multispectral data in first classification scheme.

		Reference data				User's accuracy
	Classes	Shrubland	Non-vegetated	Grassland	Total	
Classified data	Shrubland	194	0	6	200	97.00
	Non-vegetated	0	200	0	200	100.00
	Grassland	2	5	193	200	96.50
	Total	196	205	199	600	
	Producer's accuracy	98.98	97.56	96.98		
	Overall accuracy	97.83				
	Kappa	0.97				

Patterns of confusion were similar to those observed when classifying the multispectral data, but with lower classification accuracy, 97.33% was obtained using the RGB sensor. The shrubland class showed less assertiveness; with 95% user accuracy, some objects in this class were incorrectly classified as grassland. The non-vegetated class presented higher user and producer accuracy, 99% (TABLE 1.6).

Table 1.6 – Confusion matrix for RF using > 0.7 + texture feature combination in RGB data in first classification scheme.

		Reference data				User's accuracy
	Classes	Shrubland	Non-vegetated	Grassland	Total	
Classified data	Shrubland	95	0	5	100	95.00
	Non-vegetated	0	99	1	100	99.00
	Grassland	1	1	98	100	98.00
	Total	96	100	104	300	
	Producer's accuracy	98.96	99.00	94.23		
	Overall accuracy	97.33				

Kappa	0.96

The area and its percentages of vegetation cover in RGB and multispectral classification maps are summarized in Table 1.7. The total area analysed was 0.67 ha, and the most frequent class in terms of the overall area was grassland, with 47.8% and 52.4% for RGB and multispectral data, respectively. Non-vegetated areas had nearly the same values, which indicates that both sensors identified this class better than the others. In general, the two sensors showed similar values, with some confusion between grassland and shrubland, as shown previously.

Table 1.7 - Area and its percentage for different vegetation classes for RGB and multispectral sensors.

Classes	RGB		Multispectral	
	ha	%	ha	%
Grassland	0.320	47.8	0.351	52.4
Shrubland	0.240	35.8	0.211	31.5
Without vegetation	0.106	15.8	0.105	15.7
Total	**0.67 ha**			

The second classification scheme was realized to evaluate a prescribed fire using the RGB dataset. In this case, texture metrics did not improve the classification maps before or after the fire.

Two supervised classifiers in three feature combinations were compared for the classification of vegetation cover prefire and burned surfaces. As a result, in the prefire period, the MLP classifier trained with spectral features showed a higher accuracy, 96.67% (TABLE 1.8). The non-vegetated class was mapped with 92% of user's accuracy, due to confusion with grasslands (TABLE 1.9).

Table 1.8 - Accuracy metrics for second classification scheme.

Classifier	Feature combination	RGB Pre-fire		RGB Post-fire	
		Overall accuracy (%)	Kappa	Overall accuracy (%)	Kappa
MLP	**> 0.5**	96.67	0.95	98.67	0.98
	> 0.7	94.00	0.91	95.93	0.93
	> 0.7 + texture	92.67	0.89	95.93	0.93
RF	**> 0.5**	94.67	0.92	98.67	0.98
	> 0.7	92.00	0.88	96.00	0.94
	> 0.7 + texture	94.00	0.91	98.00	0.97

Table 1.9 – Confusion matrix for MLP using > 0.5 feature combination in pre-fire data in second classification scheme.

		Reference data				User's accuracy
	Classes	Shrubland	Non-vegetated	Grassland	Total	
Classified data	Shrubland	49	0	1	50	98.00
	Non-vegetated	0	46	4	50	92.00
	Grassland	0	0	50	50	100.00
	Total	49	46	55	150	
	Producer's accuracy	100.00	100.00	90.91		
	Overall accuracy	96.67				
	Kappa	0.95				

Source: from the author (2021).

Therefore, we tested the use of the best algorithm obtained in another area, for the first classification scheme, applied to this area, to evaluate the generalization capacity of the classifier, offering patterns to algorithms that they did not use in training. As a result, we found a great outcome with 95.33% overall accuracy and a 0.93 kappa index. These results show that it is possible to apply an algorithm trained in an area that has similar characteristics. Furthermore, there is the advantage of saving time by collecting samples and training the algorithm. However, in this study, we chose to use the algorithm trained for this specific area due to its higher accuracy.

The RGB postfire orthomosaic was classified with 98.67% accuracy by RF and MLP trained with spectral features. Thus, either one could be chosen for presenting the same accuracy. We adopted the MLP classifier to perform the analyses (FIGURE 1.8). This algorithm achieved 100% user accuracy for the burned and unburned classes but showed 96% user accuracy for the non-vegetated category (TABLE 1.10).

Table 1.10 – Confusion matrix for MLP using > 0.5 feature combination in postfire data in second classification scheme.

		Reference data				User's accuracy
	Classes	Shrubland	Non-vegetated	Grassland	Total	
Classified data	Shrubland	50	0	0	50	100.00
	Non-vegetated	1	48	1	50	96.00
	Grassland	0	0	50	50	100.00
	Total	51	48	51	150	
	Producer's accuracy	98.04	100.00	98.04		

Overall accuracy	98.67
Kappa	0.98

Source: from the author (2021).

Figure 1.8 - Classification maps for second scheme generated by a) MLP using > 0.5 feature combination and b) MLP using > 0.5 feature combination.
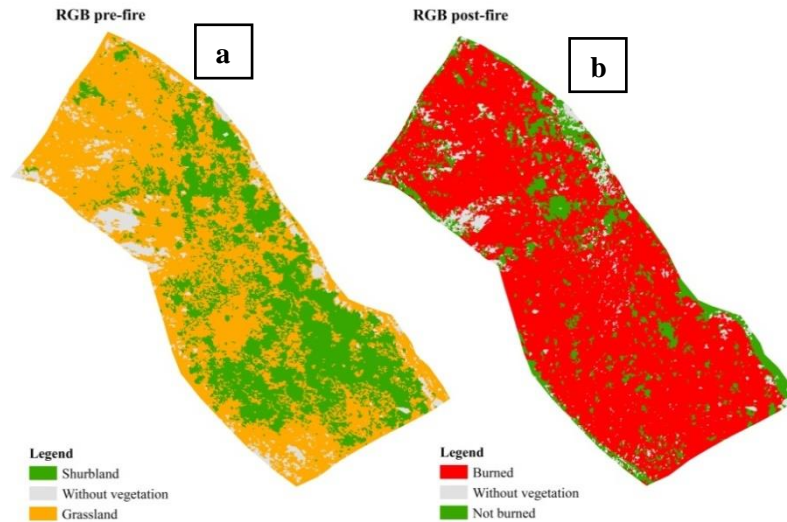
Source: from the author (2021).

Using the map produced by GEOBIA (FIGURE 1.8), we estimated the vegetation canopy before and after the prescribed fire event in an area of 0.79 ha. Most of the area was covered by grassland. It is interesting to note that there was a distinction in the area percentage of the non-vegetated class in the RGB pre- and postfire data.

Analysis of vegetation change from pre-fire and postfire revealed that 14.8% of vegetation did not burn (TABLE 1.11), complying with the characteristics of the prescribed fire.

Table 1.11 - Area and its percentage for different vegetation classes for RGB pre and post-fire.

Classes	RGB pre-fire		Classes	RGB post-fire	
	ha	%		ha	%
Grassland	0.460	58.2	**Burned**	0.625	79.1
Shrubland	0.272	34.4	**Unburned**	0.117	14.8
Without vegetation	0.053	6.7	**Without vegetation**	0.044	5.6
Total			**0.79 ha**		

Source: from the author (2021).

In the third classification scheme, we assessed a prescribed fire, made use of multispectral data, in a part of the area used for analysis in the first scheme, 0.183 ha, that

corresponded to 27.3% of the total area. Therefore, for prefire, we adopted the classification map achieved in the first scheme (FIGURE 1.9).

Figure 1.9 - Classification maps for the third scheme generated by a) MLP using > 0.5 feature combination and b) MLP using > 0.5 feature combination.
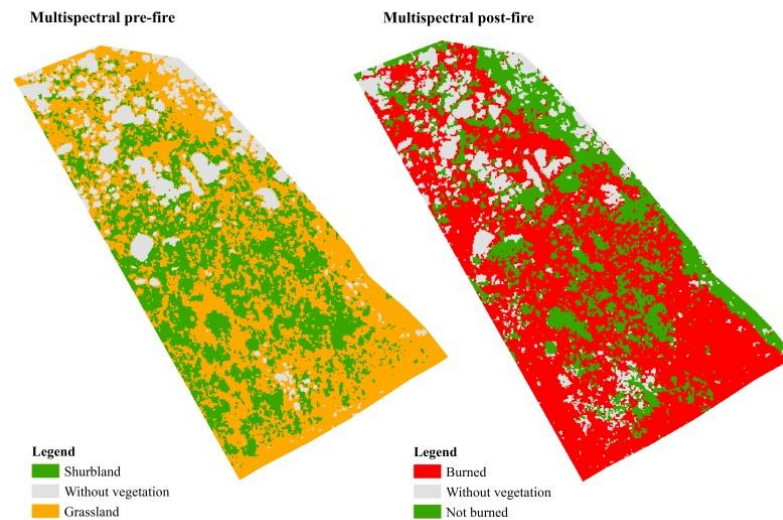
Source: from the author (2021).

The overall accuracy was 99.33% for orthomosaic postfire using the MLP algorithm (TABLE 1.12); in this case, the accuracy was the same using only spectral features and spectral added texture. We chose to use MLP trained with spectral metrics because of computational gain for not having to generate texture metrics. The map generated is shown in Figure 1.9.

Table 1.12 - Accuracy metrics for the third classification scheme.

| Classifier | Feature combination | Multispectral Post-fire | |
		Overall accuracy (%)	Kappa
MLP	> 0.5	99.33	0.99
	> 0.7	99.00	0.99
	> 0.7 + texture	99.33	0.99
RF	> 0.5	97.67	0.97
	> 0.7	98.67	0.98
	> 0.7 + texture	98.75	0.98

Source: from the author (2021).

Orthomosaic postfire was well classified, but some minor confusion occurred when one sample of burned and one of unburned vegetation were classified in the non-vegetated

category, and generated a user accuracy of 99% for these classes and 100% user accuracy for the non-vegetated class (TABLE 1.13).

Table 1.13 – Confusion matrix for MLP using > 0.5 feature combination in postfire data in third classification scheme.

	Classes	Reference data			Total	User's accuracy
		Shrubland	Non-vegetated	Grassland		
Classified data	Shrubland	99	1	0	100	99.00
	Non-vegetated	0	100	0	100	100.00
	Grassland	0	1	99	100	99.00
	Total	99	102	99	300	
	Producer's accuracy	100.00	98.04	100.00		
	Overall accuracy	99.33				
	Kappa	0.99				

Source: from the author (2021).

The area used to evaluate a prescribed fire was 0.183 ha, and 86.4% of this area was covered with vegetation before the fire event. A total of 27.3% of vegetation did not burn (TABLE 1.14) in the prescribed fire. As shown in Figure 1.6, many canopies remained alive, consistent with the purpose of low-intensity burning.

Table 1.14 - Area and its percentage for different vegetation classes for multispectral pre and post-fire.

Classes	Multispectral pre-fire		Classes	Multispectral post-fire	
	ha	%		ha	%
Grassland	0.096	52.5	Burned	0.107	58.5
Shrubland	0.062	33.9	Unburned	0.050	27.3
Without vegetation	0.025	13.7	Without vegetation	0.026	14.2
Total			0.183 ha		

Source: from the author (2021).

3. DISCUSSION

UAVs have considerable potential to improve environmental monitoring (MANFREDA et al., 2018), and their low flight altitude and speed enable the production of fine spatial resolution imagery (better than 20 cm) (ZHANG et al., 2016). Thus, multispectral and RGB UAV imagery acquired over a Campos de altitude phytophysiognomy in Itatiaia National Park was classified using machine learning and GEOBIA. The GEOBIA

segmentation process was used to generate appropriate image objects that corresponded to their respective vegetation classes. The machine learning algorithms, Random Forest and Artificial Neural Network, were used to classify these objects and were effective in separating vegetation classes and burned areas.

RF was used to reduce dimensionality, filtering irrelevant or redundant features from the dataset to avoid "the curse of dimensionality" that causes poor generalization (LIU; BELLET, 2019). Our results indicated that spectral features were more significant in discriminating different vegetation categories than the shape and texture features for all classification schemes.

Even though spectral metrics were the most frequent in Tables 1.2 and 1.3, our results confirm that the added value of texture metrics (GLCM derivatives) for RGB orthomosaic in the first classification scheme improves the accuracy by 0.33%. The inclusion of texture might facilitate the separability between classes because shrubs and grass show similar colours but different textures, and the deficiency in spectral information can be complemented by texture feature information (KWAK; NO-WOOK, 2019).

Despite this, this study demonstrated that the texture information derived from the matrix (GLCM) based on Haralick did not increase most of the final classification accuracy. Thus, spectral information was more useful than texture information.

In the first classification scheme, the shrubland class showed less assertiveness, with 95% user accuracy for RGB data and grassland with 96.5% for multispectral data, indicating relatively higher commission errors and therefore a potential wide definition of these classes in the classification.

In a study using RGB data to classify trees, shrubs, and grass, Ayhan and Kwan (2020) identified that shrubs are regarded as the most challenging shrub to classify correctly, consistent with our analyses.

The pattern of confusion between shrubs and grass in both orthomosaic analyses may be explained by high spatial resolution. As the spatial resolution becomes refined, the variance in spectral values inside land cover classes increases, and similarities in the brightness of this vegetation hamper their discrimination (LECHNER et al., 2012).

It is interesting to note that multispectral data showed superiority in an overall accuracy of 0.5% compared with RGB for the first classification scheme. These results were already expected because the multispectral data have NIR and red-edge bands that afford the highest distinctness between vegetation (NIJLAND et al., 2014). Most vegetation has a higher response in the near-infrared (NIR) and red-edge (approximately 717 nm) bands (TADDIA et

al., 2020). The absence of a NIR band potentially constrains the ability to discern vegetation from other nonvegetative land cover based on their spectral reflectance (HAMYLTON et al., 2020). Therefore, this lower accuracy is consistent with the lack of NIR and red-edge measurements with the RGB sensor.

However, the accuracy of the multispectral sensor data was slightly higher than that of RGB, which suggests that the three-band RGB works very well in distinguishing between vegetation types in *Campos de altitude*. This indicates that the higher spatial resolution of the RGB orthomosaic overcomes the limitations of the poor spectral resolution in discriminating and mapping vegetation (DÍAZ-VARELA et al., 2018).

Comparing the percentage of vegetation cover in the first scheme, we can observe that the non-vegetated class differed by only 0.1% between RGB and multispectral data, 15.8% and 15.7%, respectively, indicating the ability of the algorithms to identify this class. These results can be explained by the difference in the spectral response of the non-vegetated area coverage of vegetated areas, thus making it easier to differentiate by using the algorithms, helped by the use of indices, such as the VDVI, that are designed to extract green vegetation and the NDVI that enhances the vegetation, showing high values in regions of healthy vegetation and low values in regions of little or no vegetation (RHEW et al., 2011).

From the second scheme perspective, in prefire analyses, we obtained 92% user accuracy for the non-vegetated category, where some confusion with grassland cover occurred. This may have been due to some rocky outcrops having a similar colour to sparsely vegetated areas, included in the grass class. Therefore, as RGB does not have bands such as NIR and red-edge bands, this spectral distinction is more difficult. The same standard was detected in postfire orthomosaic, which showed 96% user accuracy for the non-vegetated category. On the other hand, the algorithm was able to achieve 100% user accuracy for the burned and unburned classes, probably because of the larger distinction between these two classes.

In terms of accuracy, we achieved satisfactory results for classification before (96.67%) and after (98.67%) the prescribed fire for RGB data. This was possible because the changes in the magnitude of spectral reflectance observed after fire can be measurable with visible wavelengths (red, green, and blue) (GUPTA; REINKE; JONES, 2013). A key point is that this promising result was obtained using a low-cost imagery solution.

We noted a distinction of 1.1% in the area in the non-vegetated category in the RGB pre- and postfire data, possibly because following the fire, the ash overlayed some areas, causing this percentage reduction.

Prescribed burning is a vegetation management tool that has been applied across the world for controlling fuel load, creating spatial discontinuities in vegetation, preventing large forest fires, and reducing fire risk, while controlled fire also offers managers the opportunity to manipulate diversity (MARINO et al., 2011; MCKENNA et al., 2019; PÉREZ-RODRÍGUEZ et al., 2020).

From a fuel perspective, following the prescribed fire, 14.8% of vegetation did not burn, and most of this percentage was composed of the canopies of the shrubs, especially those of *Cortaderia modesta* and *Machaerina ensifolia*, which are typically associated. According to Safford (2001), the dense tussocks of *C. modesta* provide protection and insulation from high temperatures and internal physical damage from fire.

This partial vegetation burn is a trait of the prescribed fire, and the vegetation is managed by controlling fire intensity to remove different percentages of fuel according to specific objectives (FERNANDES et al., 2013); consequently, this prescribed burn achieved this aim.

Several studies have been proving the effectiveness of controlled burning to cause a strong reduction of spatial continuity and surface fuel loads, leading to less fire-prone fuel, as a Schmidt et al. (2016) in wet grasslands in the Brazilian savanna; Fuentes; Duguy; Nadal-Sala (2018) in *Pinus halepensis* forest in Northeastern Spain; Carvajal-Ramírez et al. (2019) in a Mediterranean forest; Pérez-Rodríguez et al. (2020) in two prescribed fires that occurred in Spain.

Several studies have proven the effectiveness of controlled burning to cause a strong reduction in spatial continuity and surface fuel loads, leading to less fire-prone fuel, such as Schmidt et al. (2016) in wet grasslands in the Brazilian savanna; Fuentes, Duguy, Nadal-Sala (2018) in *Pinus halepensis* forest in northeastern Spain; Carvajal-Ramírez et al. (2019) in a Mediterranean forest; and Pérez-Rodríguez et al. (2020) in two prescribed fires that occurred in Spain.

Therefore, this test confirms the potential of UAV-RGB data to evaluate the effectiveness of fuel reduction and demonstrates that land managers can employ UAV technology for local fire management purposes.

Using multispectral data attached to MLP trained with spectral features to classify burned surfaces, we obtained 99.33% overall accuracy. The method showed a generally high agreement in the estimation of vegetation burned and unburned coverages. Different from the RGB result analysis, in this context, the non-vegetated category was better classified, with 100% user accuracy, in addition to the user accuracy of 99% in the two other classes; perhaps

this great outcome resulted from the additional bands, NIR, and red-edge that increased the spectral distinction.

Spectral changes due to fire effects can be observed in the electromagnetic spectrum. The burned surface demonstrates a slightly higher reflectance at the red edge and lower reflectance at the NIR band (CHUVIECO et al., 2006; SHIN et al., 2019), and the red-edge shift is known to be decreased vitality due to stress (SHIN et al., 2019) because the red edge is sensitive to the chlorophyll content in leaves, variability in leaf area, and soil background effects, which can be useful for fire damage detection (CARVAJAL-RAMÍREZ et al., 2019).

In other studies, Allison et al. (2016) and Samiappan et al. (2019) demonstrated the usefulness of multispectral bands for mapping the burned area extent and post-wildfire monitoring, which agreed with our results.

The controlled burn of this area resulted in the remaining vegetation, 27.3%, and many canopies remaining alive, as was observed in the RGB analysis, especially between the rocks and in firebreaks, consistent with the purpose of low-intensity burning. Prescribed fire is realized under specific conditions that are different from those that occur during the fire season. Thus, these burnings mainly impact surface fuels and understorey vegetation (FERNANDEZ-CARRILLO; MCCAW; TANASE, 2019), as was shown in this study. Corroborating McKenna et al. (2017) findings, the impacts of an experimental fire at the site were variable, leaving many areas unburned.

Therefore, images collected by UAVs that provide a spatial resolution of less than 1 m can be used to measure the efficacy of prescribed burnings and postfire management actions (FERNÁNDEZ-GUISURAGA et al., 2018).

The use of UAVs is a valuable tool for more cost-effective and efficient monitoring and management of natural resources in protected areas. Local and rapid changes, such as a wildfire or prescribed fire, can be easily detected and analysed using high and temporal-spatial resolution, thus offering an effective tool for management and conservation, assisting managers in decision-making.

A limitation regarding this study was the limited flight time of the UAV due to high energy consumption and the small number of available batteries (six), making it unfeasible for simultaneous image acquisition of large areas. Additionally, the location of the study area was difficult to access and precluded recharging the batteries.

Another limitation that we verified was the bias introduced through colour balancing generated by processing software in the RGB orthomosaics to reduce mosaic seam lines and vignetting. A study using an uncalibrated RGB camera is impracticable for realizing

radiometric correction and becomes limited for comparing repetitions carried out in different environmental condition changes and dates.

Despite the promising results we obtained in this study, for complementary studies, it is possible to use 3D point clouds generated by UAVs and apply these data as a feature in classification to obtain a better distinction between grass and shrubs. Moreover, multitemporal replication could also be used in the monitoring of vegetation recovery following the prescribed fire and ascertain the persistence in time of the scar, testing the maximum time after prescribed burning to conduct the UAV flight.

4. CONCLUSIONS

Our research demonstrates that both RGB and multispectral sensors performed well and enabled the discrimination of shrubs, grass, non-vegetated areas, and burned surfaces with errors in the classification lower than 10%. This confirms the suitability of this method for the detailed monitoring of vegetation cover and prescribed fire in Campos de altitude at a fine spatial resolution and represents a valuable tool for fire management applications.

Considering the accuracy figures obtained in this study, it is concluded that the prescribed fire impact on land cover was properly assessed with the proposed approach and confirmed the low-intensity burning required for fire best management practices.

As multispectral sensors are more expensive, the developed low-cost methodological approach using RGB images could provide an affordable alternative for land managers in protected areas. We demonstrated that habitat mapping and monitoring could be performed with high-spatial-resolution, true-colour images acquired from UAVs.

REFERENCES

AHMED, O. S. et al. Hierarchical land cover and vegetation classification using multispectral data acquired from an unmanned aerial vehicle. International **Journal of Remote Sensing**, v. 38, n. 8-10, p. 2037-2052, 2017.

ALLISON, R. S. et al. Airborne Optical and Thermal Remote Sensing for Wildfire Detection and Monitoring. **Sensors**, v. 16, n. 8, p. 1-29, 2016.

ALVES, D. P. et al. Artificial neural network for prediction of the area under the disease progress curve of tomato late blight. **Scientia Agricola**, v. 74, n. 1, p. 51–59, 2017.

ASHAPURE, A. et al. A Comparative Study of RGB and Multispectral Sensor-Based Cotton Canopy Cover Modelling Using Multi-Temporal UAS Data. **Remote Sensing**, v. 11, n. 23, p. 1-18, 2019.

ASSMANN, J. J. et al. Vegetation monitoring using multispectral sensors – best practices and lessons learned from high latitudes. **Journal of Unmanned Vehicle Systems**, v. 7, p. 54–75, 2019.

AXIMOFF, I.; ALEVES, R.G.; RODRIGUES, R.C. Campos de altitude do Itatiaia: aspectos ambientais, biológicos e ecológicos. **Boletim do Parque Nacional do Itatiaia**, Rio de Janeiro, n. 18, 74p., 2014.

AYHAN, B.; KWAN, C. Tree, Shrub, and Grass Classification Using Only RGB Images. **Remote Sensing**, v. 12, n. 8, p. 1-20, 2020.

BAATZ, M.; SCHAPE, A. Multiresolution segmentation: an optimization approach for high quality multi-scale image segmentation. **Journal of Photogrammetry and Remote Sensing**, v. 58, p. 12-23, 2000.

BARNES, E.M. et al. Coincident detection of crop water stress, nitrogen status and canopy density using ground-based multispectral data. In: 5th International Conference on Precision Agriculture and other resource management, 2000. **Proceedings** […] Bloomington, USA, 2000.

BARRERO, O.; PERDOMO, S. A. RGB and multispectral UAV image fusion for Gramineae weed detection in rice fields. **Precision Agriculture**, v. 19, p. 809-822, 2018.

BENZ, U. et al. Multi-resolution, object oriented fuzzy analysis of remote sensing data for GIS-ready information. **ISPRS Journal of Photogrammetry and Remote Sensing,** v.58, p. 239–258, 2004.

BREIMAN, L. Random forests. **Machine Learning**, v. 45, n. 1, p. 5–32, 2001.

BELGIU, M.; DRĂGUȚ, L. Random Forest in Remote Sensing: A Review of Applications and Future Directions. **ISPRS Journal of Photogrammetry and Remote Sensing**, v. 114, p. 24–31, 2016.

CANDIAGO, S. et al. Evaluation multispectral images and vegetation indices for precision farming applications from UAV images. **Remote Sensing**, v. 7, n. 4, p. 4026–4047, 2015.

CARVAJAL-RAMÍREZ, F. et al. Evaluation of Fire Severity Indices Based on Pre- and Post-Fire Multispectral Imagery Sensed from UAV. **Remote Sensing**, v. 11, n. 9, p. 1-19, 2019.

CHUVIECO, E. et al. Use of a Radiative Transfer Model to Simulate the Postfire Spectral Response to Burn Severity. **Journal of Geophysical Research: Biogeosciences**, v. 111, p. 1-15, 2006.

CHUVIECO, E. et al. Historical background and current developments for mapping burned area from satellite Earth observation. **Remote Sensing of Environment**, v. 225, p. 45-64, 2019.

COHEN, J. A coefficient of agreement for nominal scales. **Educational and Psychological Measurement**, v. 20, n. 1, p. 37–46. 1960.

COLOMINA, I.; MOLINA, P. Unmanned aerial systems for photgrammetry and remote sensing: A review. **ISPRS Journal of Photogrammetry and Remote Sensing,**v. 92, 79–97, 2014.

CONGALTON, R. G.; GREEN, K. **Assessing the accuracy of remotely sensed data**: Principles and Practices. 3. ed. Boca Raton: Crc Press, 2019. 346 p.

DE CASTRO, A. I. et al. An automatic random forest-obia algorithm for early weed mapping between and within crop rows using UAV imagery. **Remote Sensing**, v. 10, n. 2, p. 1-21, 2018.

DÍAZ-VARELA, R. A. et al. Sub-metric analisis of vegetation structure in bog-heathland mosaics using very high resolution rpas imagery. **Ecological Indicators**, v. 89, p. 861–873, 2018.

DUARTE-CARVAJALINO, J. M. et al. Evaluating Late Blight Severity in Potato Crops Using Unmanned Aerial Vehicles and Machine Learning Algorithms. **Remote Sensing**, v. 10, n. 10, p. 1-17, 2018.

ESCH, T. et al. Improvement of image segmentation accuracy based on multiscale optimization procedure. **IEEE Geoscience and Remote Sensing Letters**, v. 5, p. 463–467, 2008.

FENG, Q.; LIU, J.; GONG, J. UAV Remote Sensing for Urban Vegetation Mapping Using Random Forest and Texture Analysis. **Remote Sensing**, v. 7, n. 1, p. 1074–1094, 2015.

FERNÁNDEZ-GUISURAGA, J. M. et al. Using Unmanned Aerial Vehicles in Postfire Vegetation Survey Campaigns through Large and Heterogeneous Areas: Opportunities and Challenges. **Sensors**, v. 18, p. 1-17, 2018.

FERNANDEZ-CARRILLO, A.; MCCAW, L.; TANASE, M.A. Estimating prescribed fire impacts and post-fire tree survival in eucalyptus forests of Western Australia with L-band SAR data. **Remote Sensing of Environment**, v. 224, p. 133–144, 2019.

FERNANDES, P. M. et al. Prescribed burning in southern Europe: developing fire management in a dynamic landscape. **Frontiers in Ecology and the Environment**, v. 11, n. s1, p. e4-e14, 2013.

FRANKLIN, S. E.; AHMED, O. S. Deciduous tree species classification using object-based analysis and machine learning with unmanned aerial vehicle multispectral data. **International Journal of Remote Sensing**, v. 39, n. 15-16, p. 5236–5245, 2017.

FREEMAN, P.K.; FREELAND, R.S. Agricultural UAVs in the US: Potential, policy, and hype. Remote Sensing Applications: Society and Environment, v. 2, p. 35–43, 2015.

FUENTES, L.; DUGUY, B.; NADAL-SALA, D. Short-term effects of spring prescribed burning on the understory vegetation of a Pinus halepensis forest in Northeastern Spain. **Science of The Total Environment**, v. 610-611, p. 720-731, 2018.

GAŠPAROVIĆ, M. et al. An automatic method for weed mapping in oat fields based on UAV imagery. **Computers and Electronics in Agriculture**, v. 173, p. 1-12, 2020.

GAO, J. et al. Fusion of pixel and object-based features for weed mapping using unmanned aerial vehicle imagery. **International Journal of Applied Earth Observation and Geoinformation,** v. 67, p. 43–53, 2018.

GITELSON, A. A. et al. Remote sensing estimation of canopy chlorophyll content in crops. **Geophysical. Research Letter**, v. 32, p. 1-4, 2005.

GONÇALVES, J. et al. Evaluating an unmanned aerial vehicle-based approach for assessing habitat extent and condition in fine-scale early successional mountain mosaics. **Applied Vegetation Science**, v. 19, p. 132–146, 2016.

GUPTA, V.; REINKE, K.; JONES, S. Changes in the spectral features of fuel layers of an Australian dry sclerophyll forest in response to prescribed burning. **International Journal of Wildland Fire**, v. 22, n. 6, p. 862-868, 2013.

HAMYLTON, S. M. et al. Evaluating techniques for mapping island vegetation from unmanned aerial vehicle (UAV) images: Pixel classification, visual interpretation and machine learning approaches. **International Journal of Applied Earth Observation and Geoinformation**, v. 89, p. 1-14, 2020.

HARALICK, R.M.; SHANMUGAM, K.; DINSTEIN, I. Textural features for image classification. **IEEE Transactions on Systems,** v. SMC-3; n. 6, p. 610–621, 1973.

HU, L. et al. Monitoring housing rental prices based on social media: An integrated approach of machine-learning algorithms and hedonic modeling to inform equitable housing policies. **Land Use Policy**, v. 82, p. 657–673, 2019.

ICMBio – Instituto Chico Mendes de Biodiversidade. **Plano de Manejo Parque Nacional do Itatiaia Revisão – Encarte 3**. Brasília, 215p., 2014. Available: http://www.icmbio.gov.br/portal/component/content/article?id=2181:parna-do-itatiaia.

IIZUKA, K. et al. Modeling Future Urban Sprawl and Landscape Change in the Laguna de Bay Area, Philippines. **Land, v.** 6, n. 26, p. 1-21, 2017.

IIZUKA, K. et al. Advantages of unmanned aerial vehicle (UAV) photogrammetry for landscape analysis compared with satellite data: A case study of postmining sites in Indonesia. **Cogent Geoscience**, v. 4, n. 1, p. 1-15, 2018.

KULKARNI, A.D.; LOWE, B. Random Forest Algorithm for Land Cover Classification. **International Journal on Recent and Innovation Trends in Computing and Communication**, v. 4, n. 3, p. 58 – 63, 2016.

KWAK, G.; NO-WOOK, P. Impact of Texture Information on Crop Classification with Machine Learning and UAV Images. **Applied Sciences**, v. 9, n. 4, p. 1-17, 2019.

LALIBERTE, A. S. et al. Acquisition, orthorectification, and object-based classification of unmanned aerial vehicle (UAV) imagery for rangeland monitoring. **Photogrammetric Engineering & Remote Sensing**, v. 76, n. 6, p. 661-672, 2010.

LARRINAGA, A. R.; BROTONS, L. Greenness Indices from a Low-Cost UAV Imagery as Tools for Monitoring Post-Fire Forest Recovery. **Drones**, v. 3, n. 1, p. 1-16, 2019.

LAWRENCE, R. L.; WOOD, S. D.; SHELEY, R. L. Mapping invasive plants using hyperspectral imagery and Breiman Cutler classifications (RandomForest). **Remote Sensing of Environment**, v. 100, n. 3, p. 356–362, 2006.

LECHNER, A. M. et al. Characterising Upland Swamps Using Object-Based Classification Methods and Hyper-Spatial Resolution Imagery Derived From an Unmanned Aerial Vehicle. In: ISPRS Annals of the Photogrammetry, Remote Sensing and Spatial Information Sciences, v. 4, p. 101–106, 2012. **Proceedings** […] Melbourne, Australia, 2012.

LEI MA. et al. Evaluation of Feature Selection Methods for Object-Based Land Cover Mapping of Unmanned Aerial Vehicle Imagery Using Random Forest and Support Vector Machine Classifiers. **International Journal of Geo-Information**, v. 6, n. 2, p. 1-21, 2017.

LIAN, C. et al. Multiple neural networks switched prediction for landslide displacement. **Engineering Geology**, v. 186, p. 91–99, 2015.

LIU, K.; BELLET, A. Escaping the curse of dimensionality in similarity learning: Efficient Frank-Wolfe algorithm and generalization bounds. **Neurocomputing**, v. 333, p. 185–199, 2019.

MAGALLANES, S. R. S. et al. Immediate Effects of Prescribed Burning on Chemical Properties of the Cerrado Soil. **Floresta e Ambiente**, v. 27, n. 3, p. 1-6, 2020.

MAMAGHANI, B.; SALVAGGIO, C. Multispectral Sensor Calibration and Characterization for sUAS Remote Sensing. **Sensors**, v. 19, n. 20, p. 1-29, 2019.

MANFREDA, S. et al. On the Use of Unmanned Aerial Systems for Environmental Monitoring. **Remote Sensing**, v. 10, n. 4, p. 1-28, 2018.

MARINO, E. et al. Fire hazard after prescribed burning in a gorse shrubland: Implications for fuel management. **Journal of Environmental Management**, v. 92, n. 3, p. 1003–1011, 2011.

MATESE, A. et al. Intercomparison of UAV, aircraft and satellite remote sensing platforms for precision viticulture. **Remote Sensing**, v. 7, n. 3, p. 1-28, 2015.

MCKENNA, P. et al. Measuring fire severity using UAV imagery in semi-arid central Queensland, Australia. **International Journal of Remote Sensing**, v. 38, n. 14, p. 4244–4264, 2017.

MCKENNA, P. et al. Response of open woodland and grassland mine site rehabilitation to fire disturbance on engineered landforms. **Ecological Engineering**, v. 133, p. 98–108, 2019.

MICHEZ, A. et al. Mapping of riparian invasive species with supervised classification of Unmanned Aerial System (UAS) imagery. International **Journal of Applied Earth Observation and Geoinformation**, v. 44, p. 88–94, 2016.

NEVALAINEN, O. et al. Individual Tree Detection and Classification with UAV-Based Photogrammetric Point Clouds and Hyperspectral Imaging. **Remote Sensing**, v. 9, n. 3, p. 1-34, 2017.

NIJLAND, W. et al. Monitoring plant condition and phenology using infrared sensitive consumer grade digital cameras. **Agricultural and Forest Meteorology**, v. 184, p. 98–106, 2014.

PALACE, M. et al. Determining subarctic peatland vegetation using an unmanned aerial system (UAS). **Remote Sensing**, v. 10, n. 9, p. 1-20, 2018.

PEÑA, J. et al. Object-based image classification of summer crops with machine learning methods. **Remote Sensing**, v. 6, p. 5019–5041, 2014.

PÉREZ-RODRÍGUEZ, L. A. et al. Evaluation of Prescribed Fires from Unmanned Aerial Vehicles (UAVs) Imagery and Machine Learning Algorithms. **Remote Sensing**, v. 12, n. 8, p. 1-11, 2020.

PÉREZ-ORTIZ, M. et al. Selecting patterns and features for between-and withincrop-row weed mapping using UAV-imagery. **Expert Systems with Application**s, v. 47, p. 85–94, 2016.

PIVELLO, V. R. et al. Understanding Brazil's catastrophic fires: Causes, consequences and policy needed to prevent future tragedies. **Perspective in Ecology and Conservation**, v. 19, n. 3, p. 233-255, 2021.

RÄSÄNEN, A. et al. What makes segmentation good? A case study in boreal forest habitat mapping. **International Journal of Remote Sensing**, v. 34, n. 23, p. 8603–8627, 2013.

REZAEIAN, M.; AMIRFATTAHI, R.; SADRI, S. Semantic segmentation of aerial images using fusion of color and texture features. **Journal of Computing and Security**, v. 1, n. 3, p. 225-238, 2014.

RHEW, I. C. et al.Validation of the Normalized Difference Vegetation Index as a Measure of Neighborhood Greenness. **Annals of Epidemiology**, v. 21, n. 12, p. 946–952, 2011.

RODRIGUEZ-GALIANO, V. F. et al. An assessment of the effectiveness of a random forest classifier for land-cover classification. **ISPRS Journal of Photogrammetry and Remote Sensing**, v. 67, p. 93–104, 2012.

ROUSE, J. W. et al. Monitoring vegetation systems in the Great Plains with ERTS, In: S.C. Freden, E.P. Mercanti, and M. Becker. Third Earth Resources Technology Satellite–1 Syposium. **Proceedings** […] volume I: Technical Presentations, NASA SP-351, NASA, Washington, D.C., p. 309-317, 1974.

SAFFORD, H. D. Brazilian páramos I. An introduction to the physical environment and vegetation of the *campos de altitude*. **Journal of Biogeography**, v. 26, p. 693-712, 1999.

SAFFORD, H. D. Brazilian Páramos III: Patterns and Rates of Postfire Regeneration in the Campos de altitude. **Biotropica**, v. 33, n. 2, p. 282-302, 2001.

SAMIAPPAN, S. et al. Remote Sensing of Wildfire Using a Small Unmanned Aerial System: Post-Fire Mapping, Vegetation Recovery and Damage Analysis in Grand Bay, Mississippi/Alabama, USA. **Drones**, v. 3, n. 2, p. 1-18, 2019.

SCHMIDT, I. B. et al. Implementação do Programa Piloto de Manejo Integrado do Fogo em três Unidades de Conservação do Cerrado. **Biodiversidade Brasileira**, v. 6, n. 2, p. 55-70, 2016.

SHIN, J. et al. Using UAV Multispectral Images for Classification of Forest Burn Severity— A Case Study of the 2019 Gangneung Forest Fire. **Forests**, v. 10, n. 11, p. 1-15, 2019.

STEFANSKI, J.; MACK, B.; WASKE, B. Optimization of Object-Based Image Analysis With Random Forests for Land Cover Mapping. **IEEE Journal of Selected Topics in Applied Earth Observations and Remote Sensing**, v. 6, n. 6, p. 1-13, 2013.

STUMPF, A.; KERLE, N. Object-oriented mapping of landslides using Random Forests. **Remote Sensing of Environment,** v. 115, n. 10, p. 2564–2577, 2011.

TADDIA, Y. et al. Multispectral UAV monitoring of submerged seaweed in shallow water. **Applied Geomatics**, v. 12, p. 19-34, 2020.

TORRES-SÁNCHEZ, J. et al. Imagery from unmanned aerial vehicles for early site specific weed management. In: European Conference on Precision Agriculture 2013. **Proceedings** […] Wageningen, The Netherlands: Wageningen Academic Publishers, 2013.

TUCKER, C. J. Red and photographic infrared linear combinations for monitoring vegetation. **Remote Sensing of Environment**, v. 8, n. 2, p. 127–150, 1979.

VAILLANT, N. M.; FITES-KAUFMAN, J. A.; STEPHENS, S. L. Effectiveness of prescribed fire as a fuel treatment in Californian coniferous forests. **International Journal of Wildland Fire**, v. 18, n. 2, p. 165–175, 2009.

VELOSO, H.P.; RANGEL FILHO, A.L.R.; LIMA, J.C.A. **Classificação da vegetação brasileira, adaptada a um sistema universal**. Rio de Janeiro: IBGE, Departamento de Recursos Naturais e Estudos Ambientais, 124p., 1991.

VENTURI, S. et al. Unmanned aerial vehicles and Geographical Information System integrated analysis of vegetation in Trasimeno Lake, Italy. **Lakes and Reservoirs: Research and Management**, v. 21, p. 5– 19, 2016.

VERRELST, J. et al. Angular sensitivity analysis of vegetation indices derived from chris/proba data. **Remote Sensing of Environment**, v. 112, n. 5,p. 2341–2353, 2008.

WANG, J. et al. Maximum weight and minimum redundancy: a novel framework for feature subset selection. **Pattern Recognition,** v. 46, n. 6, p. 1616–1627, 2013.

WANG, X. et al. Extraction of vegetation information from visible unmanned aerial vehicle images. **Transactions of the Chinese Society of Agricultural Engineering**, v. 31, n. 5, p. 152–159, 2015.

WOEBBECKE, D. M. et al. Color indexes for weed identification under various soil, residue, and lighting conditions. **Transactions of the ASAE**, v. 38, n. 1, p. 259–269, 1995.

XU, Z. et al. Tree species classification using UAS-based digital aerial photogrammetry point clouds and multispectral imageries in subtropical natural forests. **International Journal of Applied Earth Observation and Geoinformation**, v. 92, p. 1-14, 2020.

YANG, M-D. et al. Spatial and Spectral Hybrid Image Classification for Rice Lodging Assessment through UAV Imagery. **Remote Sensing**, v. 9, n. 6, p. 1-19, 2017.

YAO, H.; QIN, R; CHEN, X. Veículo Aéreo Não Tripulado para Aplicações de Sensoriamento Remoto - Uma Revisão. **Remote Sensing**, v. 11, n. 12, p. 1-22, 2019

YU, Q. et al. Object-based Detailed Vegetation Classification with Airborne High Spatial Resolution Remote Sensing Imagery. **Photogrammetric Engineering & Remote Sensing**, v. 72, n. 7, p. 799-811, 2006.

ZHANG, H., FRITTS, J.E.; GOLDMAN, S.A. Image Segmentation Evaluation: A Survey of Unsupervised Methods. **Computer Vision and Image Understanding**, v. 110, n. 2, p. 260–280, 2008.

ZHANG, J. et al. Seeing the forest from drones: Testing the potential of lightweight drones as a tool for long-term forest monitoring. **Biological Conservation**, v. 198, p. 60–69, 2016.

ZHENG, H. et al. Evaluation of RGB, Color-Infrared and Multispectral Images Acquired from Unmanned Aerial Systems for the Estimation of Nitrogen Accumulation in Rice. **Remote Sensing**, v. 10, n. 6, p. 1-17, 2018.

ZYLSHAL, et al. A support vector machine object based image analysis approach on urban green space extraction using Pleiades-1A imagery. **Modeling Earth Systems and Environment**, v. 2, n. 54, p. 1:12, 2016.

ARTICLE 2 - Effectiveness of using remote sensing data to identify wildfires in Brazilian protected areas

Abstract

Protected areas have been experiencing increasingly frequent wildfires that influence strategies for conserving biodiversity and reducing habitat loss rates. Therefore, the accurate quantitative and qualitative spatiotemporal mapping of wildfires is valuable to improve our knowledge of drivers behind fire occurrences and to analyse the impact of fire on vegetation. The purpose of this research was to evaluate the effectiveness and availability of Landsat-8 and Sentinel-2 images to identify burned areas in Itatiaia National Park (INP). We applied the shape, theme, edge and position (STEP) method, an object-based similarity matrix, to assess the geometric and thematic similarity of burned scars. This analysis was performed to evaluate which satellite, Landsat or Sentinel, produces accurate similarity compared with the fire occurrence record (FOR). In addition, we conducted fire recurrence analysis to improve knowledge of spatiotemporal patterns of wildfires. We found that a higher recurrence of fire occurred in the buffer area, especially in the lower part of INP and near rural communities. Moreover, medium spatial resolution remote sensing images can be used to increase the accuracy of fire detection in protected areas.

Keywords: Satellite imagery. Landsat. Sentinel. STEP method. Burned area. Itatiaia National Park.

1. INTRODUCTION

In Brazil, one-third of its territory is classified as protected areas (PAs) regulated and managed by federal, state, or municipal governments that include nature reserves forming three categories of protection: the strictest level of protection; areas reserved for sustainable use; and indigenous land (OLIVEIRA et al., 2017).

Protected areas are essential strategies for conserving biodiversity, reducing habitat loss rates, and maintaining their integrity (D'AMICO et al., 2020; GRAY et al., 2016; BUTCHART et al., 2012; MARGULES; PRESSEY; WILLIAMS, 2002). These areas are important because they are designed to protect representative portions of different types of natural landscapes that help sustain life on Earth while providing many benefits to humans (FIGUEROA; SÁNCHEZ-CORDERO, 2008). However, protected areas have been experiencing increasingly frequent wildfires, as fire regimes are changing due to human activities, warming temperatures and shifting precipitation patterns (HALOFSKY; PETERSON; HARVEY, 2020; BOWMAN et al., 2020).

Forest fires are widely recognized as one of the most critical environmental disturbances because they affect atmospheric chemistry, with aerosols and greenhouse gas emissions (KNORR; JIANG; ARNETH, 2016); reduce biodiversity and water retention; and cause soil degradation and erosion through a series of modifications in their physical,

chemical and biological nature (SANSEVERO et al., 2017; REDIN et al., 2011; CHUVIECO et al., 2010).

On the other hand, fire is a natural phenomenon in many ecosystems, helping to promote diversity, maintain integrity and species composition, and contribute to natural regeneration (KELLY; BROTONS, 2017; ODION et al., 2014), and its suppression can cause a reduction in the diversity of plant species (BOND; KEELEY, 2005).

Therefore, the accurate quantitative and qualitative spatiotemporal mapping of wildfires is valuable to improve our knowledge about the drivers behind fire occurrences and to analyse the impact of fire on vegetation with the purpose of relieving current and future effects of biomass burning (BAR; PARIDA; PANDEY, 2020; FORKEL et al., 2019). In addition, this information provides aid for policy-makers and firefighters to guarantee effective and organized fire management actions (PIROMAL et al., 2008).

There are several methods to map burned areas and to generate reliable information, such as conventional methods based on extensive field visits and the use of satellite imagery. In protected areas in Brazil, the conventional method in which data are collected in situ using GPS is mostly used, but these data are often prone to error, incomplete, and limited because of inconsistent collection efforts over space and time, introducing much uncertainty (CHUVIECO et al., 2019).

Earth observations have been widely used for the assessment, mapping and monitoring of burned areas in recent decades as an alternative for compiling more trustworthy information (CHUVIECO et al., 2019). Burned area analyses are normally realized for large areas and mostly use a coarse spatial resolution (with pixels larger than 250 m); for example, products derived from Advanced Very High Resolution Radiometer (AVHRR) images with a spatial resolution of approximately 1.21 km2 at nadir (CARMONA-MORENO et al., 2005); Land Long Term Data Record (LTDR) with a 5 km pixel size (MORENO RUIZ et al., 2014; MORENO RUIZ et al., 2012); Fire CCI that is available at a 250 m pixel size (CHUVIECO et al., 2018); and Moderate Resolution Imaging Spectroradiometer (MODIS)-derived burn area products are available at a global scale with 500 m pixel size (MCD64A1) (GIGLIO et al., 2018).

However, to detect and estimate small fire patches and to obtain more precise and accurate data, medium to higher spatial and temporal resolutions are necessary. This became possible after the free availability of Landsat and Sentinel data, initiating a new era for land resource monitoring (ROY et al., 2014; DRUSCH et al., 2012), which enabled the

development of procedures for detailed and prompt postfire mapping (SMIRAGLIA et al., 2020).

In this study, we evaluated the effectiveness and availability of satellite imagery (Landsat-8 and Sentinel-2) to identify burned areas, motivating refinement of the fire occurrence records (FOR) of protected areas.

The specific objectives were: (i) to map wildfires within and surrounding the Itatiaia National Park between 2013 and 2018, (ii) characterize the occurrence and recurrence of wildfires between 2013 and 2018, (iii) to compare fire scars derived from remote sensing and field measurements.

2. MATERIALS AND METHODS

2.1. Study site

The Itatiaia National Park (INP) is a protected area located in the Atlantic rainforest in the Mantiqueira Complex (22°19'–22°45'S and 44°45'–44°50'W); it covers an area of approximately 30,000 ha plus a 3 km buffer zone extending outward from the reserve boundary (FIGURE 2.1). This buffer aims to protect INP surroundings, decreasing negative impacts. It was the first national park established in Brazil in 1937 and is composed of four municipalities, Resende and Itatiaia in Rio de Janeiro state and Bocaina de Minas and Itamonte in Minas Gerais state (ICMBio, 2014).

The phytophysiognomy of the INP is composed of *Campos de altitude* (high altitude grasslands, above 2000 m. a.s.l.), dense ombrophilous forest (submontane, montane, and high-montane), montane mixed ombrophilous forest (with Araucaria trees) and montane semideciduous forest (ICMBio, 2014).

The elevation varies between 600 m and 2,791 m a.s.l. at its peak, Agulhas Negras. The climate is influenced by this altitude variation, and is classified by Koppen as Cwb at elevations above 1,600 m a.s.l., with 1 to 3 months of drought per year. In addition, in the lower part of the park, climate is classified as Cpb, with precipitation distributed throughout the year. It ranges from 1,250 mm to 2,500 mm, and the temperature varies from 13 °C to 21 °C (ICMBio, 2014).

Figure 2.1 - Location of the study area, Itatiaia National Park, state of Minas Gerais and Rio de Janeiro, Brazil.
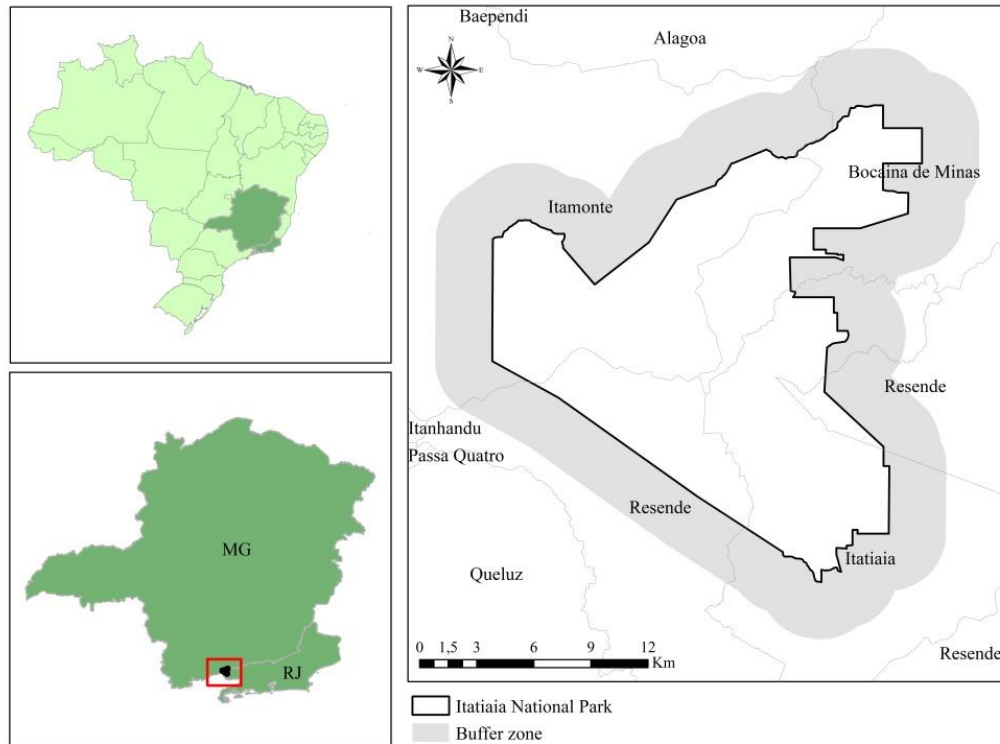
Source: from the author (2021).

2.2. Database

The database was composed by: (i) Fire Occurrence Record (FOR); (ii) remote sensing images; and (iii) hotspot datasets.

2.2.1. Fire Occurrence Record (FOR)

The FOR is an official dataset of fire that has occurred within Brazilian protected areas, available from the National Center to Prevent and Combat Forest Fire (PREVFOGO), associated with the Brazilian Institute of the Environment and Renewable Natural Resources (IBAMA). It was created in the 1990s to systematize fire occurrence and to gather information for the development of prevention and minimization strategies for the occurrence of wildfires in protected areas (BONTEMPO et al., 2011). In 2007, the Chico Mendes Institute (ICMBio) was established and became responsible for the formation of a database of the National Information System on Fire (SISFOGO); since then, only some protected areas have continued to use FOR.

In the Itatiaia National Park, FOR data have been collected *in situ* by firefighters since 2008 using the global position system (GPS) in a GIS environment. For this study, we used annual shapefiles containing wildfire information as the geolocation of occurrence and the

quantification of the burned area. This method of recording, despite being widely used by protected area managers in Brazil, may have some inaccuracy in estimating the burned area (SANTOS et al., 2018).

The FOR polygons were used as ground information regarding wildfires that occurred in the INP between 2013 and 2018 and were confronted with images from Landsat-8, Sentinel-2, and the hotspot dataset of Brazil's National Institute for Space Research (INPE).

2.2.2. Remote sensing images

In this study, we used images from two different satellites, Landsat and Sentinel. The Landsat program has been collecting Earth data for over four decades. The Operational Land Imager (OLI) aboard Landsat-8 generates images with 30 m and 60 m spatial resolution and 16-day revisit mission (WULDER et al., 2019).

The Landsat-8 OLI images (surface reflectance) were get using the Google Earth Engine (GEE) platform, which allows greater agility and efficient geospatial analyses since its processing is performed in cloud computing (GORELICK et al., 2017). Thus, a visual analysis of the images was performed annually to choose those that fit into the study period with the lowest cloud cover (TABLE 2.1).

Table 2.1 - Landsat-8 and Sentinel-2 images (dates) were used in this study.

Year	Landsat-8		Sentinel-2	
	Time 1	Time 2	Time 1	Time 2
2013	08/07/2013	10/09/2013	-	-
2014	05/06/2014	13/09/2014	-	-
2015	14/07/2015	31/08/2015	-	-
2016	14/06/2016	07/12/2016	16/06/2016	26/07/2016
2017	05/09/2017	21/092017	26/07/2017	13/11/2017
2018	06/07/2018	24/09/2018	22/05/2018	24/09/2018

Source: from the author (2021).

The Sentinel-2 constellation is part of the Copernicus Programme by the European Space Agency (ESA) and the European Union (EU), specifically designed for monitoring vegetation cover, climate change, and disaster events. Sentinel-2 provides a 5-day revisit at a spatial resolution of 10 m to 60 m (DRUSCH et al., 2012; PHIRI et al., 2020). In addition, it includes red-edge and water vapour spectral bands that are not available in OLI data.

Due to the Sentinel-2A launch date, June 2015, the images used in this study were from 2016. Sentinel-2 images with atmospheric correction in GEE were only available as of December 2018 at the time of this study. Thus, similar to Landsat-8, images with lower cloud cover were analysed and chosen (TABLE 2.1), and these scenes were acquired from their website: https://scihub.copernicus.eu/dhus/#/home. The images were available in reflectance at the top of the atmosphere and were corrected for surface reflectance using SNAP software.

For the purpose of identifying burned scars included in INP in the remote sensing images (Landsat-8 and Sentinel-2), spectral indices were calculated. As wildfires typically cause alteration in reflectance, for example, a decrease in near-infrared (NIR) due to vegetation removal and transformation of vegetation material to charcoal (FASSNACHT et al., 2021), indices were derived from these spectral relationships. The normalized burn ratio index (NBR) (KEY; BENSON, 2006) (Equation 1) was generated for two moments, before and after fire occurrences per year, and highlighted the areas with fires (TRAN et al., 2018).

$$NBR= \frac{NIR\text{-}SWIR}{NIR\text{+}SWIR} \qquad\qquad (1)$$

where: NIR= near-infrared; $SWIR$= short wave infrared.

NIR and SWIR bands are frequently used because NIR naturally reacts positively to foliar area and productivity and SWIR reacts positively to drought and non-vegetated surfaces (KEY; BENSON, 2006).

The differentiated normalized burn ratio (dNBR) (Equation 2) was used to assist the mapping of burned areas. This index is calculated by subtraction of NBR from time 1 to time 2 and generates great visualization of the scar left by the fire in the landscape. The dNBR is broadly used to discriminate burned areas and estimate vegetation burn severity (KEY; BENSON, 2006; FASSNACHT et al., 2021).

$$dNBR=NBR_{time1}\text{-}\ NBR_{time2} \qquad\qquad (2)$$

The values of both indices vary between −1 and 1. Negative NBR values close to zero indicate areas where there is little or no chlorophyll activity, such as bare soil or areas affected by wildfires. Closer to one represents vegetated areas (CHUVIECO; MARTIN; PALACIOS, 2002; ESCUIN; NAVARRO; FERÁNDEZ, 2008). A dNBR value close to one indicates a

severe impact from fire, while areas with negative values may indicate regrowth since fire (KEY; BENSON, 2006).

Therefore, after obtaining the dNBR maps from 2013 to 2018, the identification and delineation of the burned areas were realized using the density slice method, which divides the range of brightnesses in a single band into intervals and enhances determined features (CAMPBELL; WYNNE, 2011), such as wildfires in this case. Afterward, visual interpretation by a specialist in a GIS environment was realized to filter the data obtained. Despite the large time consumption, the process is considered somewhat simple and allows reliable results to be obtained (BASTARRIKA; CHUVIECO; MARTÍN, 2011).

2.3. HotSpot Dataset

The hot-pixel data between 2013 and 2018 in INP were obtained from the National Institute for Space Research (INPE), available at www.inpe.br/queimadas/bdqueimadas. We used data from all polar and geostationary satellites present on the platform. Field validation indicated that wildfires 30 m long by 1 m wide or larger were detected by polar orbiting satellites and that fire fronts must have been twice the size to be located by geostationary satellites (INPE, 2021).

The data are composed of a shapefile in vector format that contains points that represent the hotspots monitored daily. Repeated information from the same fire was removed before the analysis because, in a large wildfire, a group of adjacent pixels may be referred to as a single fire. These hotspot datasets were used for comparison with remote sensing maps and fire occurrence records.

2.4. Similarity assessment

In this study, we applied the STEP (Shape, Theme, Edge and Position) method, an object-based similarity matrix proposed by Lizarazo (2014), to assess the geometric and thematic characteristics of burn scars that occurred in INP. This analysis was conducted to compare fire monitoring inputs derived from remote sensing and *in situ* surveys.

STEP uses samples of reference and classified objects to evaluate similarity metrics. First, it needs a set of ground situations (reference objects); in this case, the FOR was used. In a second step, these data are overlaid with the samples of classified objects generated by visual interpretation of Landsat and Sentinel images. Therefore, all classified objects that intersect with the reference are selected.

Thematic quality was determined by theme similarity (T), which refers to a certain class and quantifies the area percentage of the classified object that corresponds to the class of the reference object. Geometric quality was evaluated by the edge (E), shape (S) and position (P) indices. Edge similarity compares the boundaries of the objects (internal and external), computing the percentages of the reference object's boundary concurring with the classified object's boundary. Shape similarity compares the geometry of reference and classified objects considering a compactness index. Position similarity evaluates the centroid position of classified and reference objects. Values of STEP similarity indices range from 0-1, where 0 refers to objects without similarity, and 1 indicates that there is total agreement (LIZARAZO, 2014).

The indices of similarity are generated for the individual objects and presented in a matrix in which columns indicate the classified objects and rows indicate the reference objects. This individual matrix can be aggregated by thematic class, resulting in a new matrix that expresses the integrated STEP similarity matrix, with rows and columns corresponding to the thematic classes.

2.5. Fire recurrence

Fire recurrence analysis was performed from 2013 to 2018 using annual summarized maps containing the delineated scars obtained with Landsat-8 and FOR data. The polygons were grouped by year, resulting in six layers, and fire recurrence maps were obtained by proximity analysis called spaghetti and meatballs (DIN, 2020) from the GIS. In this procedure, polygons from different years are overlaid for measuring the frequency and extend of fire occurrence overlaps. Fire recurrence is correlated with the severity of future wildfires because it affects the availability of fuel in the area.

3. RESULTS AND DISCUSSION
3.1.Burned area and fire recurrence

Burned area mapping is important to monitor land use and land cover (LULC) change, to model climatic impacts from the burning of biomass (ELHAG; BOTEVA, 2016; VIEDMA et al., 2017), to account for the environmental impacts of fires on the economy and ecology, to create reference information and to support postfire management strategies (SMIRAGLIA et al., 2020; POLYCHRONAKI; GITAS, 2012).

In this research, the total burned areas mapped from the FOR, active fires, and Landsat and Sentinel satellites are shown in Figure 2.2.

Figure 2.2 - Total burned area between 2013 and 2018. A: FORs; B: Landsat-8; C: Sentinel-2; D: active fires of INPE.
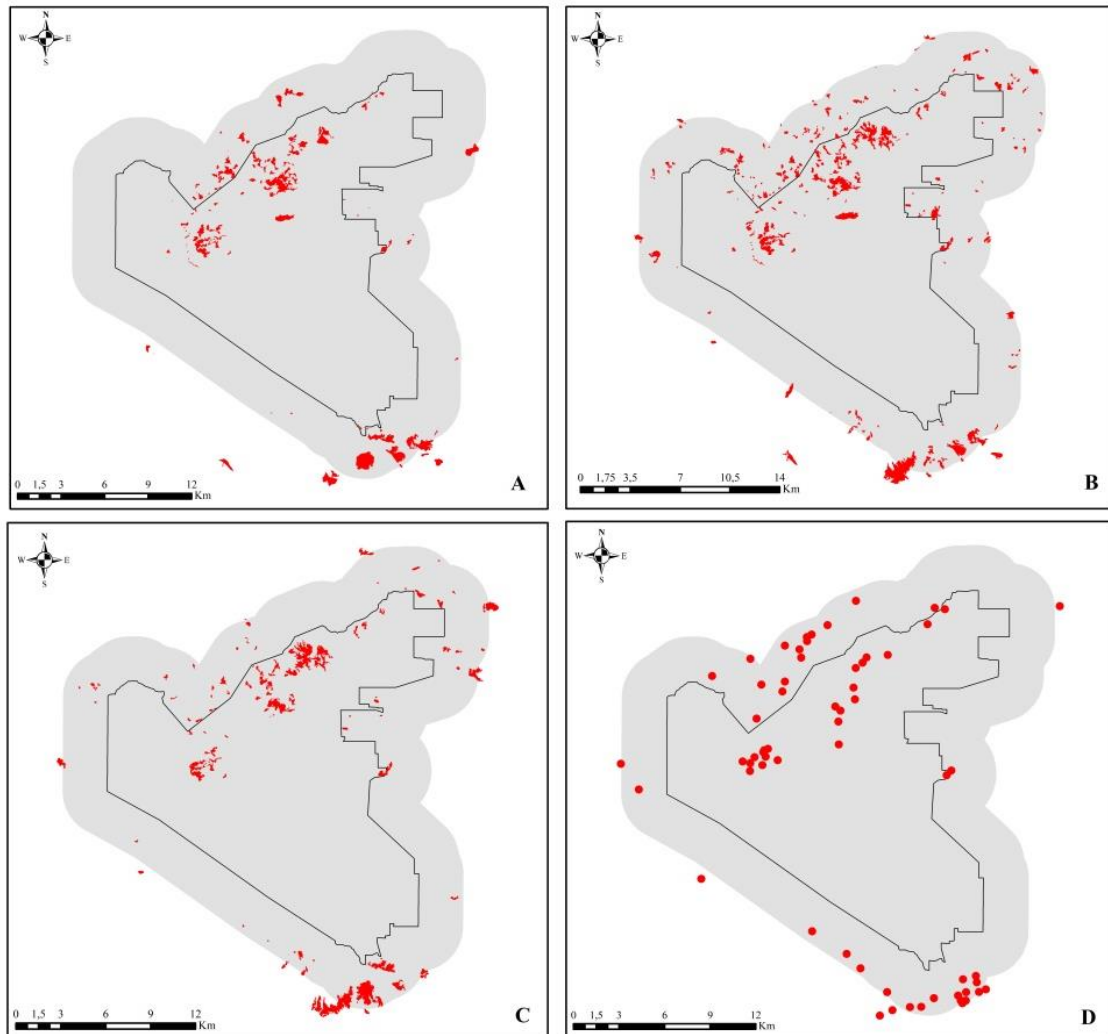
Source: from the author (2021).

According to fire occurrence records, the total area that was burned in the 2013-2018 period was 1392.3 ha (FIGURE 2.3), corresponding to 111 fires recorded within the boundaries of Itatiaia National Park and 112 in the buffer area, totaling 223 fires. This value indicates that 2.4% of this protected area (INP and buffer) was affected by fires. The years 2014 and 2016 had higher fire occurrences, resulting in 52 records for both. Despite this, 2017 had a larger area burned during the study period, with a wildfire area of 115.4 ha.

Using Landsat data, we mapped 2223.78 ha burned between 2013 and 2018 (FIGURE 2.3), contained in 274 records. Eighty-eight wildfires were found inside the park, while 186 were in the buffer zone. Comparing burned areas inside the park with those in the buffer area,

the highest difference occurred in 2015, where broad fires occurred in the buffer zone (44 patches), while there were few events into INP (5 patches).

The largest fire scar was detected in 2017, corresponding to 142.83 ha. In contrast, 2014 had the largest burned area (624.72 ha), represented by 76 polygons. The total burned area detected was 59.7% higher than the total burned areas detected using the FOR.

Similar results were found by Arruda et al. (2021), who used Landsat images as input data for mapping burned scars in the Brazilian savanna and found that these images contribute to improving the long-term temporal series of burned areas in tropical regions. Shimabukuro et al. (2020) found that Landsat-OLI had the highest values of total burned area compared with NPP-VIIRS (National Polar-Orbiting Partnership-Visible Infrared Imaging Radiometer Suite) and PROBA-V (Project for On-Board Autonomy–Vegetation), probably due to the better spatial resolution.

Figure 2.3 - Total burned area identified per year by each product (Landsat, Sentinel and FORs).
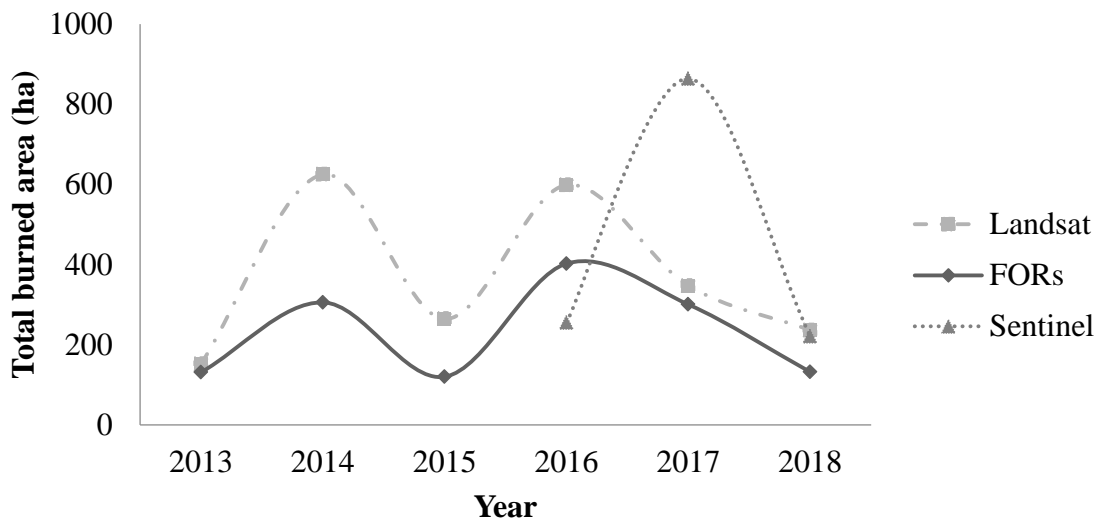
Source: from the author (2021).

From the Sentinel-2 images, we identified 34 fire occurrences within the limits of INP and 68 records in the buffer area totaling 1340.03 ha (FIGURE 2.3). Although we only used three years in this analysis, we detected a burned area near the area contained in fire occurrence records, indicating the crucial importance of temporal resolution in burned area analysis (SHIMABUKURO et al., 2020). Especially when analyzing savannas and pastures vegetation that presents rapid recovery after fire (LACOUTURE; BROADBENT; CRANDALL; 2020; WIESNER et al., 2019).

In 2017 we found the largest area burned in a single event, totaling 194.4 ha and localized in the lower part of INP. This scar was the same as that identified with Landsat images, but Sentinel images were clearer in the visualization and delineation of this scar. Furthermore, this year had the highest number of fire records (37 patches).

Clouds were the greatest difficulty in using orbital satellite images for mapping fire scars. For example, the 16-day revisit of Landsat and cloud obstruction constrain burned area mapping, even over the USA where Landsat data availability is greater than elsewhere (HAWBAKER et al., 2017; WULDER et al., 2016). This can be observed in this study when considering Landsat-8 for 2017 and Sentinel-2 for 2016, the years with the greatest cloud cover, which explains the low number of registered polygons.

The disagreements observed in the different data sources are related to the identification of burned areas by remote sensing images (Landsat and Sentinel) that were not included in the INP records. This can occur because during the fire season, fire combat is focused in areas that can cause more risk to the park and its boundaries, and it is not possible to record all occurrences, especially in the buffer zone. In addition, in this protected area, the surface relief is very uneven, which makes it difficult to accurately survey the burned area, whether small or large.

Furthermore, many government agencies collect information about fires, but records are generally prone to error, incomplete, and limited because of inconsistent collection efforts over space and time (CHUVIECO et al., 2019).

In this case, we realized that remote sensing data demonstrate the advantages of mapping burned areas at a local scale (SZPAKOWSKI; JENSEN, 2019) and can be used to promote wildfire monitoring, assessment, and prevention measures more accurately.

Based on Figure 2.4, we can observe that there was seasonality in wildfires occurrence when one year had lower occurrences than another, and the occurrences increased. This might occur due to biomass accumulation and burning in areas that have not burned in the past. However, this trend was not observed in 2018, when fire occurrence should be increased, but it remained almost constant. This may be related to the implementation of integrated management of fire in 2017.

Figure 2.4 - Total of fire occurrences identified per year by each product (Landsat, Sentinel and FORs).
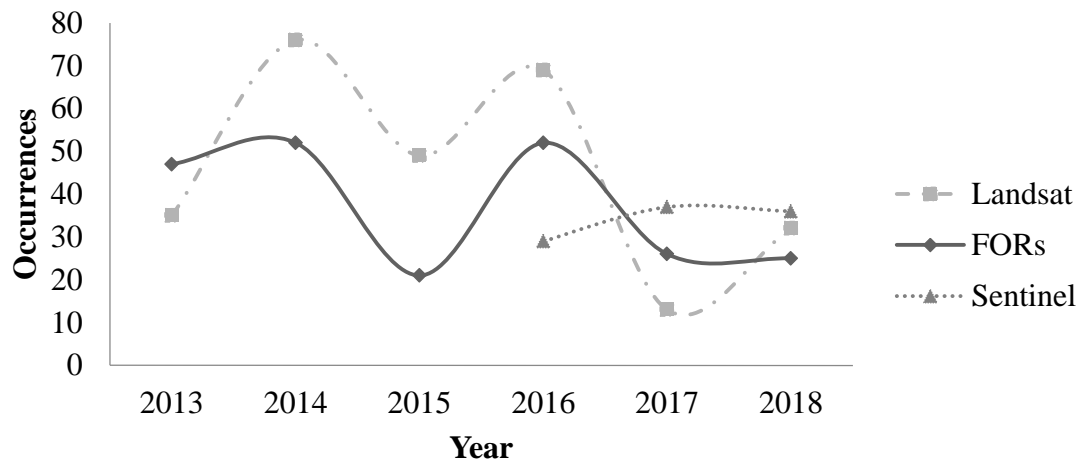
In the Itatiaia National Park and the buffer zone from January 2013 to December 2018, 62 active fires (FIGURE 2.2) were detected by the AQUA_M-T, TERRA_M-M, S-NPP-375, NOAA-15, NOAA-18, NOAA-19, GOES-16, and METOP-B satellites, which is consistent with the hotspot dataset of INPE. We observed that S-NPP-375 detected more fires than the other satellites, totaling 49 records, probably due to its higher spatial resolution when compared with other satellites. The VIIRS sensor on S-NPP enables the detection of smaller and cooler fires relative to the MODIS sensor on the Aqua and Terra satellites (CSISZAR et al., 2014).

We overlapped the hotspot dataset with the FOR and conducted a visual assessment. This analysis allowed the identification of 35 heat sources in total that were found in INP records. The other 27 hotspots were not associated with any polygons of fire.

Tomzhinski, Coura, Fernandes (2011), evaluating the detection by INPE of 101 registers in the FOR between 2008 and 2010 in Itatiaia National Park, obtained similar results in that the satellite data, converted into active fires by INPE, failed to detect 96% of the occurrences, especially those smaller than 23 ha.

When comparing the final classification of burned areas derived from Landsat images with the active fire of INPE, we observed that 36 indications of fires were correct and 26 were not linked with any fire event. On the other hand, when this analysis was performed using fires obtained with Sentinel images, 20 of the 38 heat sources were associated with identified fires.

Therefore, related to active fires detected by INPE and mapped, Sentinel-2 had the best performance, followed by Landsat-OLI and FOR data. In another study, the best

performance was achieved by the OLI+PROBA-V+VIIRS product, followed by OLI, PROBA-V, and MCD64A1 (SHIMABUKURO et al., 2020).

The lower detection of active fires compared with other sources of data is likely due to the higher spatial resolution provided by the Landsat and Sentinel imagery compared with those used by INPE products. Furthermore, active fire products give the location of all fires actively burning during the satellite overpass time. Active fire products are very sensitive to the daily dynamics of biomass burning, consequently having a short persistence of the signal, and in situations where the fire front moves quickly, there is an undersampling of fire dynamics (HUMBER et al., 2019).

Fire recurrence analysis is a valuable tool because frequent fires could cause changes in vegetation composition or structure, could result in soil erosion, could affect the resilience of ecosystems to fire and could significantly change the existing fire regime (DÍAZ-DELGADO et al., 2002; EUGENIO; LLORET, 2004; BENTO-GONÇALVES et al., 2012; FERREIRA-LEITE et al., 2016). For these reasons, it is necessary to improve our knowledge of the spatiotemporal patterns of wildfires.

Figure 2.5 shows the fire recurrence map created using Landsat and FOR data. In terms of fire recurrence, from 2013 to 2018, using Landsat images, 3.7% of all burned areas were burned between three and four times. Within the INP boundaries, mostly one to two fire recurrences were verified. The higher recurrence areas were located in the buffer zone, highlighting the lower part of the park and the areas close to rural communities in the municipality of Bocaina de Minas. According to local managers' knowledge, frequent human activities significantly increase the likelihood of wildfires in INP.

On the other hand, using FOR data, we detected between four and six fire recurrences in the buffer zone, totaling 2.9%, with a focus on the lower part of the park. Inside the boundaries of INP, the recurrence ranged between one and two, the same as that observed in Landsat images.

Figure 2.5 - Fire recurrence map of Itatiaia National Park from 2013 to 2018. A: FOR data; B: Landsat images.
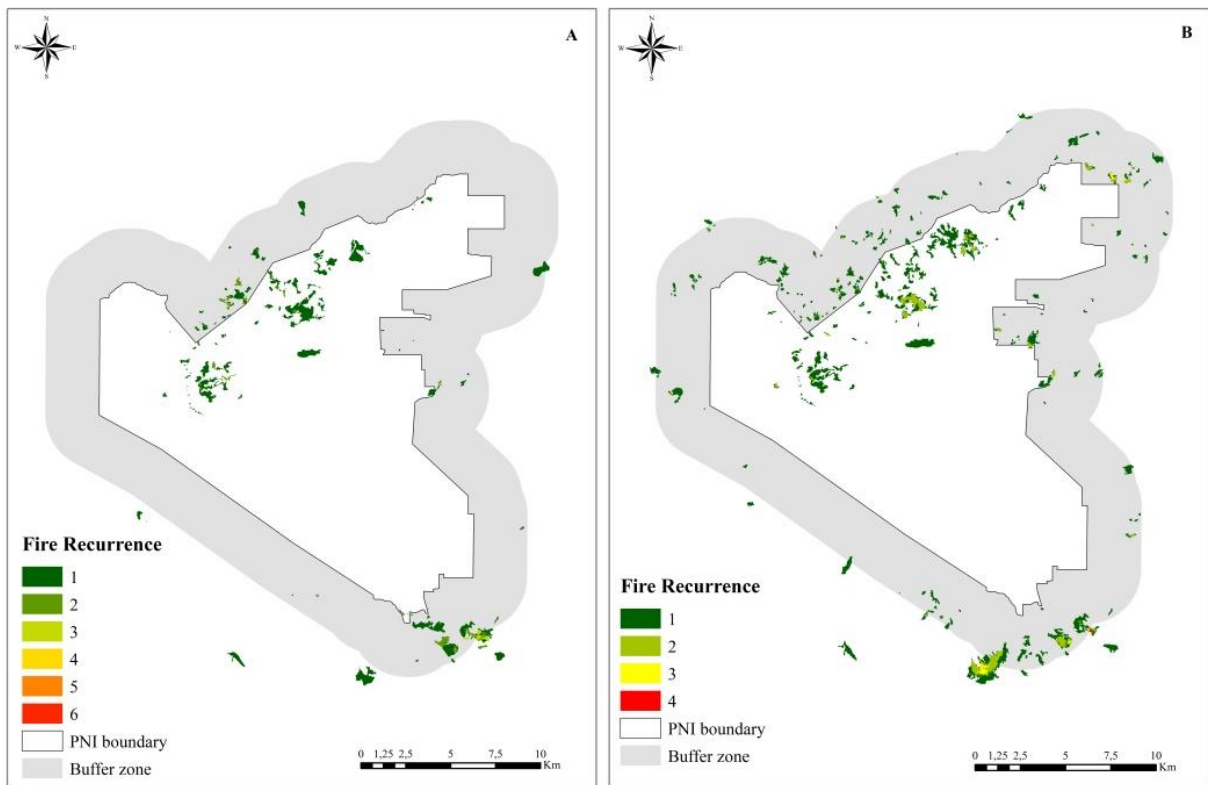
Source: from the author (2021).

The MapBiomas project provides the annual time series of LULC of all Brazilian biomes using Landsat imagery with 30 m of spatial resolution through automatic mapping based on the random forest algorithm (SOUZA JUNIOR et al., 2020). Thus, the final map of burned areas generated by Landsat-8 images and the FOR map were overlapped with the land use and land cover map provided by MapBiomas (2021) (Figure 2.6) to identify vegetation classes affected by fire between 2013 and 2018.

In reviewing the spatial distribution of the fires in Itatiaia National Park, it is clear that the fires occurred mainly in pastures and mosaics of agriculture and pasture, more specifically in the *Campos de altitude* phytophysiognomy at high altitudes. These results were expected due to the history of occurrence of fires reported in other research, such as that of Tomzhinski, Ribeiro, Fernandes (2012) and Aximoff, Rodrigues (2011).

The use of remote sensing images to map fire scars, as shown in Santos et al. (2018), may result in an underestimation due to fires that did not reach the tree canopies and therefore were not visible in the image. In INP, the areas most affected by fires are covered by *Campos de altitude* with a predominance of undergrowth, and in the case of burning in the buffer zone, pasture. As a result, this limitation found by Santos et al. (2018) was not found in this study. Contrary to the underestimation presented in Santos et al. (2018), we noticed that both

satellites (Landsat-8 and Sentinel-2) overcame the area affected by the fire contained in the FOR, despite not having identified all the burns compiled by INP.

Figure 2.6 - Land use and land cover of Itatiaia National Park and 3 km buffer zone.
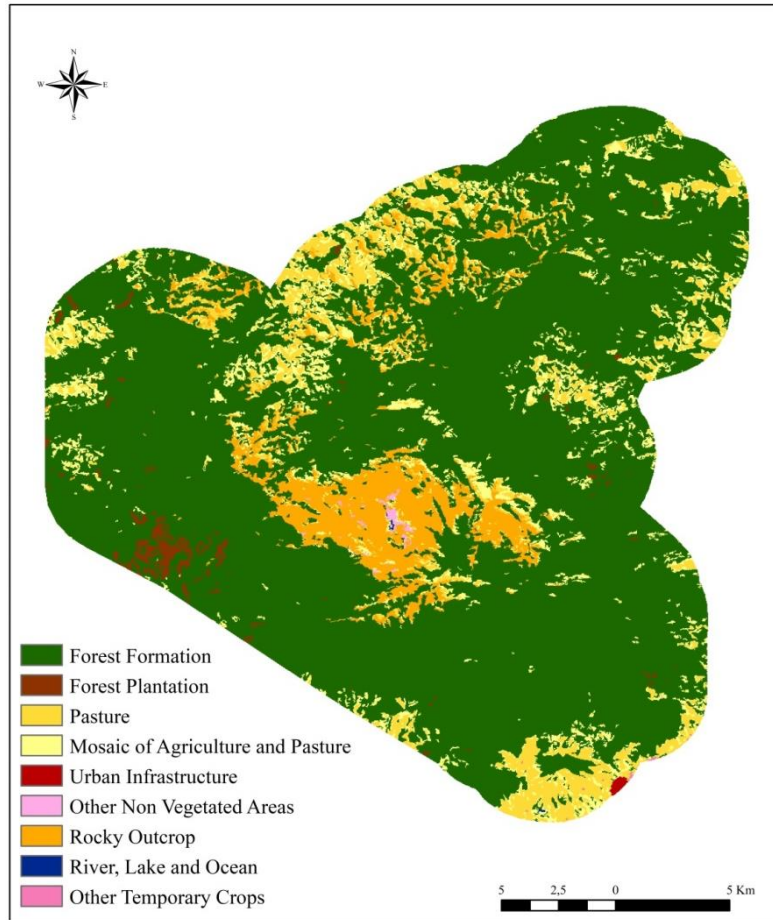
Source: MapBiomas (2021).

3.2. STEP

The similarity assessment technique used in this study was the STEP, which is based on thematic and geometric quality obtained with object-based image analysis (OBIA). In contrast to pixel-based approaches that use a confusion matrix, OBIA groups pixels resulting in the output of meaningful objects (ELLIS; MATHEWS, 2019). The STEP method uses the geometric characteristics of the objects, such as shape, edge, and position, to generate assess the similarity of objects (LIZARAZO, 2014).

Similarity metrics were evaluated for the classified objects derived from remote sensing data (Landsat and Sentinel) and for the reference objects composed of the Itatiaia National Park dataset. Table 2.2 shows the results of individual similarity matrices aggregated by thematic class. These classes in this study were composed of burned and unburned areas.

As this research aims to evaluate the ability of Landsat and Sentinel data to identify burned scars, we present only the similarity index results for the burned thematic class.

Table 2.2 - STEP index between 2013 – 2018 to burned scars polygons.

		Theme	Shape	Position	Edge
Landsat-8	2013	0.81	0.66	0.62	0.39
	2014	0.93	0.81	0.84	0.34
	2015	0.90	0.79	0.82	0.30
	2016	0.91	0.70	0.59	0.21
	2017	0.72	0.54	0.68	0.041
	2018	0.93	0.71	0.47	0.37
Sentinel-2	2016	0.93	0.81	0.76	0.61
	2017	0.72	0.44	0	0.18
	2018	0.91	0.65	0.46	0.4

Source: from the author (2021).

This study assessed the performance of two remote sensing datasets, Sentinel and Landsat, in terms of their ability to identify wildfire scars as well as FOR based on the STEP method (LIZARAZO, 2014). This method has been used in the literature to analyse similarity metrics in the mapping of field boundaries with remote sensing images (WALDNER et al., 2021) in heterogeneous urban land cover (TSOELENG; ODINDI; MHANGARA, 2020), to identify individual tree crown parameters using UAVs (YURTSEVEN et al., 2019), to detect and map land surface elevation changes using UAVs (LIZARAZO; ANGULO; RODRÍGUEZ, 2017), for the detection and identification of precipitating clouds (RAMIREZ; LIZARAZO, 2016), and in the classification of land cover in southeastern Brazil (PRADO; CARVALHO, 2016).

In this research, the reference objects used in the analysis derived from FOR totalled 116 wildfires when compared with Landsat and 43 when compared with Sentinel. These data overlapped with 109 classified objects from Landsat and 36 from Sentinel.

Position similarity according to the analysis ranged between 0.47 and 0.84 and -0.63 and 0.76 for Landsat and Sentinel data, respectively. In the position index for 2017 for the Sentinel data, a negative value occurred when the distance of the centroid among objects was greater than the value of the circular diameter within the same area. This value indicates that objects have no positional correspondence; thus, this negative value was replaced by 0.

The shape index for both satellites varied between 0.44 and 0.81. In a STEP similarity matrix, a value of 1 indicates classified objects that match the reference objects; thus, it suggests for this study that at least there was 44% shape correspondence between the analysed objects.

In terms of shape similarity, Tsoeleng; Odindi; Mhangara (2020) indicated poor shape similarity as well when evaluating natural features, except for most artificial features such as buildings, roads which are better classified in their study, achieving a high accuracy of 0.86. Waldner et al. (2021) found that the similarity of shape was the poorest of all metrics to extract fields from satellite imagery, with a value of approximately 0.6.

Edge similarity values ranged between 0.041 and 0.61. Similar results in regard to poor correspondence of edges were also found by Prado and Carvalho (2016). In their study, poor correspondence was caused by classification errors and differences between the design of objects.

This was expected in the present study and may have occurred because of the spatial resolution of the images, 30 m for Landsat images and 10 m for Sentinel images, which influenced the delineation of wildfire edges. When image classification is carried out on raster data, the boundaries of the land cover classes are based on the pixel grid structure. Nevertheless, objects with natural boundaries do not have well-defined edges and have complex boundaries that are usually affected by boundary blur (GONG, 1994).

Theme similarity presented higher figures for all years using Landsat and Sentinel data with values that varied between 0.72 and 0.93, respectively. These values demonstrate that there was more than 70% coincidence among classified burned areas and FOR data. This finding corroborates the study by Yurtseven et al. (2019), who identified that theme was the best similarity index for all polygons analysed.

Our results suggest that the best aspect analysed was theme, followed in their respective order by shape, position and edge. Figure 2.7 shows classified objects of Landsat and Sentinel that correspond to the reference objects. In this figure, it is possible to observe that there is a thematic match; nevertheless, there are differences regarding shape, position and edge, consistent with the results.

Figure 2.7 - STEP metrics for classified objects. The reference objects are presented in gray color.
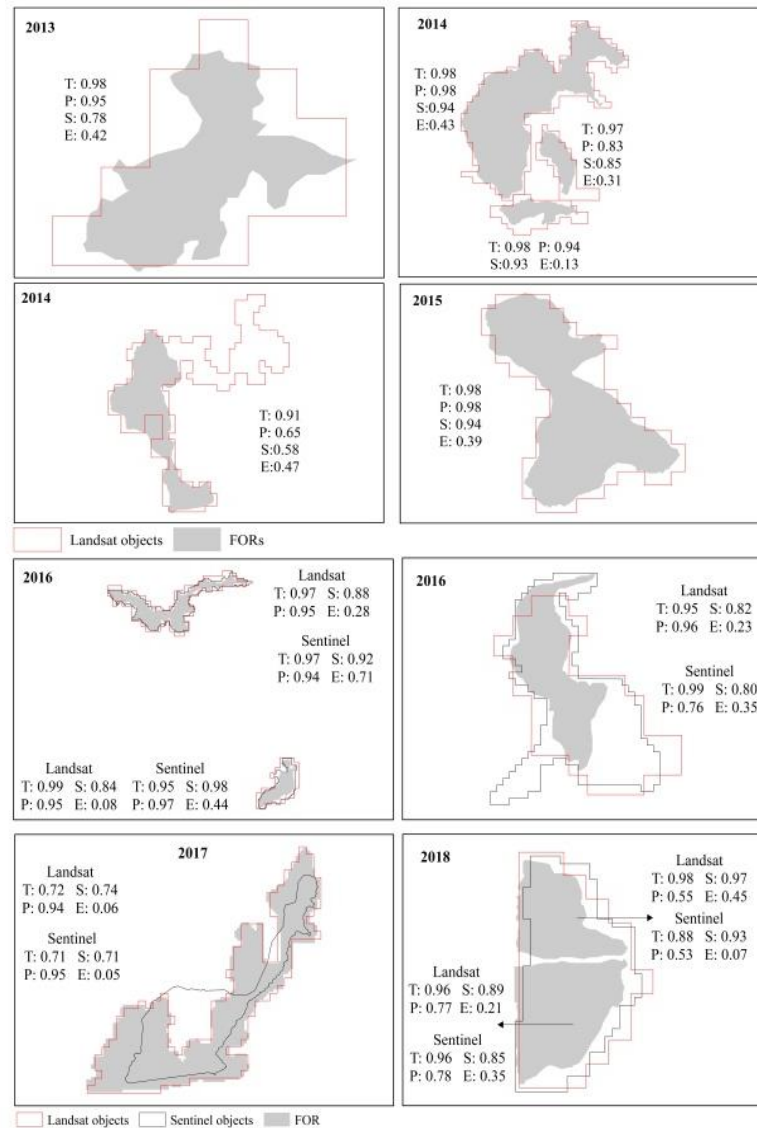
Source: from the author (2021).

From the analysis in Table 2.2, it is evident that wildfire scar data obtained with two different satellite datasets, in terms of shape, theme, position and edge similarity, present close values. In contrast, when visually observing the images, we recognize that better performance was achieved by Sentinel data, and we detect that FOR underestimate the burned area because wildfires identified in remote sensing images are larger than those found in FOR registries.

According to this study, remote sensing data can be used to improve the existing method to record fires in protected areas. The approach presented here cannot replace *in situ* observations, as they are necessary to assessing vegetation mortality and postfire impact, but it has the potential to decrease the collection time and increase the quality of fire scar delineation, especially in areas of difficult assess.

4. CONCLUSIONS

Remote sensing images are an efficient option to increase the quality of the fire occurrence records of protected areas, improving the data that will be used by managers to obtain better planning of actions regarding integrated fire management.

The higher recurrence of fire occurs in the buffer area, especially in the lower part of INP and near rural communities; in addition, the more affected vegetation is that in the *Campos de altitude* in the highest summits of Itatiaia. Therefore, the fire recurrence map added to the survey of the causes of forest fires and the socioeconomic needs for the use of fire provides important information for the planning and execution of specific strategies aimed at protecting and managing protected areas.

REFERENCES

ARRUDA, V. L. S. et al. An alternative approach for mapping burn scars using Landsat imagery, Google Earth Engine, and Deep Learning in the Brazilian Savanna. **Remote Sensing Applications: Society and Environment**, v. 22, p. 1-11, 2021.

AXIMOFF, I. O que Perdemos com a Passagem do Fogo pelos Campos de altitude do Estado do Rio de Janeiro? **Biodiversidade Brasileira**, n. 2, p. 180-200, 2011.

BASTARRIKA, A.; CHUVIECO, E.; MARTÍN, M.P. Mapping burned areas from Landsat TM/ETM+ data with a two-phase algorithm: balancing omission and commission erros. **Remote Sensing of Environment**, v. 115, n. 4, p. 1003-1012, 2011.

BAR, S.; PARIDA, B. R.; PANDEY, A. C. Landsat-8 and Sentinel-2 based Forest fire burn area mapping using machine learning algorithms on GEE cloud platform over Uttarakhand, Western Himalaya. **Remote Sensing Applications: Society and Environment**, v. 18, p. 1-11, 2020.

BENTO-GONÇALVES, A. et al. Fire and soils: key concepts and recent advances. **Geoderma**, v. 191, p. 3–13, 2012.

BOWMAN, D. M. J. S. et al. Vegetation fires in the anthropocene. **Nature Reviews Earth & Environment**, v. 1, p. 500–515, 2020.

BOND, W. J.; KEELEY, J. E. Fire as a global "herbivore": The ecology and evolution of flammable ecosystems. **Trends in Ecology & Evolution**, v. 20, n. 7, p. 387–394, 2005.

BONTEMPO, G. C. et al. Registro de Ocorrência de Incêndio (ROI): evolução, desafios e recomendações. **Biodiversidade Brasileira**, n. 2, p. 247-263, 2011.

BUTCHART, S. H. M. et al. Protecting Important Sites for Biodiversity Contributes to Meeting Global Conservation Targets. **PLOS ONE**, v. 7, n. 3, 2012.

CAMPBELL, J. B.; WYNNE, R. H. **Introduction to Remote Sensing**. 5. ed. The Guilford Press, 2011. 662 p.

CARMONA-MORENO, C. et al. Characterizing interannual variations in global fire calendar using data from Earth observing satellites. **Global Change Biology**, v. 11, n. 9, p.1537-1555, 2005.

CHUVIECO, E., MARTIN, M.P., PALACIOS, A. Assessment of different spectral indices in the red-near-infrared spectral domain for burned land discrimination. **International Journal of Remote Sensing**, v. 23, n. 23, p. 5103-5110, 2002.

CHUVIECO E. et al. Development of a frame work for fire risk assessment using remote sensing and geographic information system technologies. **Ecological Modelling**, v. 221, n. 1, p. 46–58, 2010.

CHUVIECO, E. et al. Generation and analysis of a new global burned area product based on MODIS 250 m reflectance bands and thermal anomalies. **Earth System Science Data**, v. 10, p. 2015-2031, 2018.

CHUVIECO, E. et al. Historical background and current developments for mapping burned area from satellite Earth observation. **Remote Sensing of Environment**, v. 225, p. 45-64, 2019.

CSISZAR, I. et al. Active fires from the Suomi NPP Visible Infrared Imaging Radiometer Suite: Product status and first evaluation results. **Journal of Geophysical Research: Atmospheres**, v.119, n. 2, p. 803–816, 2014.

D'AMICO, A. R. et al. Environmental diagnoses and effective planning of Protected Areas in Brazil: Is there any connection? **PLoS ONE**, v. 15, n. 12, p. 1-13, 2020.

DIN, A. Applying Spaghetti and Meatballs to Proximity Analysis. **Cityscape: A Journal of Policy Development and Research**, v. 22, n. 2, p. 133-148, 2020.

DRUSCH, M. et al. Sentinel-2: ESA's optical high-resolution mission for GMES operational services. **Remote Sensing of Environment**, v. 120, n.15, p.25-36, 2012.

ELLIS, E. A.; MATHEWS, A. J. Object-based delineation of urban tree canopy: assessing change in Oklahoma City, 2006–2013. **Computers, Environment and Urban Systems**, v. 73, p. 85-94, 2019.

ELHAG, M.; BOTEVA, S. Mediterranean land use and land cover classification assessment using high spatial resolution data. **IOP Conference Series: Earth and Environmental Science**, v. 44, p. 1-13, 2016.

GIGLIO, L. et al. The collection 6 MODIS burned area mapping algorithm and product. **Remote Sensing of Environment**, v. 217, p. 72-85, 2018.

ICMBio – Instituto Chico Mendes de Biodiversidade. **Plano de Manejo Parque Nacional do Itatiaia Revisão – Encarte 3**. Brasília, 215p., 2014. Available: http://www.icmbio.gov.br/portal/component/content/article?id=2181:parna-do-itatiaia.

INPE – Instituto Nacional de Pesquisas Espaciais. **Programa Queimadas**. 2021. Available: https://queimadas.dgi.inpe.br/queimadas/portal/informacoes/perguntas-frequentes.

KEY, C. H.; BENSON, N. C. Landscape assessment (LA): sampling and analysis methods. In: LUTES, D. C. et al. **FIREMON:** Fire Effects Monitoring and Inventory System. U.S. Department of Agriculture, Forest Service, Rocky Mountain Research Station, Fort Collins, CO, USA, 2006, p. LA-1-55.

DÍAZ-DELGADO, R. et al. Satellite evidence of decreasing resilience in Mediterranean plant communities after recurrent wildfires. **Ecology**, v. 83, n. 8, p.2293-2303, 2002.

EUGENIO, M.; LLORET, F. Fire recurrence effects on the structure and composition of Mediterranean *Pinus halepensis* communities in Catalonia (northeast Iberian Peninsula). **Ecoscience**, v.11, n. 4, p.446-454, 2004.

ESCUIN, S.; NAVARRO, R.; FERNÁNDEZ, P. Fire severity assessment by using NBR (Normalized Burn Ratio) and NDVI (Normalized Difference Vegetation Index) derived from LANDSAT TM/ETM images. **International Journal of Remote Sensing**, v. 29, n. 4, p. 1053-1073, 2008.

FASSNACHT, F. E. et al. Explaining Sentinel 2-based dNBR and RdNBR variability with reference data from the bird's eye (UAS) perspective. **International Journal of Applied Earth Observation and Geoinformation**, v. 95, p. 1-19, 2021.

FERREIRA-LEITE. et al. Incidence and recurrence of large forest fires in mainland Portugal. **Natural Hazards**, v. 84, p. 1035–1053, 2016.

GONG, P. Reducing boundary effects in a kernel-based classifier. **International Journal of Remote Sensing**, v. 15, n. 5, p. 1131–1139, 1994.

FIGUEROA, F., SÁNCHEZ-CORDERO, V. Effectiveness of natural protected areas to prevent land use and land cover change in Mexico. **Biodiversity and Conservation**, v. 17, p. 3223–3240, 2008.

FORKEL, M. Emergent relationships on burned area in global satellite observations and fire-enabled vegetation models. **Biogeosciences**, v. 16, p. 57–76, 2019.

GRAY, C. L. et al. Local biodiversity is higher inside than outside terrestrial protected areas worldwide. **Nature Communications**, v. 7, p. 1-7, 2016.

GORELICK, N. Google Earth engine: planetary-scale geospatial analysis for everyone. **Remote Sensing of Environment**, v. 202, p. 18-27, 2017.

HALOFSKY, J. E.; PETERSON, D. L.; HARVEY, B. J. Changing wildfire, changing forests: the effects of climate change on fire regimes and vegetation in the Pacific Northwest, USA. **Fire Ecology**, v. 16, n. 4, p. 1-26, 2020.

HAWBAKER, T. J. Mapping burned areas using dense time-series of Landsat data. **Remote Sensing of Environment**, v. 198, n. 1, p. 504-522, 2017.

HUMBER, M. L. et al. Spatial and temporal intercomparison of four global burned area products. **International Journal of Digital Earth**, v. 12, n. 4, p. 460–484, 2019.

KELLY, L. T.; BROTONS, L. Using fire to promote biodiversity. **Science**, v. 355, n. 6331, p.1264-1265, 2017.

KNORR, W.; JIANG, L.; ARNETH, A. Climate, CO_2 and human population impacts on global wildfire emissions. **Biogeosciences**, v. 13, p. 267–282, 2016.

LACOUTURE, D. L.; BROADBENT, E. N.; CRANDALL, R. M. Detecting Vegetation Recovery after Fire in A Fire-Frequented Habitat Using Normalized Difference Vegetation Index (NDVI). **Forests**, v. 11, p. 1-12, 2020.

LIZARAZO, I. Accuracy Assessment of Object-Based Image Classification: Another STEP. **International Journal of Remote Sensing**, v. 35, n. 16, p. 6135–6156, 2014.

LIZARAZO, I.; ANGULO, V.; RODRÍGUEZ, J. Automatic mapping of land surface elevation changes from UAV-based imagery. **International Journal of Remote Sensing**, v. 38, n. 8-10, p. 2603-2622, 2017.

MapBiomas - Projeto de Mapeamento Anual do Uso e Cobertura da Terra no Brasil. **Collection of Brazilian Land Cover & Use Map Series**. 2021. Available: http://mapbiomas.org.

MARGULES, C. R.; PRESSEY, R. L.; WILLIAMS, P. H. Representing biodiversity: Data and procedures for identifying priority areas for conservation. **Journal of Biosciences**, v. 27, p.309-326, 2002.

MORENO RUIZ, J. A. et al. Burned area mapping time series in Canada (1984–1999) from NOAA-AVHRR LTDR: A comparison with other remote sensing products and fire perimeters. **Remote Sensing of Environment**, v.117, n. 15, p. 407-414, 2012.

MORENO RUIZ, J. A. et al. Burned area mapping in the North American boreal forest using Terra-MODIS LTDR (2001−2011): a comparison with the MCD45A1, MCD64A1 and BA GEOLAND-2 products. **Remote Sensing**, v. 6, n. 1, p. 815-840, 2014.

ODION, D. C. et al. Examining historical and current mixed-severity fire regimes in ponderosa pine and mixed-conifer forests of western North America. **PLoS ONE**, v. 9, n. 2, p. 1-14, 2014.

OLIVEIRA, U. et al. Biodiversity conservation gaps in the Brazilian protected areas. **Scientific Reports**, v. 7, n. 9141, p. 1-9, 2017.

PIROMAL, R. A. S. Utilização de dados MODIS para a detecção de queimadas na Amazônia. **Acta Amazonica**, v. 38, n. 1, p.77-84, 2008.

PRADO, D. F. C.; CARVALHO, L. M. T. application of object-based accuracy assessment for land cover classification using rapideye images in Southeastern Brazil. In: GEOBIA 2016: Solutions and Synergies, 2016. **Proceedings** […] University of Twente Faculty of Geo-Information and Earth Observation (ITC).

POLYCHRONAKI, A.; GITAS, I. Z. Burned area mapping in Greece using SPOT-4 HRVIR images and object-based image analysis. **Remote Sensing,** v. 4, n. 2, p. 424–438, 2012.

PHIRI, D. et al. Sentinel-2 Data for Land Cover/Use Mapping: A Review. **Remote Sensing**, v. 12, n 14, p. 1-35, 2020.

REDIN, M. et al. Impactos da queima sobre atributos químicos, físicos e biológicos do solo. **Ciência Florestal**, v. 21, n. 2, p. 381-392, 2011.

RAMIREZ, S.; LIZARAZO, I. Decision tree classification model for detecting and tracking precipitating objects from series of meteorological images. In: GEOBIA 2016: Solutions and Synergies, 2016. **Proceedings** [...] University of Twente Faculty of Geo-Information and Earth Observation (ITC).

ROY, D.P. Landsat-8: science and product vision for terrestrial global change research. **Remote Sensing of Environment**, v. 145, n. 5, p. 154–172, 2014.

SANSEVERO, J. B. B. et al. Past land-use and ecological resilience in a lowland Brazilian Atlantic Forest: implications for passive restoration. **New Forest**, v. 48, p. 573–586, 2017.

SMIRAGLIA, D. et al. Agreement Index for Burned Area Mapping: Integration of Multiple Spectral Indices Using Sentinel-2 Satellite Images. **Remote Sensing**, v. 12, n. 11, p. 1-17; 2020.

SHIMABUKURO, Y. E. et al. Mapping Burned Areas of Mato Grosso State Brazilian Amazon Using Multisensor Datasets. **Remote Sensing**, v. 12, n. 22, p. 1-23, 2020.

SOUZA JUNIOR, C. M. Reconstructing three decades of land use and land cover changes in Brazilian biomes with Landsat Archive and Earth Engine. **Remote Sensing**, v. 12, n. 17, p. 1-27, 2020.

SANTOS, J. F. C. et al. Potentials and limitations of remote fire monitoring in protected areas. **Science of The Total Environment**, v. 616-617, p. 1347-1355, 2018.

SZPAKOWSKI, D. M.; JENSEN, J. L. R. A Review of the Applications of Remote Sensing in Fire Ecology. **Remote Sensing**, v. 11, n. 22, p. 1-31, 2019.

TRAN, B. N. et al. Evaluation of spectral indices for assessing fire severity in Australian temperate forests. **Remote Sensing**, v. 10, n. 11, p. 1-18, 2018.

TSOELENG, L. T.; ODINDI, J.; MHANGARA, P. A Comparison of Two Morphological Techniques in the Classification of Urban Land Cover. **Remote Sensing**, v. 12, n. 7, p. 1-14, 2020.

TOMZHINSKI, G. W.; RIBEIRO, K. T.; FERNANDES, M. C. Análise Geoecológica dos Incêndios Florestais do Parque Nacional do Itatiaia. **Boletim do Parque Nacional do Itatiaia**, Rio de Janeiro, n. 15, 164 p., 2012.

TOMZHINSKI, G. W.; COURA, P. H. F.; FERNANDES, M. C. Avaliação da Detecção de Focos de Calor por Sensoriamento Remoto para o Parque Nacional do Itatiaia. **Biodiversidade Brasileira**, n. 2, p. 201-211, 2011.

VIEDMA, O. Recent land-use and land-cover changes and its driving factors in a fire-prone area of southwestern Turkey. **Journal of Environment Management**, v. 197, p. 719–731, 2017.

WALDNER, F. et al. Detect, Consolidate, Delineate: Scalable Mapping of Field Boundaries Using Satellite Images. **Remote Sensing**, v. 13, n. 11, p. 1-24, 2021.

WIESNER, S. et al. The role of understory phenology and productivity in the carbon dynamics of longleaf pine savannas. **Ecosphere**, v. 10, n. 4, p. 1-20, 2019.

WULDER, M. A. et al. The global Landsat archive: status, consolidation, and direction. **Remote Sensing of Environment**, v. 185, p. 271-283, 2016.

WULDER, M. A. et al. Current status of Landsat program, science, and applications. **Remote Sensing of Environment**, v. 225, p. 127-147, 2019.

YURTSEVEN, H. et al. Determination and accuracy analysis of individual tree crown parameters using UAV based imagery and OBIA techniques. **Measurement**, v. 145, p. 651-664, 2019.

ARTICLE 3 - Short-term assessment of vegetation recovery post wildfires and prescribed fire of Atlantic Rainforest protected area

Abstract

Understanding fire processes across the landscape is an important way for land managers to make more informed decisions about how and where to allocate limited resources across their landscape to mitigate future burns. In this study, we evaluated short-term effects and vegetation recovery in prescribed fires and wildfires in the Itatiaia National Park, Brazil. Six wildfires and two prescribed fires were assessed, fire severity was obtained using the dNBR index derived from Sentinel-2 images, and post-fire recovery per fire severity classes was quantified using time series of the NBR index. Results show that the wildfires were more severe than prescribed fires. Vegetation recovers quickly, with NBR stabilizing in the maximum in 11 months, where wildfires showed a time to recovery similar to prescribed fire due to the weather influence. The results of this research are important to integrated fire management (IFM) in protected areas, assisting strategies for the ecosystem's recovery and the adoption of preventive measures to avoid the occurrence of large wildfires.

Keywords: Change detection. Itatiaia National Park. NBR. Fire severity. Sentinel-2.

1. INTRODUCTION

In recent years, fire occurrences and heat sources have been increasingly detected in Brazil, where more than 312.140 km^2 were burned in 2020 (INPE, 2020). The fire patterns are controlled by the weather (BARBERO et al., 2020). As climate change worsens, the risk of wildfires increases because the fire season tends to start earlier and end later (SUN et al., 2019; JOLLY et al., 2015).

Projections indicate that by the end of the 21st century the duration of the fire season and the fire frequency will increase significantly (SUN et al., 2019). Thus, a better understanding of fire and recovery processes across the landscape is needed. These outcomes become important to land managers because if they know the drivers of burn severity and recovery, they could make more informed decisions about how and where to allocate limited resources across their landscape to mitigate future burns (FRANCO; MUNDO; VEBLEN, 2020; BONNEY; HE; MYINT, 2020).

In general, when a fire event occurs, most of the ecosystems are modified, with partial or total vegetation burn, resulting in disturbance in biological activity, generating environmental, economic and social costs (VIANA-SOTO et al., 2017; BASTOS et al., 2011). A burning event depends on a variety of biological and environmental factors and the interaction between them, like its intensity, duration, extent, and period of the year when it occurs (SHIMABUKURO et al., 2020; BASTOS et al., 2011). Thus, it is complex to mapping

and modeling post-fire patterns because these factors will the resilience of vegetation. However, accurate mapping is a key issue in spatial forest ecology that is related to fire (TEODORO; AMARAL, 2019).

In Brazilian protected areas, frequency and severity of wildfires are estimated subjectively according to the size of the burned area using GPS measurements. This procedure can underestimate the affected area because the data may be incomplete and limited due to the inconsistent collection efforts over space and time (CHUVIECO et al., 2019).

In this context, remote sensing can be a useful tool to improve the quality and quantity of data demanded by managers and for monitoring and mapping burned areas, fire severity and vegetation recovery after fire with more precision. Especially with the recent improvement of spatial and temporal resolution of the Sentinel-2 satellite and its free access (AMOS; PETROPOULOS; FERENTINOS, 2019). As a result, the information is obtained rapidly and at large spatial scales, providing more frequent acquisitions and making possible the detailed monitoring that is necessary to reveal the short-term, post-fire dynamics in ecosystems that recover quickly, like tropical savannas and grasslands (PÉREZ-CABELLO; MONTORIO; ALVES, 2021).

These fire information (fire severity, vegetation recovery) can be derived by spectral indices, like the normalized burn ratio (NBR) and the delta NBR (dNBR). The NBR index is considered more suitable among the spectral indices for describing fire severity through dNBR because relates vegetation moisture content by combining the near-infrared (NIR) and shortwave infrared (SWIR) parts of the electromagnetic spectrum, which are influenced by fire (VERAVERBEKE et al., 2011). The dNBR has become increasingly applied because previous research has demonstrated its efficient (FASSNACHT et al., 2021; SANTOS et al., 2018; LHERMITTE et al., 2011).

Although multispectral satellite data have been widely used in fire mapping and monitoring, to date, there has been a lack of knowledge about differences in fire severity and in rates of vegetation recovery associated with different disturbance types, like prescribed fire and wildfires in the same area.

In this context, the main goal of this study was to gain further insights into the short-term effects of prescribed and wildfires in the Itatiaia National Park (INP).

The specific objectives were: (i) to evaluate vegetation recovery performed per fire severity classes, (ii) to identify if the vegetation recovery is different between wildfires and prescribed fires, (iii) to contribute with more information about prescribed fires to the promotion of sustainable fire management practices in protected areas.

2. MATERIALS AND METHODS

2.1. Study area

The study area comprises a protected area called Itatiaia National Park (INP) (22º19'–22º45'S and 44º45'–44º50'W), which is located in the Serra da Mantiqueira within the Atlantic Rainforest biome, southeastern Brazil. The biome is classified as one of the 36 biodiversity hotspots in the world (CEPF, 2016). The INP boundaries cover the States of Rio de Janeiro (Resende and Itatiaia municipalities) and Minas Gerais (Bocaina de Minas and Itamonte municipalities) and have an area of approximately 30,000 ha plus a 3 km buffer zone around the limit (ICMBio, 2014) (FIGURE 3.1).

Figure 3.1 - Itatiaia National Park location, state of Minas Gerais and Rio de Janeiro, Brazil.
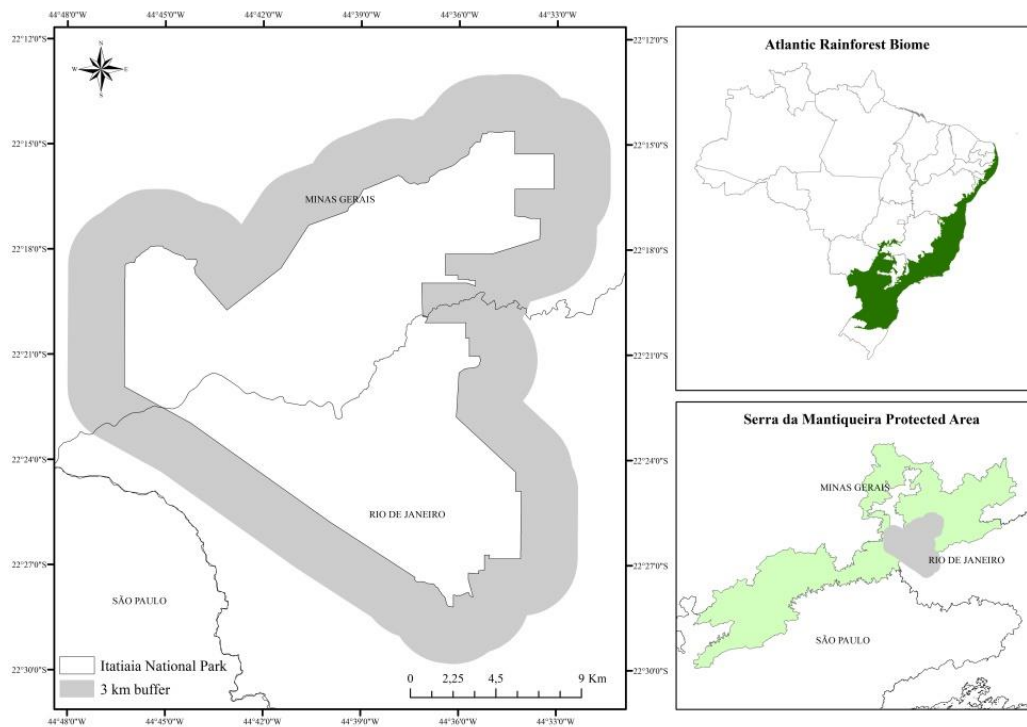
Source: from the author (2021).

The INP altitudes varies from 540 to 2,791 m above sea level, with the highest summits of the park being the Pico das Agulhas Negras. The climate in the region is mesothermic type (Cwb) according to the Köppen classification (ALVARES et al., 2013) and is influenced by altitude variation. The climate in the upper part of the park is defined as Cwb and shows a mild and rainy season during summer, and the yearly average temperature is

11.5° C with an 8.4° C average during the winter. The lower part presents Cpb type with rainfall distributed throughout the year (ICMBio, 2014).

The Itatiaia National Park vegetation is characterized as dense Atlantic Rainforest, with phytophysiognomies that follow an elevation gradient, as montane mixed ombrophilous forest, characterized by the presence of Araucaria trees, high-montane, sub-montane and montane forest, and *Campos de altitude* (Brazilian paramos), above to 2,300 m (ICMBio, 2014; VELOSO; RANGEL FILHO; LIMA, 1991).

The climate and landscape of the INP make it vulnerable to wildfires, especially during drier periods and in the high part of the park. Spatial records of fires have been kept since 1937, although data collection is sparse until 2008 when the Fire Occurrence Records (FORs) was implemented and fire events started to be collected with GPS. Belchior et al. (2020) found that between 2008 and 2016 a total of 3,435.64 hectares were burned in the INP, with higher fire recurrences shown in anthropic fields and pastures related to livestock use. Similar results were presented by Tomzhinski; Ribeiro; Fernandes (2012) analyzing fire occurrence between 1937 and 2011 and found that 78% of wildfires were located in altitudes above 2,000 m and the August and September months presented higher occurrences.

We selected, for this study, six wildfire events and two prescribed fire events within the boundaries of the INP (FIGURE 3.2). The analysis units were composed of forest fires that occurred between 2019-2020 and two prescribed burns. One of these was the first prescribed fire experiment conducted at the INP for reducing fuel load in 2017. The other one aimed at establishing a firebreak prior to the dry season of 2019.

These two methods of fire use are management actions expected in Integrated Fire Management for reducing catastrophic fires. The major difference between these strategies used in the INP is that the prescribed fire is realized in the large area with a controlled perimeter applied in specific environmental conditions and the fire behavior to create spatial discontinuities in the vegetation. In the prescribed fire realized in 2017, the environmental condition was characterized by higher humidity and lower temperature, providing a front propagation speed slower than 1 m/minute and a fire intensity varying between 57.6 e 2,831.1 kW/m (MOTTA et al., 2019).

On the other hand, firebreak is a type of prescribed fire where the vegetation is burned to create barriers against fire propagation with the function of increasing the success of forest fire control.

Figure 3.2 – Units of study composed of wildfires and prescribed fires.
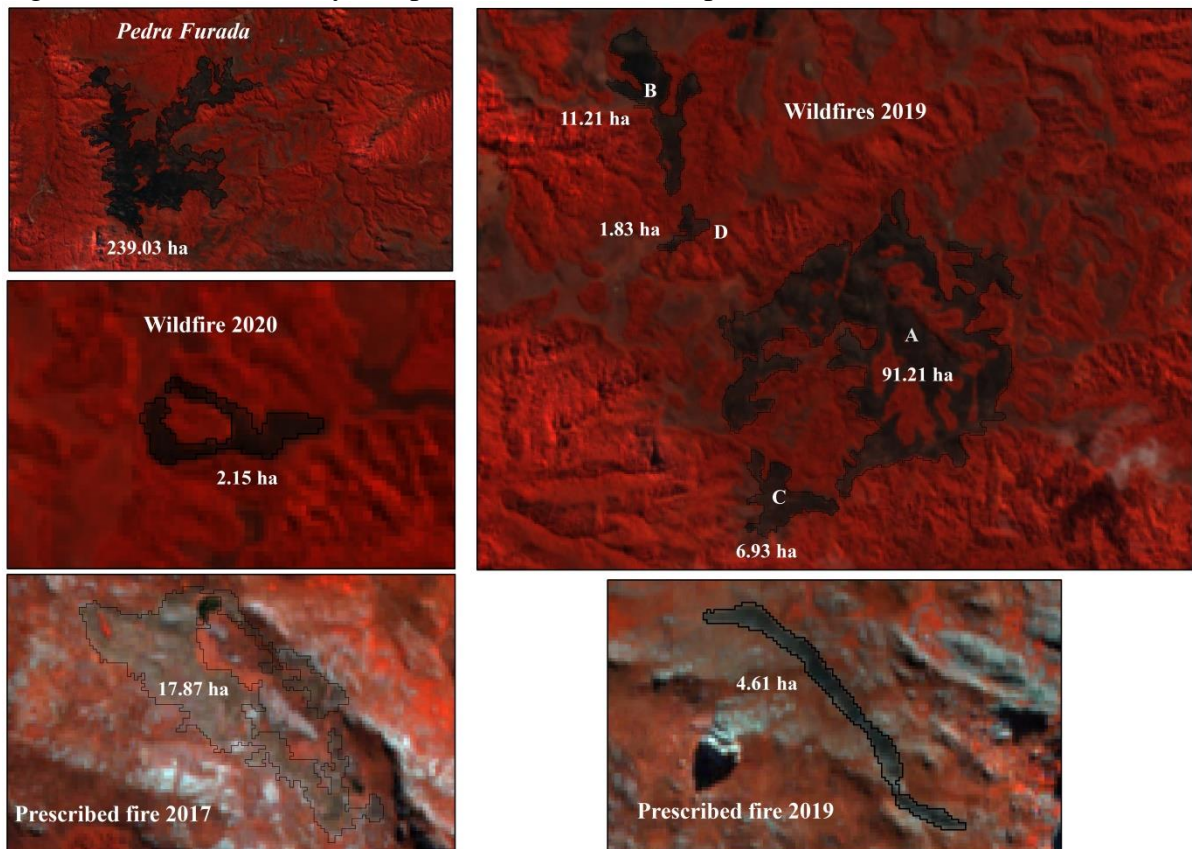
Source: from the author (2021).

2.2. Database

2.2.1. Remote sensing images

Sentinel-2 images were used in this research. Their major characteristics guiding this choice are free access, short revisit period, and high spatial resolution, which provide opportunities for mapping land cover and changes at fine spatial scale within short periods of time, e.g., a wildfire event (PHIRI et al., 2020).

Sentinel-2 is part of the Earth observation mission from the Copernicus Programme (DRUSCH et al., 2012) and compared to other medium spatial resolution satellites, as Landsat, offers improved data, especially in temporal and spatial resolution (NOVELLI et al., 2016). Its valuable trait is high temporal resolution of five days, multispectral imagery, and free access data. Also, this satellite has visible and near-infrared (NIR) bands with a spatial resolution of 10 m, the infrared bands have 20 m spatial resolution and the other bands have 60 m (RAIYANI et al., 2021).

The images were processed using Google Earth Engine (GEE) due to its cloud computing power and readily available imagery. It is a geospatial processing platform that was launched by Google in 2010 and represents a new generation that gives free access to use

a vast catalog of satellite imagery, allowing efficient geospatial analyses as parallelized processing on a global scale using Google's cloud (TAMIMINIA et al., 2020; GORELICK et al., 2017). In addition, it is not necessary to download any data nor to install any software in order to conduct processing tasks in GEE (AMANI et al., 2020).

Using GEE, we performed visual analyses to select cloud-free surface reflectance images and to compose time series of each study area.

Images from 2019 and 2020 were available with Level-2A of processing (bottom-of-atmosphere-reflectance). Images from 2017 were downloaded from the Copernicus SciHub website (https://scihub.copernicus.eu) with Level-1C of processing (top-of-atmosphere-reflectance) and converted to bottom-of-atmosphere-reflectance in QGIS using Dark Object Subtraction (DOS1), an atmospheric correction method that presents good performance compared with other more complex methods (PRIETO-AMPARAN et al., 2018).

2.2.2. Fire severity and monitoring post-fire recovery

The NBR index (KEY; BENSON, 1999) (Equation 1) was calculated and vegetation recovery analysis was conducted in the GIS environment.

This index is broadly used in fire analysis because relates vegetation moisture content by combining the near-infrared (NIR) and shortwave infrared (SWIR), parts of the electromagnetic spectrum (VERAVERBEKE et al., 2011). NIR and SWIR reflectance are frequently used because they are oppositely affected by fires, SWIR reflectance increase while NIR reflectance decrease with the transformation of vegetation to charcoal (FASSNACHT et al., 2021; KEY; BENSON, 2006). So, higher NBR values indicate healthy vegetation. On the other hand, lower values suggest bare soil and recently burned areas (PÁDUA et al. 2020; PRODAN; RACETIN 2019).

$$NBR = \frac{NIR\text{-}SWIR}{NIR\text{+}SWIR} \qquad\qquad (1)$$

Where *NIR* describes near-infrared and *SWIR* represents short wave infrared.

The current study used the index that relates NBR post and pre-fire to calculate the burn severity, called Differenced Normalized Burn Ratio (dNBR) (Equation 2), this index is calculated by subtracting a postfire NBR image from the pre-fire NBR image (FASSNACHT et al., 2021; KEY; BENSON, 2006). This index was chosen because previous research

demonstrates that it is more sensitive to changes in vegetation water content and chlorophyll, consequently useful to evaluate fire severity (FASSNACHT et al., 2021; SANTOS et al., 2018; LHERMITTE et al., 2011; CARVALHEIRO et al., 2010; EIDENSHINK et al., 2007).

dNBR positive value or close to one represents areas with high/severe impact of fire, while areas with values closer or lower than zero indicate an unburned area or vegetation regrowth (PADUA et al., 2020; KEY; BENSON, 2006).

$$dNBR= NBR_{pre-fire}- NBR_{post-fire} \qquad (2)$$

In this context, the fire severity level classification used was proposed by the United States Geological Survey (USGS) that constitute seven classes (TEODORO; AMARAL, 2019) (TABLE 3.1), but in this study, we used just four classes. dNBR value -0.1 was rated as unburned and above 0.66 was classified as a high severity area.

Table 3.1 - Values derived from dNBR indicating fire severity and classified based on the USGS.

| dNBR	Fire Severity Level	Legend color
-0.1 - 0.1	Unburned	
0.1 - 0.27	Low-severity	
0.27 - 0.44	Moderate-low severity	
0.44 - 0.66	Moderate-high severity	
> 0.66	High-severity	

We used time-series analysis of NBR temporal patterns to identify vegetation response after fire and vegetation recovery, which is considered complete when postfire NBR values approach the pre-fire ones. We used NBR average values per burn severity level, which allowed us to examine the overall change through time, reducing the influence of the pixels that are unlikely to change as a result of fire, e.g., bare land and rock outcrops (LACOUTURE; BROADBENT; CRANDALL, 2020). The major aim of this analysis was to comprehend the duration of burn scar on the landscape within different levels of burn severity.

3. RESULTS

For all study areas, there was a lack of useable images, especially in November, December, and January due to high cloud cover.

The fire severity map was calculated using the dNBR from all study areas and is presented in Figure 3.3. These maps allowed estimation and delimitation of the area of each severity level. The greater the difference (pre and post-fire), the higher the severity.

Figure 3.3 - Fire severity classes calculated by Sentinel-2 dNBR index to study areas.
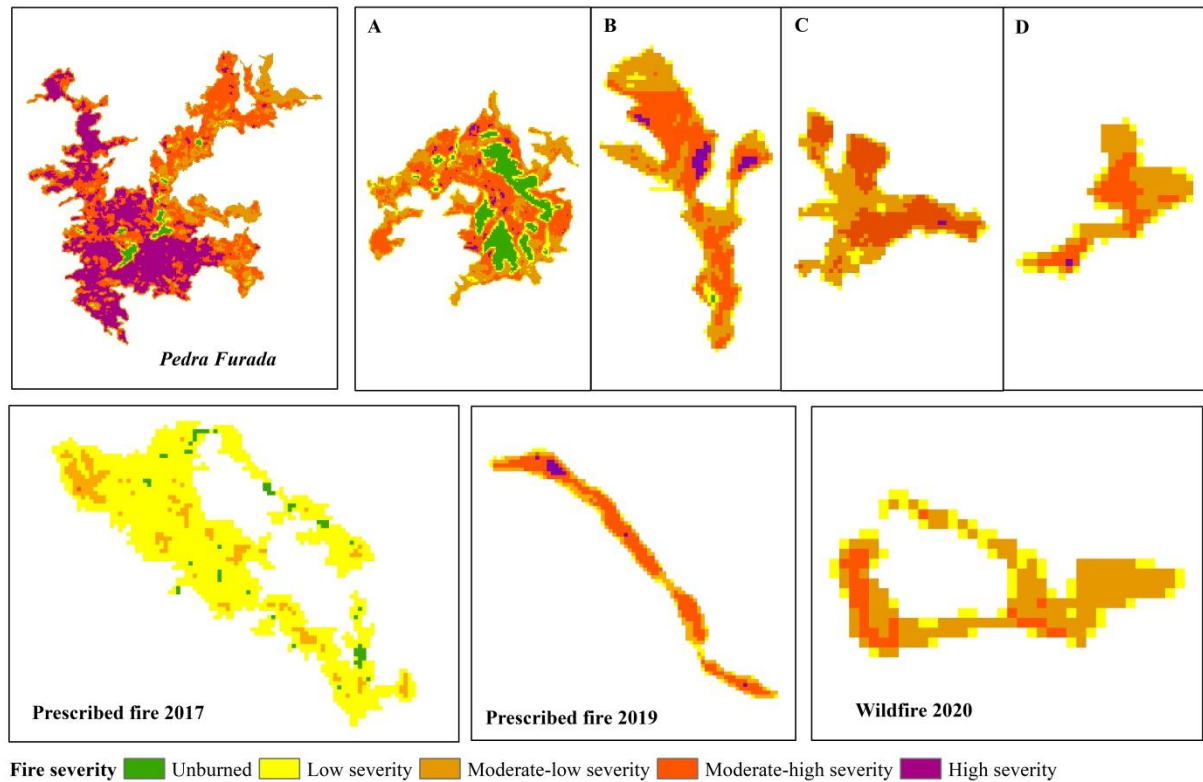
Source: from the author (2021).

From the 17.9 ha representing the prescribed fire realized in May 2017, 0.56 ha was estimated not to have been affected by the fire, the presence of these patches can be addressed to the characteristic of prescribed fire. The low severity level showed the higher percentage of burned area (87.1%) corresponding to 15.59 ha, and 1.71 ha showed a moderate-low severity. Only 0.01 ha presented moderate-high severity.

Our results indicate that the firebreak realized in 2019 produced a burned area of 4.61 ha, where 49.5% of the site experienced moderate-high severity and 36.4% moderate-low severity. Low severity composed 10.6% of the area and just 3.5% showed high severity.

The *Pedra Furada* forest fire has burned 239.03 ha, the greater percentage of the burned area showed moderate-high (37%) and high severity (34.7%). The moderate-low severity comprised 21.5% of the site area and only 12.83 ha and 3.5 ha were presented in low severity and unburned area, respectively.

Assessing the four forest fires that happened in August 2019 (A, B, C, and D) we found that 91.21 ha, 11.21 ha, 6.93 ha, and 1.83 ha were respectively burned. In all cases, the higher percentage of burned area was classified as moderate-low and moderate-high severity, quantifying 69.8%, 83.3%, 87.6%, and 81.4%, respectively. High severity represented an area of 1.55 ha, 0.44 ha, 0.02 ha, and 0.01ha. Unburned areas were only present in two of these events (A and B) that correspond to an area of 13.72 ha (15.04%) and 0.02 ha (0.18%).

The last forest fire evaluated occurred between 01/07/2020 and 04/25/2020 and burned 2.15 ha. Both moderate-low and low severity classes represented the majority of the burned area (a total of 86.55%, corresponding to 1.86 ha), the rest of area was defined as moderate-high severity (equivalent to 13.5%). This event did not present unburned and high severity areas.

A multitemporal approach was used to evaluate the progress of vegetation recovery using NBR temporal variation. The NBR average value was extracted for each severity level and unburned area for all fire events, as well as for the whole area affected by the fire (FIGURE 3.4).

When analyzing the values obtained from the whole area of the 2017 prescribed fire, we observed a decline of NBR values in 81.8% after the fire disturbance, which corresponds to the loss of vegetation over the considered scar that resulted from the fire. However, from August to October another decrease in NBR was detected presenting a negative value. Seven months after prescribed fire the NBR average had reached 77.3% of pre-fire value, but 50 days without cloud-free images did not allow us to identify the moment that vegetation recovery was completed.

Observing NBR temporal trends per severity level we detected that low severity followed the unburned area tendency, except immediately after the fire, when low severity presented NBR decrease of 80.95%. This fact may occur because this area was less affected by the fire. On the other hand, moderate-low and moderate-high severity showed greater post-fire NBR decline, but an increase six months after the fire event.

As the results presented in Figure 3.4 for a prescribed fire realized in May 2019, there is an evident decline of NBR value for the whole area after fire (from 0.20 to -0.22). Six months after fire, this area presents positive values of NBR but just achieved 25% of pre-fire value. For this site, we identify a lack of usable images between 11/04/2019 to 04/25/2020, so in this period it was not possible to be conclusive about vegetation recovery.

Figure 3.4 – Vegetation recovery per fire severity classes calculated by Sentinel-2 dNBR index to study areas.

A

B

C

D
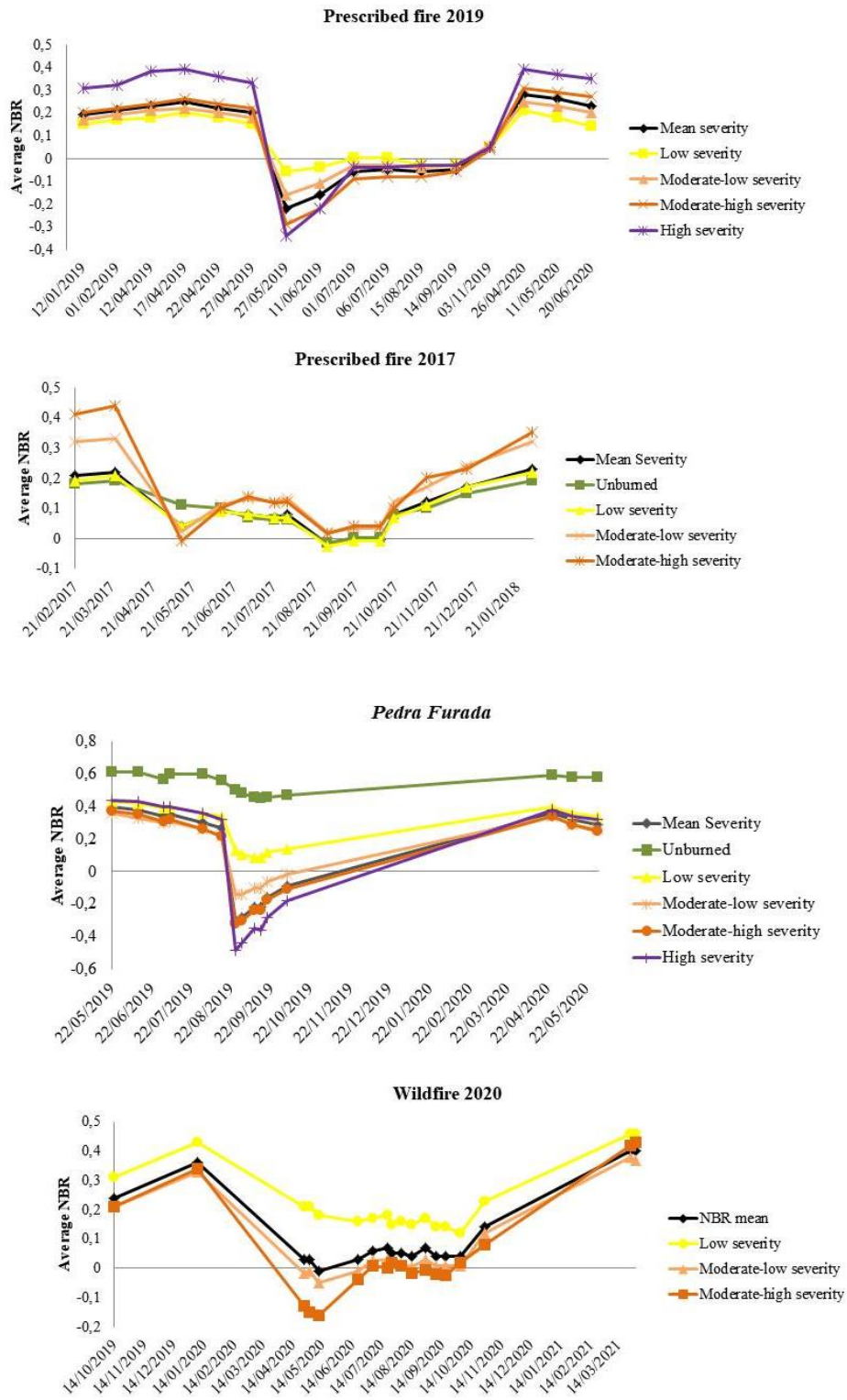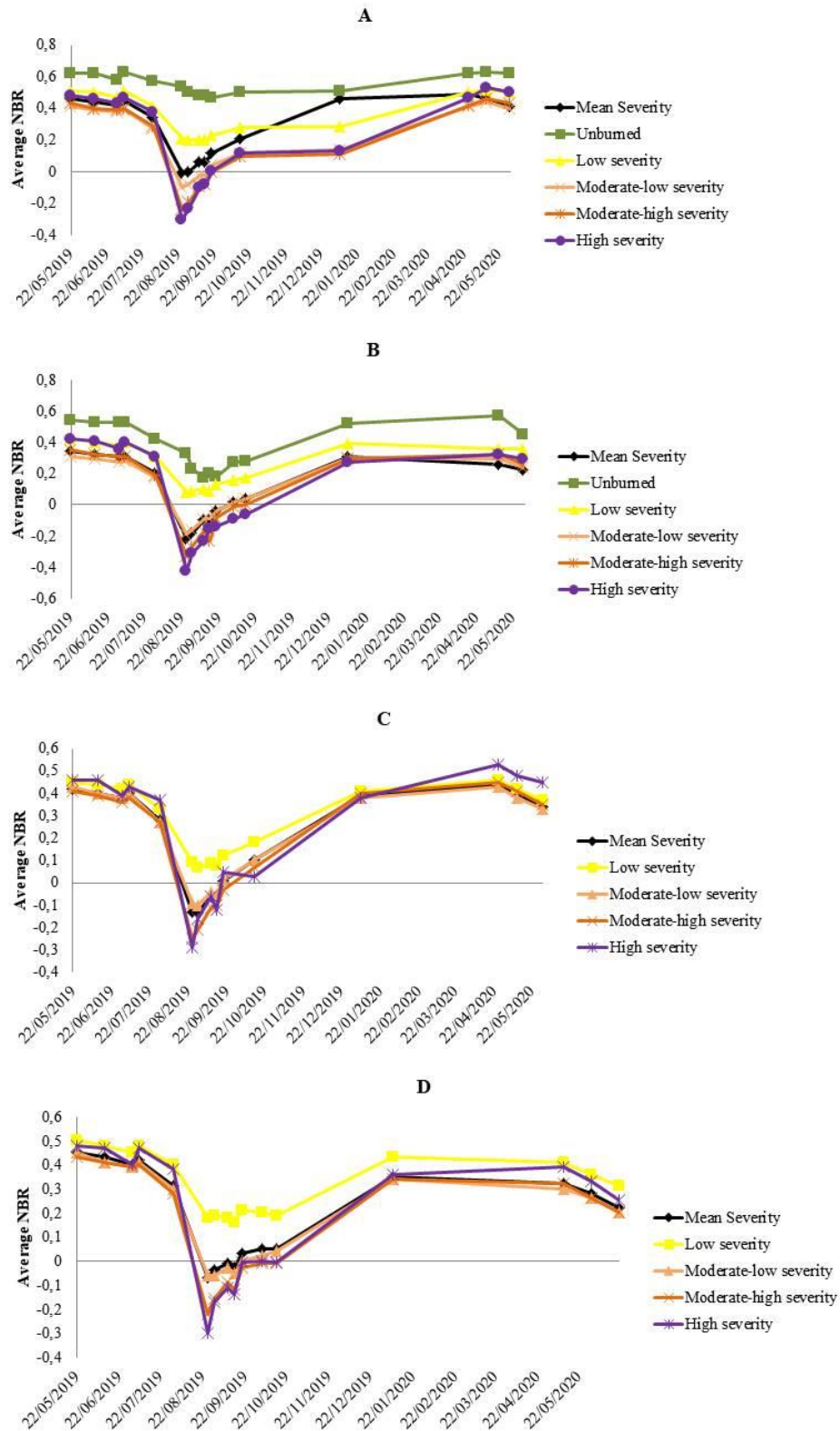
Source: from the author (2021).

The average NBR value of the high-severity area presented higher post-fire increases with the growth of -0.34 to -0.03 from May to August while the low severity areas increase

from -0.06 to -0.03 in the same period. For the moderate-low and moderate-high severity, similar growth NBR values were detected.

Evaluating *Pedra Furada* forest fire we observed that it occurred between 08/15/2019 to 08/24/2019, in the fire season. Before the occurrence of fire, the mean NBR value was around 0.3 for the whole area and 0.6, 0.35, 0.25, 0.25, and 0.35 for unburned, low-severity, moderate-low severity, moderate-high severity, and high severity, respectively. After the fire, NBR values were reduced to negative values in general in moderate-low, moderate-high, and high severity areas. Although in the unburned area the NBR value were kept almost constant. In this case, the gap of images was six months (10/05/2019 to 04/25/2020), so we could not detect the time of vegetation recovery.

The four forest fires that occurred spatially aggregated in August 2019 were analyzed. For the total area of Fire A, before the disturbance occurrence, the mean NBR value was around 0.35. Fires B, C, and D, presented mean values of 0.2, 0.3, and 0.3, respectively.

Two of these (A and B) showed unburned areas, where one present constant NBR values over the months and the other demonstrate a small decrease in NBR, probably caused by the influence of weather in vegetation phenology. In all fires the higher NBR decrease was identified in high severity areas, on the other hand, the lower decrease was observed in low-severity areas. The trend of high-severity areas, which presents a higher post-fire increase, was found in all fires.

The re-establishment time of these wildfires was similar, where NBR values returned to pre-fire levels in five months' time, January 2020, despite the exact moment not being exactly determined due to the lack of images during an 82 days period.

Finally, we assessed the area burned between 2020/01/07 to 2020/04/25, and an immediate decrease in NBR value was observed after the fire for the whole area, but this reduction was not so drastic as in the other forest fires. The low-severity area presented a small decline in values (51.2%) after the fire. The fire did not generate high severity impacts, however, moderate-low and moderate-high severity showed NBR reduction below zero, -0.015, and -0.13 respectively. These characteristics were different from other fires perhaps due to its occurrence out of the fire season.

We were incapable to define the precise time of NBR value near the value before the fire because of the absence of cloud-free images between 2020/10/28 to 2021/03/27, the same that happened with other sites. Still, according to the data, 11 months after fire the vegetation was already recovered. Differing from other fires, like *Pedra Furada* that presented recovery 8 months after the disturbance.

4. DISCUSSION

4.1. Fire severity

The detectability of a fire scar with remote sensing images is generally based on the fire severity and the vegetation type (VERAVERBEKE et al., 2010). The fire severity can be defined as the magnitude of changes in vegetation and soil caused by fire (ESCUIN; NAVARRO; FERNANDEZ, 2008; LENTILE et al., 2006) and is an important method to analyze impacts of wildfires on the landscape (SZPAKOWSKI; JENSEN, 2019).

The wildfires can burn a totality of vegetation or cause injury; however, both of these affect the reflectance of the vegetation. So, when vegetation is disturbed by fire the NIR reflectance reduces (FASSNACHT et al., 2021) because this part of the electromagnetic spectrum greatly depends on the spongy mesophyll and the fire affects it, resulting in a decrease (CHO et al., 2012). While, SWIR reflectance increases due to the decrease of the leaf water content (KEY; BENSON, 2006; MARTÍN; CHUVIECO, 1998).

Due to the spectral regions being changed by fire, vegetation indexes (VIs) like NDVI, NBR, RBR, CBI, are commonly used to assess fire severity (SHVETSOV et al., 2019; CHEN et al., 2010; ESCUIN; NAVARRO; FERNANDEZ, 2008) and vegetation recovery monitoring (ADAGBASA; ADELABU; OKELLO, 2020; SHVETSOV et al., 2019; VIANA-SOTO; AGUADO; MARTÍNEZ, 2017; GITAS et al., 2012; CHEN et al., 2010).

Even though there are many indexes, we choose the NBR because it shows a good performance for this purpose (FASSNACHT et al., 2021; SANTOS et al., 2018; LHERMITTE et al., 2011; ESCUIN; NAVARRO; FERNANDEZ, 2008).

In this study, we applied the dNBR in Sentinel-2 images, which is the difference between pre-fire NBR values and post-fire values. As a result, this difference can identify the fire severity levels (LI et al., 2018).

The prescribed fire realized in May 2017 generated a greater percentage of low severity with a small area represented as high severity. While the firebreak of 2019 resulted in more areas classified in moderate-high and moderate-low severity and presented a small percentage of high severity like the other prescribed fire. As these prescribed fires were applied to grass- and shrub-like vegetation of the *Campos de altitude*, they are expected to be less severe due to the lower fuel loads and short duration of burning (NEARY; LEONARD, 2020).

They realized under specific environmental conditions with controls over burning operations, predetermined duration, and a lower rate of spread (NEARY; LEONARD, 2020;

FERNANDEZ-CARRILLO; MCCAW; TANASE, 2019). In addition, it is a common fuel reduction technique used for fire prevention (PÉREZ-RODRÍGUEZ et al., 2020). As a result, wildfires usually are more severe than prescribed fires (NEARY; LEONARD, 2020).

On the other hand, the wildfires analyzed have in common that they present the majority of burned areas classified as high and moderate severity. This fact was expected because the wildfires generally are more intense and decontrolled, causing more injuries in the vegetation. Similar results were found by Pádua et al. (2020), where a total of 86% of burned area, corresponding to 311 ha, were found within high and moderate severity classes.

An exception was a wildfire that occurred in 2020 between January and April. In this case, most part of the burned area was categorized as moderate-low and low-severity. This pattern was similar to the prescribed fire, but different from the other wildfires investigated, probably be due to its occurrence out of the fire season, which goes from July until September (TOMZHINSKI; RIBEIRO; FERNANDES, 2012). In this period of the year, the air is more humid and there is more rainfall, resulting in less susceptibility to burning.

4.2. Vegetation recovery

As fire severity affects the spatial configurations of burned and unburned patches and influences ecological processes of post-fire recovery and succession (LI et al., 2018; DÍAZ-DELGADO et al., 2003), we assessed vegetation recovery per fire severity class.

Monitoring of vegetation recovery, defined as the capability to return pre-fire condition or natural state (BARTELS et al., 2016) is an important metric to determine the short and long-term impacts of fire, to analyze ecosystem resilience, and to determinate landscape dynamics (PÉREZ-CABELLO; MONTORIO; ALVES, 2021).

The dNBR index was used to assess fire severity, and vegetation recovery was obtained by monitoring NBR index of Sentinel-2 images. Thus, the recovery information can be derived from medium spatial resolution remotely sensed datasets, especially because of free and open data access, an important achievement of recent years (KENNEDY et al., 2014).

In burned areas by prescribed fire and by wildfires, NBR values decreased at the same time as the fire severity raised (FIGURE 3.4). Observing the prescribed fire that happened in 2017, we detected that the low-severity areas present similar behavior to unburned areas. Corroborating with a wildfire that happened in 2017 in riparian vegetation, shrubland communities, maritime pine, and deciduous species, that show similar values of NDVI between low-severity and unburned areas (PÁDUA et al., 2020).

The results for this prescribed fire show that between August and October all severity classes, especially low-severity and unburned areas, presented a decline in NBR values higher than immediately post-fire. However, the NBR values return to grow in November, allowing us to observe the phenological stages of vegetation. These events probably happen because of climate influence. August to October correspond to the end of Winter and the beginning of the Spring, which in INP is marked by lower temperature, an average of 8.4 ℃, 1 to 3 months of dry weather and frost is common (ICMBio, 2014). Besides, November corresponds to middle Spring approaching Summer, which presents higher temperatures (up to 26º C) and more regular rainfall, with higher intensity in December and January (ICMBio, 2014), resulting in greater chlorophyll content due to increase the vegetation growth.

Lazzeri et al. (2021) analyzed *Pinus pinaster* vegetation recovery using RBR index and found results that agree with the ones found in the present study, growth of vegetation in spring and midsummer and quiescence stage in autumn and winter, with the establishment of arboreal dominant vegetation being observed only after Spring.

The temporal trend of NBR demonstrates that for all wildfires and prescribed fire studied the high and moderate severity classes presented the lowest post-fire NBR values. Similar results were found by Pádua et al. (2020) and Navarro et al. (2017). Another tendency observed was a lower reduction of NBR values in low-severity and almost constant growth for this area, while in high-severity areas, greater post-fire NBR increases were detected. Our study also corroborates with other research like Bright et al. (2019) using NBR in coniferous forest; Shvetsov et al. (2019) in larch and scots pine forest using NBR; Chu; Guo; Takeda (2017) in Siberian larch forest using dNBR, dNDVI, and dNDMI indexes; Jin et al. (2012) in Canadian boreal forests using EVI index.

In this study, this fact can be possibly justified by the rapid regeneration of some species, as *Machaerina ensifolia* and *Cortaderia modesta*. These species are abundant in the high fields of INP, which have physical characteristics as dense tussocks that provide safety and insulation from high temperatures allowing for damage protection and survival after fire (SAFFORD, 2001).

A similar result was found in Chapada Diamantina National Park, where the authors found rapid regrowth capacity in the high-altitude vegetation fields (SANTOS et al., 2020). In mountainous grassland ecosystems, at the Golden Gate Highlands National Park, 48% of the park recovered to pre-fire conditions due to the fast response of the vegetation in African grasslands that are perennial and adapted to wildfires (ADAGBASA; ADELABU; OKELLO, 2020). In addition, chaparral vegetation demonstrates quick response after fire and many of

the plant species are fitted to regrow and establish following fires, even when high severity occurred (LENTILE et al., 2007).

The analysis of vegetation recovery showed that the prescribed fires took from 7 to 11 months to return to the same spectral response as before the occurrence of the fires, whereas in areas affected by wildfires, it took from 5 to 11 months.

The wildfires showed recovery times similar to the prescribed fire. This fact was not expected; however, it can be explained by the season of occurrence of wildfires, at the end of Winter, being benefited by the beginning of Spring and consequently by the improvement in temperature and rainfall, leading to greater vegetation development (MENESES, 2021). While the prescribed fires were applied at the end of Autumn and the beginning of Winter and its recovery is influenced by lower temperature and sometimes by the frost, which can cause quiescence stage.

This pattern found in our results was similar to other studies, like Lacouture; Broadbent; Crandall (2020) which analyzed sandhill pine savannas; Wiesner et al. (2019) that detected rapid NDVI increase after spring, growing season fires, in pine savannas, and Meneses (2021) that obtained shrubland recovery faster than tree species, and this process was influenced by the season, being more efficient in the Spring and at the beginning of the Summer.

In contrast, higher recovery rates were found in an area composed largely of pines with some oaks, yaupon and juniper where three years after the fire the NDVI values return to before fire levels (LEE; CHOW, 2015). In addition, land-cover occupied by woodland-shrub type needed 20 months to vegetation recovery and another area with Sclerophyllous vegetation needed 24 months (GOUVEIA, PÁSCOA, DaCAMARA, 2018).

We can conclude that forest vegetation requires longer periods of time to return a spectral response similar to pre-fire, while savannas and grasslands recovery after fire is swifter, as found by Lacouture et al. (2020); Wiesner et al. (2019), and Pereira et al. (2016).

An important reservation of this study is only a spectral analysis was realized. In this manner, we could not infer about vegetation composition and abundance. The limitation of spectral analysis is that recovery of specific vegetation types or species may not be identifiable (MENG et al., 2014). However, it is useful for monitoring the time the scar remains in the area and identifying for how long after the fire event the scar can still be detected.

To sum up, despite there being some challenges to overcome, as the cloud cover, monitoring post-fire can be achieved using NBR values derived from Sentinel-2 satellite.

Although the temporal window used in our research was relatively short, it allowed to infer an estimated time to recovery in each area, but we were unable to precisely identify time-to-vegetation recovery due to the lack of usable images. The same issue was found by Lacouture et al. (2020) which identified that the growing season weather increased the time-to-vegetation recovery, but also limited the availability of satellite images.

5. CONCLUSIONS

High-severity areas present greater post-fire increases in the temporal trend of NBR, while low-severity shows almost constant growth.

The method demonstrates the ability to infer and estimate time-to-vegetation recovery. Wildfires present a time to recovery similar to prescribed fire due to the influence of the weather.

Prescribed fires produce more moderate and low-severity areas while wildfires cause a higher percentage of burned areas categorized in moderate and high severity. So, prescribed fires in INP achieved their aim presenting low impact on land cover.

The use of Sentinel-2 images is efficient to obtain fire severity and assess post-fire regeneration and in aiding with decision-making in the context of protected areas management.

REFERENCES

ADAGBASA, E. G.; ADELABU, S. A.; OKELLO, T. W. Development of post-fire vegetation response-ability model in grassland mountainous ecosystem using GIS and remote sensing. **ISPRS Journal of Photogrammetry and Remote Sensing**, v. 164, p. 173-183, 2020.

ALVARES, C. A. et al. Köppen's climate classifcation map for Brazil. **Meteorologische Zeitschrift**, v. 22, n. 6, p. 711–728, 2013.

AMANI, M. et al. Google Earth Engine Cloud Computing Platform for Remote Sensing Big Data Applications: A Comprehensive Review. **IEEE JOURNAL OF SELECTED TOPICS IN APPLIED EARTH OBSERVATIONS AND REMOTE SENSING**, v. 13, p. 5326-5350, 2020.

AMOS, C.; PETROPOULOS, G. P.; FERENTINOS, K. P. Determining the use of Sentinel-2A MSI for wildfire burning & severity detection. **International Journal of Remote Sensing**, v. 40, n. 3, p. 905-930, 2019.

BARBERO, R. et al. Attributing Increases in Fire Weather to Anthropogenic Climate Change Over France. **Frontiers in Earth Science**, v. 8, p. 1-11, 2020.

BARTELS, S. F. et al. Trends in post-disturbance recovery rates of Canada's forests following wildfire and harvest. **Forest Ecology and Management**, v. 361, p. 194–207, 2016.

BASTOS, A. et al. Modelling post-fire vegetation recovery in Portugal. **Biogeosciences**, v.8, p. 3593–3607, 2011.

BELCHIOR, I. B. et al. Occurrence and recurrence of forest fires in Itatiaia National Park between 2008 and 2016. **Biodiversidade Brasileira**, v. 10, n. 1, p. 72, 2020.

BONNEY, M. T.; HE, Y.; MYINT, S. W. Contextualizing the 2019–2020 Kangaroo Island Bushfires: Quantifying Landscape-Level Influences on Past Severity and Recovery with Landsat and Google Earth Engine. **Remote Sensing,** v. 12, n. 23, p. 1-29, 2020.

BRIGHT, B. C. et al. Examining post-fire vegetation recovery with Landsat time series analysis in three western North American forest types. **Fire Ecology**, v.15, n. 8, p. 1-14, 2019.

CARVALHEIRO, L. C. et al. Forest fires mapping and monitoring of current and past forest fire activity from Meteosat Second Generation Data. **Environmental Modelling & Software**, v. 25, n. 12, p. 1909–1914, 2010.

CEPF - Critical Ecosystem Partnership Fund. **Announcing the World's 36th Biodiversity Hotspot: The North American Coastal Plain (2016, November).** Available: http://www.cepf.net/news/top_stories/Pages/Announcing-the-Worlds-36th-   Biodiversity-Hotspot.aspx.

CHEN, X. et al. Detecting post-fire burn severity and vegetation recovery using multitemporal remote sensing spectral indices and field-collected composite burn index data in a ponderosa pine forest. **International Journal of Remote Sensing**, v. 33, n. 23, p. 7905-7927, 2010.

CHO, M. A. et al. Potential utility of the spectral red-edge region of sumbandilasat imagery for assessing indigenous forest structure and health. **International journal of applied Earth observation and Geoinformation**, v. 16, p. 85–93, 2012.

CHU, T.; GUO, X.; TAKEDA, K. Effects of burn severity and environmental conditions on post-fire regeneration in Siberian larch forest. **Forests**, v. 8, n.3, p. 1-27, 2017.

CHUVIECO, E. et al. Historical background and current developments for mapping burned area from satellite Earth observation. **Remote Sensing of Environment**, v. 225, p. 45-64, 2019.

DÍAZ-DELGADO, R.; LLORET, F.; PONS, X. Influence of fire severity on plant regeneration by means of remote sensing imagery. **International Journal of Remote Sensing**, v. 24, n. 8, p. 1751–1763, 2003.

DRUSCH, M. et al. Sentinel-2: ESA's optical high-resolution mission for GMES operational services. **Remote Sensing of Environment**, v. 120, n.15, p.25-36, 2012.

EIDENSHINK, J. C. et al. A project for monitoring trends in burn severity. **Fire Ecology**, v. 3, n. 1, p.3-21, 2007.

ESCUIN, S.; NAVARRO, R.; FERNÁNDEZ, P. Fire severity assessment by using NBR (Normalized Burn Ratio) and NDVI (Normalized Difference Vegetation Index) derived from LANDSAT TM/ETM images. **International Journal of Remote Sensing**, v. 29, n. 4, p. 1053-1073, 2008.

FASSNACHT, F. E. et al. Explaining Sentinel 2-based dNBR and RdNBR variability with reference data from the bird's eye (UAS) perspective. **International Journal of Applied Earth Observation and Geoinformation**, v. 95, p. 1-19, 2021.

FERNANDEZ-CARRILLO, A.; MCCAW, L.; TANASE, M. A. Estimating prescribed fire impacts and post-fire tree survival in eucalyptus forests of Western Australia with L-band SAR data. **Remote Sensing of Environment**, v. 224, p. 133–144, 2019.

FRANCO, M. G.; MUNDO, I. A.; VEBLEN, T. T. Field-Validated Burn-Severity Mapping in North Patagonian Forests. **Remote Sensing**, v.12, n. 2, p. 1-18, 2020.

GITAS, I. et al. **Advances in Remote Sensing of Post-Fire Vegetation Recovery Monitoring - A Review**. Remote Sensing of Biomass - Principles and Applications. Temilola Fatoyinbo, IntechOpen, DOI: 10.5772/20571. 2012.

GORELICK, N. Google Earth engine: planetary-scale geospatial analysis for everyone. **Remote Sensing of Environment**, v. 202, p. 18-27, 2017.

GOUVEIA, C.; PÁSCOA, P.; DaCAMARA, C. **Post-Fire Vegetation Recovery in Iberia Based on Remote-Sensing Information**. Forest Fire, Janusz Szmyt, IntechOpen, DOI: 10.5772/intechopen.72594. 2018

ICMBio – Instituto Chico Mendes de Biodiversidade. **Plano de Manejo Parque Nacional do Itatiaia Revisão – Encarte 3**. Brasília, 215p., 2014. Available: http://www.icmbio.gov.br/portal/component/content/article?id=2181:parna-do-itatiaia.

INPE – **INSTITUTO NACIONAL DE PESQUISAS ESPACIAIS.** Available: https://queimadas.dgi.inpe.br/queimadas/portal. 2020.

JIN, Y. et al. The influence of burn severity on post-fire vegetation recovery and albedo change during early succession in North American boreal forests. **Journal of Geophysical Research**, v. 117, p. 1-15, 2012.

JOLLY, W. M. Climate-induced variations in global wildfire danger from 1979 to 2013. **Nature Communication**, v. 6, n. 7537, p. 1-11, 2015.

KENNEDY, R. E. et al. Bringing an ecological view of change to Landsat-based remote sensing. **Frontiers in Ecology and the Environment**, v. 12, n. 6, p. 339-346, 2014.

KEY, C. H.; BENSON, N. C. Landscape assessment (LA): sampling and analysis methods. In: LUTES, D. C. et al. **FIREMON:** Fire Effects Monitoring and Inventory System. U.S. Department of Agriculture, Forest Service, Rocky Mountain Research Station, Fort Collins, CO, USA, 2006, p. LA-1-55.

KEY, C. H.; BENSON, N. C. Measuring and remote sensing of burn severity. In: Paper Presented, 1999. **Proceedings** […] Joint Fire Science Conference and Workshop.

LACOUTURE, D. L.; BROADBENT, E. N.; CRANDALL, R. M. Detecting Vegetation Recovery after Fire in A Fire-Frequented Habitat Using Normalized Difference Vegetation Index (NDVI). **Forests**, v. 11, p. 1-12, 2020.

LAZZERI, G. et al. Multitemporal Mapping of Post-Fire Land Cover Using Multiplatform PRISMA Hyperspectral and Sentinel-UAV Multispectral Data: Insights from Case Studies in Portugal and Italy. **Sensors**, v. 21, p. 1-28, 2021.

LEE, R. J.; CHOW, T. E. Post-wildfire assessment of vegetation regeneration in Bastrop, Texas, using Landsat imagery. **GIScience & Remote Sening**, v. 52, n. 5, p. 609–626, 2015.

LENTILE, L. B. et al. Remote sensing techniques to assess active fire characteristics and post fire effects. **International Journal of Wildland Fire**, v. 194, p. 319–345, 2006.

LENTILE, L. B. et al. Post-Fire Burn Severity and Vegetation Response Following Eight Large Wildfires Across the Western United States. **Fire Ecology**, v. 3, n. 1, p. 91-108, 2007.

LHERMITTE, S. et al. Assessing intra-annual vegetation regrowth after fire using the pixel based regeneration index. **ISPRS Journal ff Photogrammetry and Remote Sensing**, v. 66, n. 1), p.17-27, 2011.

LI, X. et al. Post-Fire Vegetation Succession and Surface Energy Fluxes Derived from Remote Sensing. **Remote Sensing**, v. 10, n. 7, p. 1-19, 2018.

MARTÍN, M. P. I.; CHUVIECO, E. Cartografía de grandes incêndios forestales en la península ibérica a partir de imágenes NOAA-AVHRR. **Serie Geográfica**, v. 7, p. 109-128, 1998.

MENESES, B. M. Vegetation Recovery Patterns in Burned Areas Assessed with Landsat 8 OLI Imagery and Environmental Biophysical Data. **Fire**, v. 4, n. 4, p. 1-20, 2021.

MENG, R., Remote sensing analysis of vegetation recovery following short-interval fires in Southern California shrublands. **PloS One**, v. 9, n.10, p. 1-12, 2014.

MOTTA, M. S. et al. Intensidade do fogo em uma queima prescrita no Parque Nacional do Itatiaia. In: Wildfire Conference, 2019. **Proceedings** […] Número especial: Biodiversidade Brasileira.

NAVARRO, G. et al. Evaluation of forest fire on Madeira Island using Sentinel-2A MSI imagery. **International Journal of Applied Earth Observation and Geoinformation**, v. 58, p. 97-106, 2017.

NEARY, D. G.; LEONARD, J. M. **Effects of Fire on Grassland Soils and Water: A Review**. Grasses and Grassland Aspects. Valentin Missiakô Kindomihou, IntechOpen, DOI: 10.5772/intechopen.90747. 2020.

NOVELLI, A. Performance evaluation of object based greenhouse detection from Sentinel-2 MSI and Landsat 8 OLI data: A case study from Almería (Spain). **International Journal of Applied Earth Observation and Geoinformation**, v. 52, p. 403–411, 2016.

PÁDUA, L. et al. Effectiveness of Sentinel-2 in Multi-Temporal Post-Fire Monitoring When Compared with UAV Imagery. **ISPRS International Journal of Geo-Information**, v. 9, n. 4, p. 1-15, 2020.

PÉREZ-CABELLO, F.; MONTORIO, R.; ALVES, D. B. Remote sensing techniques to assess post-fire vegetation recovery. **Current Opinion in Environmental Science & Health**, v. 21, p.1-9, 2021.

PÉREZ-RODRÍGUEZ, L. A. et al. Evaluation of Prescribed Fires from Unmanned Aerial Vehicles (UAVs) Imagery and Machine Learning Algorithms. **Remote Sensing**, v. 12, n. 8, p. 1-11, 2020.

PEREIRA, P. et al. Short-term vegetation recovery after a grassland fire in Lithuania: The effects of fire severity, slope position and aspect. **Land Degradation & Development**, v. 27, p. 1523–1534, 2016.

PHIRI, D. et al. Sentinel-2 Data for Land Cover/Use Mapping: A Review. **Remote Sensing**, v. 12, p. 1-35, 2020.

PRIETO-AMPARAN, J. A. et al. Atmospheric and Radiometric Correction Algorithms for the Multitemporal Assessment of Grasslands Productivity. **Remote Sensing,** v. 10, n. 2, p.1-23, 2018.

PRODAN, A.; RACETIN, I. Analysis of burned vegetation recovery by means of vegetation indices. **International Multidisciplinary Scientific GeoConference: SGEM**, v. 19, p. 449–456, 2019.

RAIYANI, K. et al. Sentinel-2 Image Scene Classification: A Comparison between Sen2Cor and a Machine Learning Approach**. Remote Sensing**, v. 13, p. 1-22, 2021.

SAFFORD, H. D. Brazilian Páramos III: Patterns and Rates of Postfire Regeneration in the Campos de altitude. **Biotropica**, v. 33, n. 2, p. 282-302, 2001.

SANTOS, S. M. B. et al. Assessment of Burned Forest Area Severity and Postfire Regrowth in Chapada Diamantina National Park (Bahia, Brazil) Using dNBR and RdNBR Spectral Indices. **Geosciences**, v. 10, n. 3, p. 1-19, 2020.

SANTOS, J. F. C. et al. Potentials and limitations of remote fire monitoring in protected areas. **Science of The Total Environment**, v. 616-617, p. 1347-1355, 2018.

SHIMABUKURO, Y. E. et al. Mapping Burned Areas of Mato Grosso State Brazilian Amazon Using Multisensor Datasets. **Remote Sensing**,v.12, n. 22, p. 1-23, 2020.

SHVETSOV, E. et al. Assessment of post-fire vegetation recovery in Southern Siberia using remote sensing observations. **Environmental Research Letters**, v. 14, n. 5, p. 1-13, 2019.

SUN, Q. et al. Global heat stress on health, wildfires, and agricultural crops under different levels of climate warming. **Environment International**, v. 128, p. 125-136, 2019.

SZPAKOWSKI, D. M.; JENSEN, J. L. R. A Review of the Applications of Remote Sensing in Fire Ecology. **Remote Sensing**, v. 11, n. 22, p. 1-31, 2019.

TAMIMINIA, H. et al. Google Earth Engine for geo-big data applications: A meta-analysis and systematic review. **ISPRS Journal of Photogrammetry and Remote Sensing**, v. 164, p. 152-170, 2020.

TEODORO, A.; AMARAL, A. A Statistical and Spatial Analysis of Portuguese Forest Fires in Summer 2016 Considering Landsat 8 and Sentinel 2A Data. **Environments**, v. 6, n. 3, p. 1-17, 2019.

TOMZHINSKI, G. W.; RIBEIRO, K. T.; FERNANDES, M. C. Análise Geoecológica dos Incêndios Florestais do Parque Nacional do Itatiaia. **Boletim do Parque Nacional do Itatiaia**, Rio de Janeiro, n. 15, 164 p., 2012.

VELOSO, H.P.; RANGEL FILHO, A.L.R.; LIMA, J.C.A. **Classificação da vegetação brasileira, adaptada a um sistema universal**. Rio de Janeiro: IBGE, Departamento de Recursos Naturais e Estudos Ambientais, 124p., 1991.

VERAVERBEKE, S. et al. A time-integrated MODIS burn severity assessment using the multi-temporal differenced normalized burn ratio ($dNBR_{MT}$) **International Journal of Applied Earth Observation and Geoinformation**, v. 13, n. 1, p. 52–58, 2011.

VERAVERBEKE, S. et al. The temporal dimension of differenced normalized burn ratio (dNBR) fire/burn severity studies: The case of the large 2007 peloponnese wildfires in greece. **Remote Sensing of Environment**, v. 114, p. 2548–2563, 2010.

VIANA-SOTO, A.; AGUADO, I.; MARTÍNEZ, S. Assessment of postfire vegetation recovery using fire severity and geographical data in the mediterranean region (Spain). **Environments**, v. 4, n. 4, p. 1-17, 2017.

WIESNER, S. et al. The role of understory phenology and productivity in the carbon dynamics of longleaf pine savannas. **Ecosphere**, v. 10, n. 4, p. 1-20, 2019.